SATELLITE-BASED APPROACH FOR MONITORING AND MAPPING THE SUBMERGED AQUATIC VEGETATION IN THE EUTROPHIC SHALLOW BASIN OF LAKE BIWA, JAPAN

SHWETA YADAV

2017

ACKNOWLEDGEMENTS

I would like to express my deep gratitude to my supervisor Professor Minoru Yoneda and also to Professor Yosuke Alexandre Yamashiki for their constant guidance and supervision throughout my doctoral research, which helped me to accomplish the task of my Ph.D. thesis.

I would also like to extend my sincere thanks to Professor Tamura Masayuki, and Associate Professor Junichi Susaki for their immense support and valuable suggestions, which helped me to enhance my knowledge and understanding during my research. My gratitude extends to Professor Yoshihisa Shimizu for the constructive comments during my defense. Also thankful to Associate Professor Yoko Shimada for giving the much-needed suggestions during my research period.

I owe my thanks to Dr. Kanako Ishikawa and other staff members from Lake Biwa Environmental Research Institute (LBERI) for conducting the lake surveys with us and for sharing the information. Also grateful to Japan Water Agency (JWA) for providing the required data for research.

I am thankful to the Ministry of Education, Culture, Sports, Science, and Technology (MEXT) of Japan, for the financial support during my stay at Kyoto University.

I also thanks and acknowledge the timely help from Ms. Hanae Hoshihara during my stay in Kyoto. I convey my appreciation to Ms. Thuong Nguyen and Mr. Xuankun Li for their help during my experiments and thesis writing. Also, I am grateful to all my friends and lab members of Environmental Risk Analysis for being so supportive and encouraging throughout my research at Kyoto University.

At last, I would like to take this opportunity to convey my thanks to my beloved parents and entire family members for their love and care. To all of you and to all those I did not mention, I say thanks for helping me to reach here.

Satellite-Based Approach for Monitoring and Mapping the Submerged Aquatic Vegetation in the Eutrophic Shallow Basin of Lake Biwa, Japan

ABSTRACT

Human beings are intrinsically related to the inland water ecosystem and the diverse services it offers. Over the past decades, there has been renewed interest in submerged aquatic vegetation (SAV), both for its ecological importance and nuisance overgrowth of invasive species, in the freshwater ecosystems. When present, large SAV beds sequester nutrients, provide habitats for the fish and other invertebrates, prevent sediment re-suspension and consequently maintains a clear water condition in shallow water bodies. Hence, a lake with aquatic plants holds a high ecological value. Conversely, the massive overgrowth of invasive SAV species associated primarily with the anthropogenic nutrient enrichment in freshwater ecosystems likely to impact environmentally or economically. In particular, invasive aquatic plants alter the nutrient cycles, affects biodiversity and obstruct navigation, fishery, and other recreational activities. In Japan, over 40 alien aquatic plant species have already been naturalized and proliferated in many lakes and river beds. Most dominant alien species commonly found in Japanese lakes comprise *Egeria Densa* and *Elodea Nuttallii.* A long-term monitoring and early detection of these species remain a challenge for water managers.

Remote sensing provides a non-destructive, repeatable and cost-effective technique for monitoring the aquatic vegetation over the large lakes. However, due to the presence of optically active components (OAC) in the water column of the lakes, the identification and quantification of SAV always remain a challenge, particularly in eutrophic shallow lakes. On the other hand, to account for the spatial heterogeneity in the complex aquatic environment, the hyperspectral imagery was widely used for SAV mapping. The cost and complexity (e.g., sensitive detectors, fast computers) associated with the hyperspectral images makes it economically and technically less feasible for long-term monitoring of the large areas. In this study, we explored multispectral satellite remote sensing and developed a satellite-based approach for SAV detection, identification and quantification (i.e., SAV coverage area and biomass estimation) for the eutrophic shallow lake.

The main aim of this dissertation was to develop a satellite-based (i.e., Landsat-8 OLI) approach and to identify and quantify the SAV in the shallow eutrophic south basin of Lake Biwa, for the peak growth period of SAV (i.e., mainly in September), from 2013 to 2016. Hence, before the application of satellite remote sensing in a eutrophic lake, the comprehensive understanding of the influence of OAC on the detection of SAV in water is essential. Thus, this study is further divided into three main objectives (given below).

As our first objective, we identified the influence of optically active components and water depth, on the detection of dominant SAV species (in the south basin of Lake Biwa) using the Landsat-8 OLI image, particularly for *Egeria Densa* and *Potamogeton Maackianus*. The Bio-Optical model was applied to simulate the SAV species reflectance at the changing concentration of optically active components and water depths. The phytoplankton and Non-phytoplankton Suspended Solids (NPSS) were identified as the dominant optically active components substantially attenuating the SAV species reflectance with the increase in concentration and water depth, in the eutrophic lake. The maximum canopy depth estimated for *Egeria Densa* and *Potamogeton Maackinus*, using the Bio-Optical model and the SAV classified image, was 1.0 m and 1.1 m, respectively. The result shows that when the chlorophyll concentration is >20 μg/L and NPSS is >10 mg/L, the canopy depth reduced to < 0.3 m and <0.2 m, respectively. The *in-situ* measured data and classified SAV image confirmed the maximum canopy depth (i.e., 0.40 m - 1.1 m canopy depth), for the SAV detection using the Landsat-8 image, in the south basin of Lake Biwa.

As our second objective, the identified dominant optically active components in the Lake Biwa were assessed both by Lab experiment and Landsat-8 image. A new spectral decomposition algorithm was developed and applied to the Landsat-8 image, to estimate the chlorophyll concentration in the lake. The satellite-derived chlorophyll map shows the increased chlorophyll concentration in the 2013 and 2016 (> 30 μg/L), particularly towards the eastern shoreline and towards the outlet of the basin. The estimated chlorophyll using the satellite image was in line with the observed data (2014 and 2016) with an overall RMSE of 6.15 and 6.28 μg/L. The depth-invariant regression model developed to evaluate the water transparency of the south basin of Lake Biwa. Furthermore, the satellite-derived water transparency result confirmed the reduced water clarity due to increased chlorophyll concentration in 2013 and 2016, with < 1% (1 km^2) and 15% (8 km^2) of the basin area has the

water transparency > 3.0 m than 2014 with 54% (28 km^2). The green and red band of Landsat-8 gave the best result (R^2 = 0.77) for water clarity estimation. The satellite-derived water transparency of the south basin was 2.2 m (October 2013), 2.9 m (September 2014), 2.6 m (September 2015) and 2.0 m (September 2016), respectively. The result further confirmed the reduced water clarity in the eastern and southern side of the basin which receives the water from the number of rivers.

In the third objective, we applied the multispectral Landsat-8 OLI image to assess the SAV distribution and biomass (2013-2016) in the south basin. The SAV coverage area was mapped with the classification accuracy of 84.6% and omission and commission error of 23.5% and 18.8 %, respectively. The obtained result shows that several factors such as water depth (or SAV depth in water), SAV coverage area, SAV canopy depth, the concentration of OAC and SAV coverage area along with species reflectance, significantly affects the detection of SAV in the lake. In this study, the detected SAV coverage area using the Landsat-8 image is; 21% (2013), 18% (2014), 30% (2015 and 40% (2016) of the basin area. The result shows that SAV distribution in the basin increases following the clear water year 2014 (2014-2015 coverage area: 9.6 km^2 – 15.7 km^2), whereas decrease following the turbid water year (2013 -2014 coverage area: 10.7 km^2 – 9.6 km^2)).

The developed biomass estimation model successfully applied to the Landsat-8 image, which gives an overall RMSE of 0.13 kg DW m^{-2}. An upsurge in SAV biomass to 16% (2014), 55% (2015) and 34% (2016), was noted when compared to the biomass in 2013. When compared with 2013, the SAV biomass for the classified pixels is 55% (1852 Ton) more in 2015, followed by 2014 and 2016 with 34 % (1160 Ton) and 16% (529 Ton), in the south basin of Lake Biwa. The result further indicates the importance of water clarity in the mapping of SAV. However, long term monitoring of SAV (with monthly variations) is required to show the influence of water clarity on SAV distribution and biomass.

Present work corresponds well with the work by Lake Biwa Environmental Research Institute (LBERI), Japan. Thus, this work will be extremely beneficial for the effective SAV control and management efforts, by the concerned lake management authority and other stakeholders. In future, the developed remote sensing technique can potentially be applied for monitoring the SAV in other shallow lakes.

TABLE OF CONTENT

LIST OF FIGURES

Chapter 1 Introduction

Chapter 2 Literature Review

Chapter 3 Detection Depth Estimation of Submerged Aquatic Vegetation

LIST OF TABLES

Chapter 3 Detection Depth Estimation of Submerged Aquatic Vegetation

Chapter 4 Mapping of Optically Active Components using Satellite Image

Chapter 5 Mapping of Submerged Aquatic Vegetation using Satellite Image

LIST OF ABBREVIATIONS

SAV	Submerged Aquatic Vegetation
OAC	Optically Active Components
Chl-a	Chlorophyll-A
NPSS	Non-Phytoplankton Suspended Solids
CDOM	Colored Dissolved Organic Matter
SDA	Spectral Decomposition Algorithm
SMA	Spectral Mixture Analysis
SAM	Spectral Angle Mapper
DOC	Dissolved Organic Matter

UNITS

DW	Dry Weight
Kg DW m^{-2}	Kilogram Dry Weight per square meter
g DW m^{-2}	Gram Dry Weight per square meter
g WT m^{-2}	Gram Wet Weight per square meter
T	Ton
T DW	Ton Dry Weight

Chapter 1

INTRODUCTION

1.1 Research Background

Submerged Aquatic vegetation (SAV) are the foundation of healthy and flourishing inland water ecosystems. They are the rooted plants remains submerged throughout their growth period and typically limited to the shallow waters where sufficient light can reach to the bottom substrate [1–3]. When present, extensive SAV beds sequester nutrients, provide habitats for the fish and other invertebrates, prevent sediment re-suspension and thus maintains a clear water condition in shallow water bodies (Scheffer and Jeppesen, 1998; Takamura *et al.*, 2003). Dense macrophyte cover competes for the nutrients and releases the allelochemicals that are suspected to inhibit the growth of phytoplankton and avert eutrophication[6]. Re-establishment of SAV has also been recognized as an important ecological technique for the restoration of the eutrophicated shallow lakes [7,8].

Apart from climate change, the human interferences in the ecosystem processes contributing to the loss and alteration of biodiversity of the inland and coastal waters. Over the past few decades, the excessive nutrient loading from agriculture areas emerged as the direct driver of the ecosystem change leading to the biological invasion by non-native species and the loss of native species in many lakes worldwide [9]. Conversely, the massive overgrowth of invasive SAV species associated primarily with the anthropogenic nutrient enrichment in freshwater ecosystems likely to impact environmentally or economically. In particular, invasive aquatic plants alter the nutrient cycles, degrade water quality, dominate native species, obstruct navigation, fishery and other recreational activities (Lovell, Stone and Fernandez, 2006; Santos, Anderson and Ustin, 2011). Currently, 15 taxa of aquatic plants species are listed as the world's worst invasive species by IUCN [12]. The invasive range is predicted to increase by two folds in Europe and America by 2070 with increased gas emission scenario [9]. In Japan, over 40 alien aquatic plant species have already been naturalized and proliferated in many lakes and river beds [13]. Some of the SAV species listed among the 100 worst alien species in Japan are shown in Figure 1.1. Most dominant alien species commonly found in Japanese lakes comprise *Egeria Densa* and *Elodea Nuttallii*.

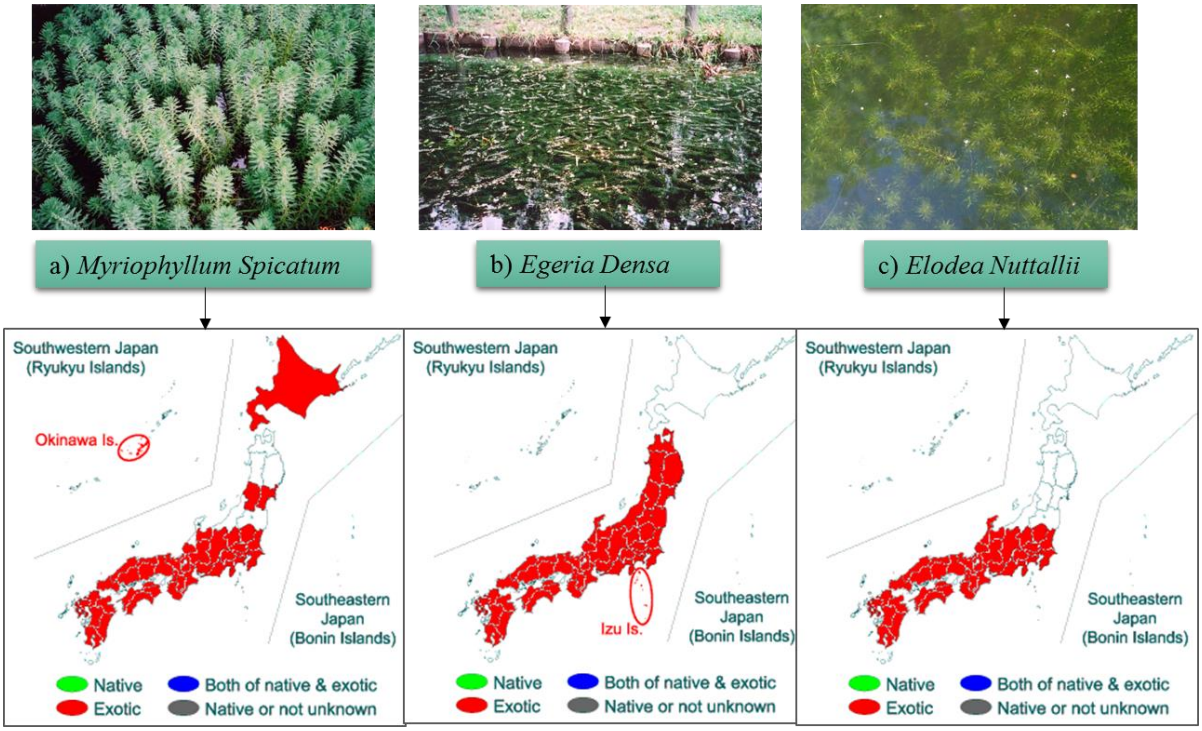

Figure 1.1. SAV alien species and their distribution in Japan (from the list of 100 worst alien species in Japan). (Source: National Institute for Environmental Studies, Japan (https://www.nies.go.jp/biodiversity/invasive/index_en.html)).

Previous work has demonstrated the feasibility of mapping and monitoring the SAV cover in the large lakes using satellite remote sensing [3,14–16]. Aerial photographs and high resolution airborne hyperspectral images have been used for vegetation mapping to overcome the spatial heterogeneity in the optically complex aquatic environment [2,17,18]. However, due to the large area coverage, ease of data acquisition, and low cost associated with the medium resolution satellite image (e.g., Landsat TM/ETM/OLI, Spot, Terra/Aster) they are widely used for mapping SAV along with other limnologic parameters [14,19,20]. Satellite remote sensing is a potential tool for monitoring the growth and characteristics of SAV in fresh waters [3,21–25]. The principles behind aquatic vegetation and terrestrial vegetation spectral characteristics are same; however, aquatic plants are not easily detectable due to the complex aquatic environment than its terrestrial counterparts [22].

In an optically shallow water, the detection of SAV using remote sensing is often hindered by the absorption and scattering processes of the optically active components (OAC) mainly phytoplankton (chlorophyll a), non-phytoplankton suspended sediments (NPSS) and cDOM (chromophoric dissolved organic matter) [22,26–29]. The presence of OAC potentially diminishes the water transparency which limits the plant growth and reduces the possibility

to detect the submerged plants using satellite images [30,31]. In order to map the SAV species in lake water, their reflectance must cross the air-water interface, which is not possible in the highly turbid water. Nevertheless, if the water is less turbid and the SAV signal is significantly contributing to the water leaving reflectance, then it is possible to map the distribution of SAV using satellite image [18,30]. Hence, water clarity is one of the important factors which substantially influences the detection of SAV by the satellite remote sensing [15]. In a eutrophic lake, the mixed pixel effect due to the presence of OAC can result in misclassification. Thus, it is essential to have a water clarity information before SAV classification. Consequently, in some studies, the satellite images were used to estimate the water transparency [32] and optical depth (water clarity or transparency) assessment [21], before SAV abundance mapping. Most frequently used approach for water clarity estimation involves the linear regression of the satellite bands and the *in-situ* water clarity data [32–34].

In addition, several remote sensing techniques have been used for SAV spectral analysis and bottom mappings. Some of the frequently used techniques are, vegetation presence frequency [16], vegetation indices [32,35], radiative transfer model and linear mixture approach [26,36], modular inversion program and Water Color Simulator (WASI) [18,37] and classification tree model [44,45]. Moreover, high spatial resolution imagery such as Quickbird multispectral image was applied in some studies for SAV mapping [40]. Techniques such as Spectral Angle Mapper (SAM)[41], Spectral Mixture Analysis (SMA)[2], Continuum Removal and Minimum Noise Fraction (MNF)[24] were successfully applied mainly on hyperspectral images for aquatic vegetation mapping and identification [2,18,23,24,42]. However, the application of these techniques on medium resolution satellite image such as Landsat-8 is still insufficient, especially for classifying and mapping the SAV in the shallow eutrophic lakes.

Furthermore, to quantitatively assess the growth of SAV communities, biomass estimation is essential. Biomass of SAV is also an important factor indicating the productivity of the lake ecosystem. However, excessive plant material (i.e., the biomass) also contributes to the plant nuisance problem in the shallow waters [43–45]. Remote sensing techniques such as Submerged Aquatic Vegetation Mapping Algorithm (SAVMA) was used to estimate the SAV biomass (mainly *Cladophora*) by assigning the average dry weight density obtained from the field survey to the identified SAV area (i.e., grouped as the dense and less dense *Cladophora* area) [21]. Whereas, in some studies, aquatic vegetation biomass estimation model was

developed by establishing a relationship between Normalized Difference Vegetation Index (NDVI) and the observed biomass of aquatic plants, using the multispectral satellite images [32]. In the former case, a different set of dry weight estimates is required to estimate the biomass for other time of the year. Whereas, in the latter case, the NDVI values of SAV can be influenced by the presence of phytoplankton's, particularly in eutrophic lakes [35]. The time-specific and location-specific approach may not be applicable in other optically shallow lakes.

Thus, in this study, we developed a new biomass estimation approach based on the spectral decomposition algorithm. In this algorithm, the mixed pixel reflectance is expressed as a linear combination of the dominant OAC (i.e., endmembers). The spectral decomposition algorithm has previously been used only for water quality monitoring for the shallow lakes using three main OAC, i.e., clear water, NPSS and phytoplankton [46,47]. Nevertheless, in optically shallow waters, the upward irradiance just below the water surface is the sum of the flux backscattered by the water column and the flux reflected by the bottom [26,48–51]. Thus, when analyzing the remote sensing data for an optically shallow lakes, the influence of the bottom albedo has to be included [18,48]. Specifically, for the lakes with long stands of dense vegetation substrate which are substantially contributing to the water leaving reflectance. However, the influence of the bottom substrate has not been accounted using the same algorithm in the previous studies, which could be due to the different environmental conditions of their study areas.

1.2 Problem Statement

The overabundance of SAV species in the water bodies often affects the lake ecosystems and the services it offers to human beings. The SAV species with relatively fast growth rate such as *Egeria Densa* (also known as Brazilian waterweed) which can thrive in low light conditions to a water depth of 4 m, can invade freshwater systems with its dense canopy formation and affects the biogeochemical cycle of the lake ecosystem [52]. The invasive species potentially compete for the nutrients and sunlight thus eliminates the native species in the lake. On the other hand, the proliferation of invasive species in a water body affects the navigation, fishing and other recreational activities. The spread of these SAV species is found in many parts of the world such as lakes in Asia, Africa, North and South America, Australia and New Zealand. In some countries huge amount of money spent in harvesting and

eradication of invasive species. The estimated control and eradication cost of invasive species in the United States was USD $100 million [11].

Lake Biwa is the largest and an ancient freshwater lake in Japan which holds great economic and ecologic importance for the region. Over the past 20 years, the shallow basin of the lake was largely reclaimed for the construction purposes which shifted the shoreline inwards consequently changed the landscape and the shore vegetation [53]. The ecosystem of the lake has greatly been affected by various kinds of human activities. Eutrophication of the lake occurred during the economic growth period after the 1960s. Following this, the lake was invaded by various types of alien flora and fauna species which had the adverse effect on indigenous fish and aquatic plant species. The Lake underwent the ecological regime shift from the phytoplankton-dominated turbid water lake to macrophyte-dominated clear water lake in 1994. The regime-shift was believed to be triggered by the acute water shortage, when the water level in the lake declined to -1.23 m below sea level, in the same year. This reduced water level allowed sufficient light penetration in the water column for aquatic vegetation to grow (Figure 1.2).

a) September 2013 b) October 2013 c) September 2015

d) September 2016 e) September 2016

Figure 1.2. In-field images of the SAV in the south basin. The September and October 2013 images of the SAV at the lake bottom provided by Japan Water Agency ((a) and (b)), September 2015 and 2016 images were taken during field survey by LBERI (c) and September 2016 images were taken during the *in-situ* measurement ((d) and (e)).

Consequently, submerged macrophyte recovered in the lake (particularly in the southern basin), with increased transparency and improved water quality [53,54]. However, the areal coverage of submerged macrophyte in the shallow southern basin (surface area 52 km^2), increased dramatically from 6 km^2 in 1994 to 50 km^2 in 2014, covering more than 90% of the basin area [17,55]. The dense community of submerged macrophyte lowered the oxygen saturation to less than 50% just above the lake bottom and adversely impacted the navigation and fisheries in recent years [56,57]. In Lake Biwa, the dispersal and biomass of native SAV species, *Vallisneria Asiatica* var. Biwaensis reduced drastically, followed by the rapid invasion by 141 alien species where alien submerged vegetation species reported are *Egeria Densa*, *Elodea Nuttallii,* and *Myriophyllum Brasiliense*, in past few decades [54]. Furthermore, large masses of submerged macrophyte detach from the bottom and drift up to the lake shore every year, affects the landscape value of the lake. To avert the nuisance overgrowth of SAV, local authorities and the Shiga prefectural government invested sizable effort and expense in harvesting the submerged macrophyte, as an effective macrophyte control effort. Changes in SAV percent cover, stand height and biomass are monitored annually using the traditional site-specific diver survey collecting the sample from a grid size of 50 * 50 cm, which cannot accurately account for the spatial variation in the basin. On the other hand, some researchers have reported success in detecting and qualitatively characterizing macrophyte using Hydroacoustic for over two decades, fully quantitative assessment has been hampered by hardware and software limitations. Till date, the basin wise assessment of the spatial extent of SAV cover and biomass is limited, primarily because the *in-situ* survey of large lakes like Lake Biwa is infeasible and cost-prohibitive [17,54,55,58].

1.3 Research Area Description

Lake Biwa (35⁰ 20' 59.48'' N and 136⁰ 10' 33.16'' E) is located in the central Honshu Island, southwest of Japan. It is 670 km² in area and has total catchment area of 3838 km² (Figure 1.3).

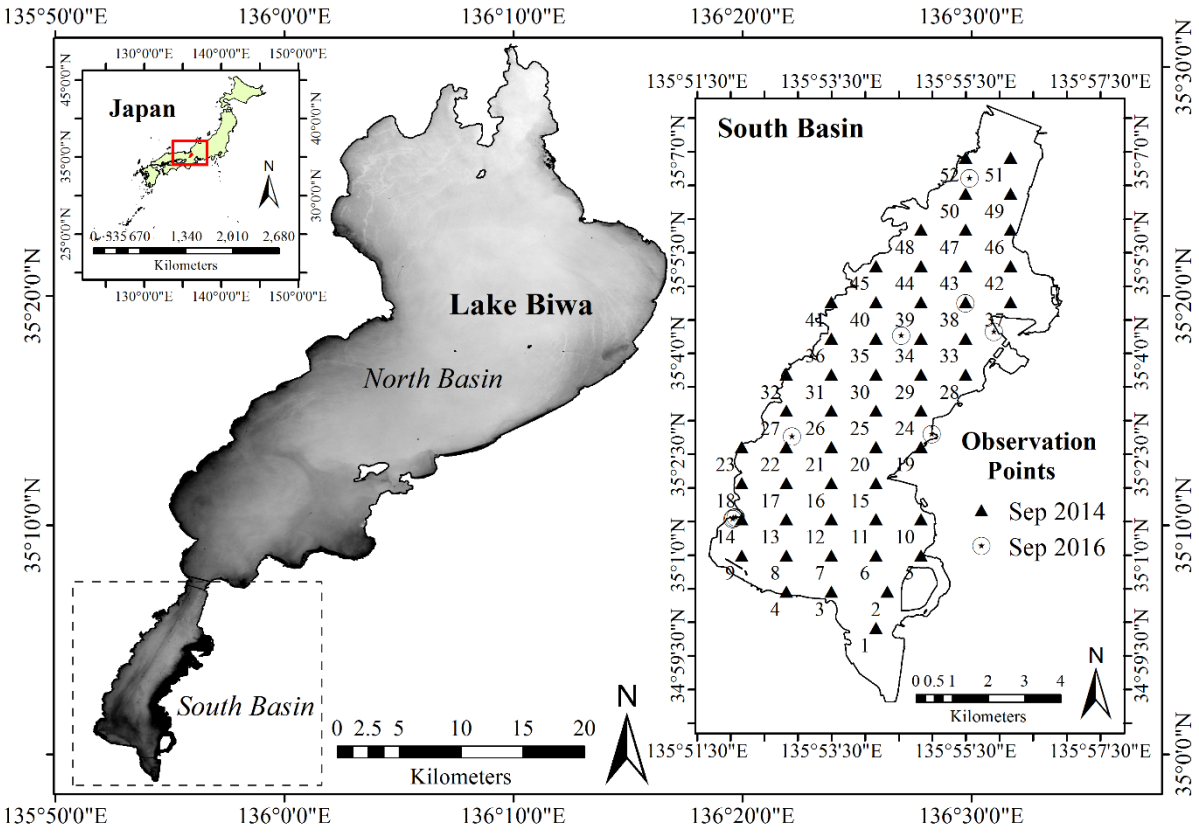

Figure 1.3. Geographical location of Lake Biwa and its southern basin with water quality and SAV observation points.

The lake comprises of two contrasting basins, the north basin which is mesotrophic and deep (mean depth 44 m) and the south basin eutrophic and shallow (mean depth 3.5 m). The area ratio of two basins is 11:1. The water level in the Lake Biwa is controlled by the Seta River Weir located in the south basin. The standard water level in the lake is 85 m above sea level. Water level does not change significantly in the lake (except in 1994 (-1.2 m)). For SAV growth period the maximum and minimum water level observed were +0.3 m to -0.5 m (i.e., from the standard water level), respectively [17,53]. Several small rivers drain into Lake Biwa which has the Seta River as the only natural outlet in the south basin. The lake serves as an important water source for agriculture, industries, and fishery while also provide drinking water for over 14 million people in the Kansai region. In 1993, Lake Biwa was designated as a registered wetland under the Ramsar Convention. The land use change in the catchment attributed

mainly to the ongoing urbanization and change in industrial structure, where most of the city area is located in the southern basin contributing to eutrophication. In addition, the southern basin is also surrounded by the farmland, mainly comprising paddy fields. To curb the eutrophication and to restore the lake ecosystem, Shiga prefectural government enacted the Ordinance on Prevention of Eutrophication of Lake Biwa in 1979 followed by the formulation of the Water Quality Conservation Plan in 1986. As a result, the overall water quality of the lake improved significantly consequently the growth of submerged macrophyte in increased notably in the south basin [53].

Recently, the total submerged macrophyte biomass in the south basin doubled up from 9623-ton dry weight (2007) to 18173-ton dry weight (2014), approximately. According to Haga and Ishikawa (2016), the dominant SAV species in the south basin are *Potamogeton Maackianus*, *Elodea Nuttallii*, *Hydrilla Verticillata* and *Egeria Densa* [55]. As of September 2014 (the peak growth period of SAV), the average concentration of chlorophyll-a (Chl-a), suspended sediment (SS) and dissolved organic carbon (DOC) measured in the south basin is 10.9 μg/L, 1.1 mg/L, and 1.5 mg/L, respectively.

1.3.1 Research Objectives

The main aim of this dissertation was to develop a satellite-based (i.e., Landsat-8 OLI) approach and to identify and quantify the SAV in the shallow eutrophic south basin of Lake Biwa, for the peak growth period of SAV (i.e., mainly in September), from 2013 to 2016. The main aim is further into three objectives they are:

1 To evaluate the influence of optically active components (OAC) on the reflectance of SAV. And to determine the detection depth of SAV in a eutrophic basin of the large lake.
2 To estimate and map the concentration of the dominant optically active component (i.e., mainly chlorophyll) in the lakes basin using satellite remote sensing approach. And to generate satellite-derived water clarity map of the basin.
3 To quantify the coverage area and biomass of SAV using multispectral satellite remote sensing (Landsat-8 OLI) for the eutrophic lake (2013-2016).

1.3.2 Research Scope

This dissertation involves the both laboratory experiment, field-survey, and model simulation in order to fulfill the purpose of this research. The detailed scope of the study are:

1. To simulate the SAV species reflectance (*Potamogeton Maackianus* and *Egeria Densa*) and to determine the influence of the OAC on SAV signal at the changing concentration and water depth. And to identify the dominant OAC (using Bio-Optical Model).
2. To determine the SAV canopy depth and estimate the detection depth of species using the satellite image and Bio-Optical Model.
3. To map the dominant OAC (i.e., chlorophyll-a) using the Landsat-8 satellite image (2013-2016)and determine the concentration of chlorophyll in the south basin of Lake Biwa (using ENVI 5.2, ArcMap 10.3.1 and 6S radiative transfer code, R statistical software).
4. To develop the satellite-based water transparency retrieval algorithm and map the water clarity of the basin (2013-2016).
5. To isolate the SAV pixels from the turbid water pixels (from selected endmembers) in the eutrophic lake using the binary decision tree classification approach (i.e., spectral mixture analysis, spectral angle mapper, minimum noise fraction transformation in ENVI 5.2).
6. To determine the detected SAV coverage area for the peak growth period (i.e., mainly in September or October (2013 to 2016)).
7. To develop a new satellite-based SAV biomass estimation approach (i.e., It involves the development of new spectral decomposition algorithm taking into account the bottom albedo for the shallow eutrophic lake).
8. To determine the change in SAV distribution (i.e., coverage area) and the SAV biomass for the peak growth period of SAV from 2013 to 2016.

1.4 Methodological Framework

The research methodology developed based on the objectives mentioned above (Figure 1.4)

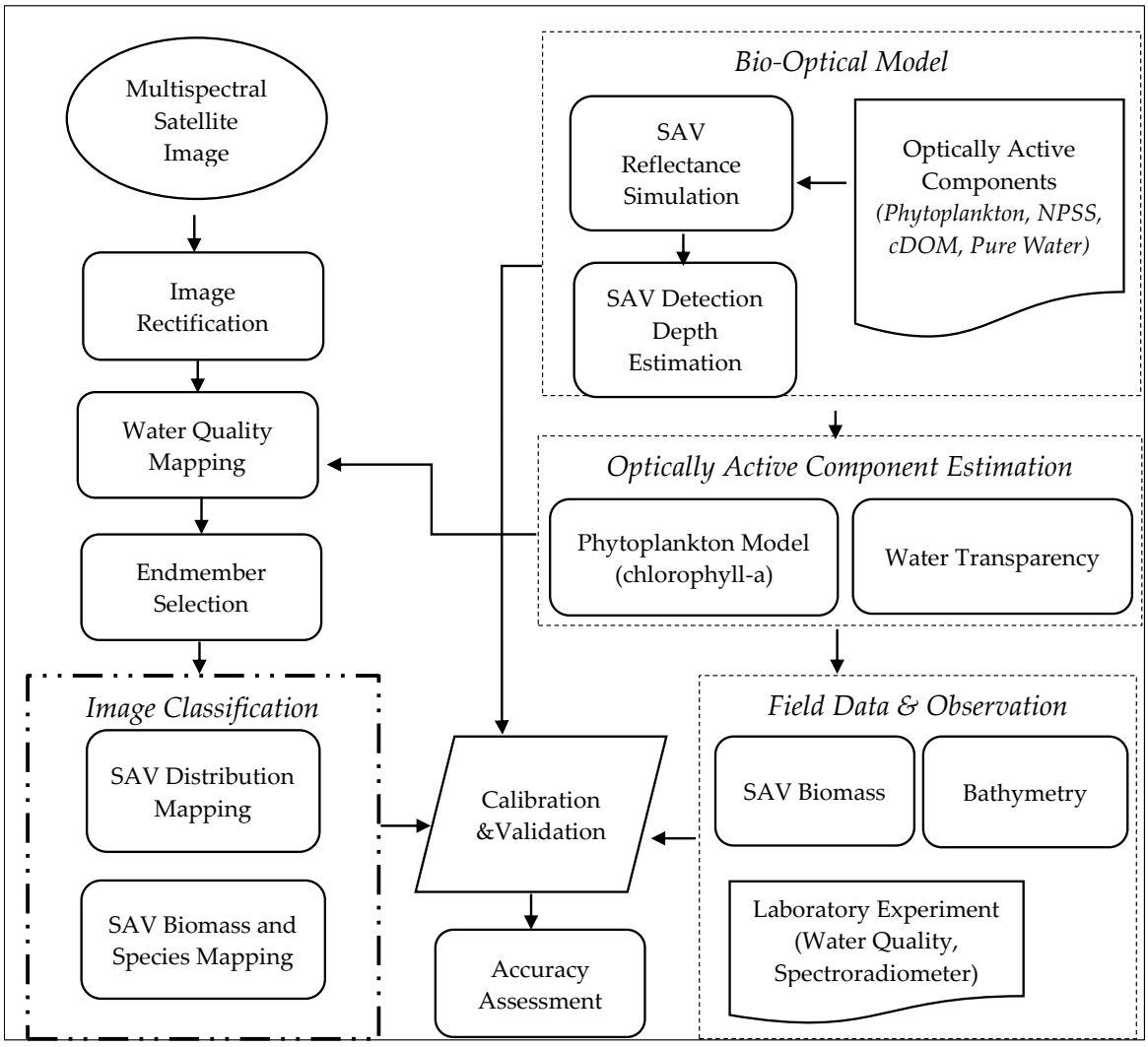

Figure 1.4 Schematic of the Research Methodology.

1.5 Research Outline

This dissertation includes six chapters. The description of the chapters is given below.

***Chapter1*:** Gives the research background of the present study, which also highlights the main purpose of the study including the research objectives, study area description, and research approach.

***Chapter 2*:** A detailed literature review related to the limnology and the remote sensing is presented in this chapter. Review of the past research work conducted on the SAV, giving the details of the methods used in the monitoring of SAV. Furthermore, the chapter provides

the detail description of SAV species, optical remote sensing of water, SAV mapping and monitoring requirements using remote sensing approach.

Chapter 3: This chapter deals with the SAV detection depth estimation using the satellite image (i.e., Landsat-8 in this study). The detection depth of two SAV species *Potamogeton Maackianus* (native species) and *Egeria Densa* (alien species) was estimated using the Bio-Optical model and *in-situ* measurements. The Bio-Optical model was used to simulate the SAV species reflectance at four different scenarios (i.e., clear water, chlorophyll dominated water, non-phytoplankton (NPSS) dominated water, and colored dissolved organic matter (cDOM)). The dominant optically active components (OAC) influencing the SAV detection in the water was identified. In addition, the Normalized Difference Vegetation Index (NDVI) was estimated for simulated scenarios. The SAV species detection was then determined using the different threshold values of NDVI (0.0, mean, minimum). The phytoplankton and NPSS were identified as the dominant OAC. The detection depth of SAV obtained in this study is 0.1 m to 1 m, whereas, the detection depth reduces to < 0.3 m when chlorophyll > 20μg/L and < 0.2 m when NPSS > 10 mg/L.

Chapter 4: Deals with the mapping of the optically active components using the satellite remote sensing approach. Initially, this study shows the water quality analysis, laboratory experiment, and *in-situ* measurement data. Later part of the study shows the development of new Spectral Decomposition Algorithm for the estimation of the OAC (i.e., chlorophyll-a in this study) concentration in the shallow eutrophic lake. The Landsat-8 band combination of blue (band-2), green (band-3), red (band-4) and NIR (band-5) gave the best result for chlorophyll-a estimation model (R^2 = 0.83) with an overall RMSE of 6.15 μg/L (2014; 29 locations) and 6.28 μg/L (2016 surveyed location) gives an R^2 = 0.78. Result also shows the increased chlorophyll concentration (> 90 μg/L) in the 2013 and 2016, then 2014 and 2015 (< 80 μg/L). Furthermore, a satellite-based water transparency retrieval algorithm was developed to estimate the water clarity (i.e., optical depth) in the lake. Developed water transparency retrieval algorithm gave the best result with Landsat-8 depth invariant green and red band (R^2 = 0.77) and an overall RMSE of 0.38 m. Maximum water transparency obtained is in 2014 (6.4 m) with chlorophyll-a concentration, followed by 2016 (5.5 m), 2015 (5.1 m) and 2013 (3.7 m).

Chapter 5: Shows the mapping of the SAV distribution and its biomass using the satellite remote sensing (i.e., Landsat-8 image) for SAV growth period in September-October (2013-2016). The chapter gives the details about the classification techniques used to isolate the SAV pixels from the other turbid water pixel. The techniques involved in the SAV classification are the Spectral Mixture Analysis (SMA), Spectral Angle Mapper (SAM), Minimum Noise Fraction (MNF) transformation, Binary Decision Tree along with NIR, SWIR and NDVI bands. The Submerged Aquatic Vegetation (SAV) classified in the eutrophic lake with an overall accuracy of 84.6% and the user accuracy of 74.6% using a Landsat-8 image. SAV Classification accuracy achieved for other years are: 70.5% (October 2013), 76.4% (September 2015) and 82.3% (September 2016). In addition, the developed new Spectral Decomposition algorithm was used to estimate the SAV biomass for the classified pixels. The biomass estimation model gave the R^2 of 0.79 for the SAV classified area with an overall RMSE 0.26 kg DW m^{-2} (2014) and 0.013 kg DW m^{-2} (2016 surveyed locations). The estimated SAV biomass for detected pixels is 3390 T (2013), 3919 T (2014), 5242 T (2015), and 4550 T (2016). The study shows that the developed SAV biomass estimation approach is successfully applied for the eutrophic shallow basin for SAV biomass estimation and could be tested on the other shallow lake using the satellite image.

Chapter 6: Gives the important findings of the study and highlights the particular conclusion drawn from the obtained results in Chapter 3, Chapter4 and Chapter 5. Furthermore, the future recommendations are also given in this chapter.

References

1. Carpenter, S. R.; Lodge, D. M. Effects of submersed macrophytes on ecosystem processes. *Aquatic Botany* **1986**, *26*, 341–370.
2. Hestir, E. L.; Khanna, S.; Andrew, M. E.; Santos, M. J.; Viers, J. H.; Greenberg, J. A.; Rajapakse, S. S.; Ustin, S. L. Identification of invasive vegetation using hyperspectral remote sensing in the California Delta ecosystem. *Remote Sensing of Environment* **2008**, *112*, 4034–4047.
3. Luo, J.; Li, X.; Ma, R.; Li, F.; Duan, H.; Hu, W.; Qin, B.; Huang, W. Applying remote sensing techniques to monitoring seasonal and interannual changes of aquatic vegetation in Taihu Lake, China. *Ecological Indicators* **2016**, *60*, 503–513.
4. Scheffer, M.; Jeppesen, E. Alternative stables states. In *The Structuring Role of Submerged Macrophytes in Lakes*; Erik Jeppesen, Martin Søndergaard, Morten Søndergaard, K. C., Ed.; Springer New York, 1998; pp. 397–406.
5. Takamura, N.; Kadono, Y.; Fukushima, M.; Nakagawa, M.; Kim, B. Effects of aquatic macrophytes on water quality and phytoplankton communities in shallow lakes. *Ecological Research* **2003**, *18*, 381–395.
6. Van Donk, E.; Van de Bund, W. J. Impact of submerged macrophytes including charophytes on phyto- and zooplankton communities: Allelopathy versus other mechanisms. *Aquatic Botany* **2002**, *72*, 261–274.
7. Pan, G.; Yang, B.; Wang, D.; Chen, H.; Tian, B. hui; Zhang, M. lan; Yuan, X. zheng; Chen, J. In-lake algal bloom removal and submerged vegetation restoration using modified local soils. *Ecological Engineering* **2011**, *37*, 302–308.
8. Zhang, S. Y.; Liu, A. F.; Ma, J. M.; Zhou, Q. H.; Xu, D.; Cheng, S. P.; Zhao, Q.; Wu, Z. Bin Changes in physicochemical and biological factors during regime shifts in a restoration demonstration of macrophytes in a small hypereutrophic Chinese lake. *Ecological Engineering* **2010**, *36*, 1611–1619.
9. Gillard, M.; Thi??baut, G.; Deleu, C.; Leroy, B. Present and future distribution of three aquatic plants taxa across the world: decrease in native and increase in invasive ranges. *Biological Invasions* **2017**, 1–12.
10. Santos, M. J.; Anderson, L. W.; Ustin, S. L. Effects of invasive species on plant communities: An example using submersed aquatic plants at the regional scale. *Biological Invasions* **2011**, *13*, 443–457.
11. Lovell, S. J.; Stone, S. F.; Fernandez, L. The economic impacts of aquatic invasive species: A review of the literature. *Agricultural and Resource Economics Review* **2006**, *35*, 195–208.
12. Lowe, S.; Browne, M.; Boudjelas, S.; De Poorter, M. 100 of the world's worst invasive alien species. A selection from the Global Invasive Species Database. *The Invasive Species Specialist Group (ISSG) a specialist group of the Species Survival Commission (SSC) of the World Conservation Union (IUCN)* **2000**, 12.
13. Kadono, Y. Alien Aquatic Plants Naturalized in Japan: History and Present Status. *Global Environmental Research ©2004 AIRIES* **2004**, *8*, 163–169.
14. Brooks, C.; Grimm, A.; Shuchman, R.; Sayers, M.; Jessee, N. A satellite-based multi-temporal assessment of the extent of nuisance Cladophora and related submerged aquatic vegetation for the Laurentian Great Lakes. *Remote Sensing of Environment* **2015**, *157*, 58–71.
15. Nelson, S. A. C.; Cheruvelil, K. S.; Soranno, P. A. Satellite remote sensing of freshwater macrophytes and the influence of water clarity. *Aquatic Botany* **2006**, *85*, 289–298.
16. Zhang, Y.; Liu, X.; Qin, B.; Shi, K.; Deng, J.; Zhou, Y. Aquatic vegetation in response to increased eutrophication and degraded light climate in Eastern Lake Taihu: Implications for lake ecological restoration. *Scientific Reports* **2016**, *6*, 23867.
17. Hamabata, E.; Kobayashi, Y. Present status of submerged macrophyte growth in Lake Biwa: Recent recovery following a summer decline in the water level. *Lakes and Reservoirs: Research and Management* **2002**, *7*, 331–338.
18. Pinnel, N. A method for mapping submerged macrophytes in lakes using hyperspectral remote sensing, Technical University of Munich, 2007.

19. Güttler, F. N.; Niculescu, S.; Gohin, F. Turbidity retrieval and monitoring of Danube Delta waters using multi-sensor optical remote sensing data: An integrated view from the delta plain lakes to the western-northwestern Black Sea coastal zone. *Remote Sensing of Environment* **2013**, *132*, 86–101.
20. Pacheco, A.; Horta, J.; Loureiro, C.; Ferreira Retrieval of nearshore bathymetry from Landsat 8 images: A tool for coastal monitoring in shallow waters. *Remote Sensing of Environment* **2015**, *159*, 102–116.
21. Shuchman, R. A.; Sayers, M. J.; Brooks, C. N. Mapping and monitoring the extent of submerged aquatic vegetation in the laurentian great lakes with multi-scale satellite remote sensing. *Journal of Great Lakes Research* **2013**, *39*, 78–89.
22. Silva, T. S. F.; Costa, M. P. F.; Melack, J. M.; Novo, E. M. L. M. Remote sensing of aquatic vegetation: Theory and applications. *Environmental Monitoring and Assessment* **2008**, *140*, 131–145.
23. Williams, D.; Rybicki, N.; Lombana, A.; O'Brien, T.; Gomez, R. Preliminary investigation of submarged aquatic vegetation mapping usingyperspectral remote sensing. *Environmental Monitoring and Assessment* **2003**, *81*, 383–392.
24. Underwood, E.; Ustin, S.; DiPietro, D. Mapping nonnative plants using hyperspectral imagery. *Remote Sensing of Environment* **2003**, *86*, 150–161.
25. Ackleson, S. G.; Klemas, V. Remote sensing of submerged aquatic vegetation in lower chesapeake bay: A comparison of Landsat MSS to TM imagery. *Remote Sensing of Environment* **1987**, *22*, 235–248.
26. Mobley, C. D. Radiative Transfer in the Ocean. *Encyclopedia of Ocean Sciences: Second Edition* **2008**, 619–628.
27. Reinart, A.; Paavel, B.; Tuvikene, L. Effect of coloured dissolved organic matter on the attenuation of photosynthetically active radiation in Lake Peipsi. *Proc. Estonian Acad. Sci. Biol. Ecol.* **2004**, *53*, 88–105.
28. Sogandares, F. M.; Fry, E. S. Absorption spectrum (340-640 nm) of pure water. *Applied Optics* **1997**, *36*, 8699–8709.
29. Sváb, E.; Tyler, A. N.; Preston, T.; Présing, M.; Balogh, K. V. Characterizing the spectral reflectance of algae in lake waters with high suspended sediment concentrations. *International Journal of Remote Sensing* **2005**, *26*, 919–928.
30. Zou, W.; Yuan, L.; Zhang, L. Analyzing the spectral response of submerged aquatic vegetation in a eutrophic lake, Shanghai, China. *Ecological Engineering* **2013**, *57*, 65–71.
31. Watanabe, F. S. Y.; Imai, N. N.; Alcântara, E. H.; Rotta, L. H. da S.; Utsumi, A. G. Signal Classification of Submerged Aquatic Vegetation Based on the Hemispherical-Conical Reflectance Factor Spectrum Shape in the Yellow and Reg Regions. *Remote Sensing* **2013**, *5*, 1856–1874.
32. Ma, R.; Duan, H.; Gu, X.; Zhang, S. Detecting Aquatic Vegetation Changes in Taihu Lake, China Using Multi-temporal Satellite Imagery. *Sensors* **2008**, *8*, 3988–4005.
33. Gholizadeh, M. H.; Melesse, A. M.; Reddi1, L. A Comprehensive Review on Water Quality Parameters Estimation Using Remote Sensing Techniques. *Sensors* **2016**, *16*, 1298.
34. Knight, J. F.; Voth, M. L. Application of MODIS Imagery for Intra-Annual Water Clarity Assessment of Minnesota Lakes. *Remote Sensing* **2012**, *4*, 2181–2198.
35. Oyama, Y.; Matsushita, B.; Fukushima, T. Distinguishing surface cyanobacterial blooms and aquatic macrophytes using Landsat / TM and ETM + shortwave infrared bands. *Remote Sensing of Environment* **2015**, *157*, 35–47.
36. Villa, P.; Mousivand, A.; Bresciani, M. Aquatic vegetation indices assessment through radiative transfer modeling and linear mixture simulation. *International Journal of Applied Earth Observation and Geoinformation* **2014**, *30*, 113–127.
37. Heege, T.; Bogner, a; Pinnel, N.; Bostater, C. R.; Santoleri, R. Mapping of submerged aquatic vegetation with a physically based process chain. *Remote Sensing of the Ocean and Sea Ice 2003* **2004**, *5233*, 43–50.
38. Jiang, H.; Zhao, D.; Cai, Y.; An, S. A Method for Application of Classification Tree Models to Map

Aquatic Vegetation Using Remotely Sensed Images from Different Sensors and Dates. *Sensors* **2012**, *12*, 12437–12454.
39. Hestir, E. L.; Greenberg, J. A.; Ustin, S. L. Classification trees for aquatic vegetation community prediction using imaging spectroscopy. *IEEE Journal of Selected Topics in Applied Earth Observations and Remote Sensing* **2012**, *5*, 1572–1584.
40. Karabulut, O.; Akyurek, Z.; Beklioglu, M. Identification and mapping of submerged plants in a shallow lake using quickbird satellite data. *Journal of Environmental Management* **2009**, *90*, 2138–2143.
41. Kruse, F. A.; Lefkoff, A. B.; Boardman, J. W.; Heidebrecht, K. B.; Shapiro, A. T.; Barloon, P. J.; Goetz, A. F. H. The spectral image processing system (SIPS)—interactive visualization and analysis of imaging spectrometer data. *Remote Sensing of Environment* **1993**, *44*, 145–163.
42. Goodwin, N.; Coops, N. C.; Stone, C. Assessing plantation canopy condition from airborne imagery using spectral mixture analysis and fractional abundances. *International Journal of Applied Earth Observation and Geoinformation* **2005**, *7*, 11–28.
43. Madsen, J. D. Biomass Techniques for Monitoring and Assessing Control of Aquatic Vegetation. *Lake and Reservoir Management* **1993**, *7*, 141–154.
44. Armstrong, R. A. Remote sensing of submerged vegetation canopies for biomass estimation. *International Journal of Remote Sensing* **1993**, *14*, 621–627.
45. Duarte, C. M.; Kalff, J. Biomass density and the relationship between submerged macrophyte biomass and plant growth form *. *Hydrobiologia* **1990**, *196*, 17–23.
46. Oyama, Y.; Matsushita, B.; Fukushima, T.; Matsushige, K.; Imai, A. Application of spectral decomposition algorithm for mapping water quality in a turbid lake (Lake Kasumigaura, Japan) from Landsat TM data. *ISPRS Journal of Photogrammetry and Remote Sensing* **2009**, *64*, 73–85.
47. Oyama, Y.; Matsushita, B.; Fukushima, T.; Nagai, T.; Imai, A. A new algorithm for estimating chlorophyll-a concentration from multi-spectral satellite data in case II waters: a simulation based on a controlled laboratory experiment. *International Journal of Remote Sensing* **2007**, *28*, 1437–1453.
48. Lee, Z.; Carder, K. L.; Mobley, C. D.; Steward, R. G.; Patch, J. S. Hyperspectral remote sensing for shallow waters. I. A semianalytical model. *Applied optics* **1998**, *37*, 6329–38.
49. Mumby, P. J.; Green, E. P.; Edwards, A. J.; Clark, C. D. Measurement of seagrass standing crop using satellite and digital airborne remote sensing. *Marine Ecology Progress Series* **1997**, *159*, 51–60.
50. Kirk, J. T. O. *Light and photosynthesis in aquatic ecosystems*; 3rd ed.; Cambridge University Press, 2011.
51. Lyzenga, D. R. Passive remote sensing techniques for mapping water depth and bottom features. *Applied Optics* **1978**, *17*, 379.
52. Yarrow, M.; Marín, V. H.; Finlayson, M.; Tironi, A.; Delgado, L. E.; Fischer, F. The ecology of egeria densa planchon (liliopsida: Alismatales): A wetland ecosystem engineer. *Revista Chilena de Historia Natural* **2009**, *82*, 299–313.
53. *Lake Biwa: Interactions between Nature and People*; Kawanabe, H.; Nishino, M.; Maehata, M., Eds.; Springer Dordrecht Heidelberg New York London, 2012.
54. Nishino, M. Biodiversity of Lake Biwa. In *Lake Biwa: Interactions between Nature and People*; Kawanabe, H.; Nishino, M.; Maehata, M., Eds.; 2012; pp. 1–732.
55. HAGA, H.; Ishikawa, K. Spatial Distribution of Submerged Macrophytes in the Southern Lake Biwa basin in the summer of 2014, in comparison with those in 2002, 2007 and 2012. *Japanese Journal of Limnology (Rikusuigaku Zasshi)* **2016**, *77*, 55–64.
56. Haga, H.; Ashiya, M.; Ohtsuka, T.; Matsuda, M.; Tuji, A.; Baba, K.; Numahata, S.; Yamane, T. Relationship between dissolved oxygen concentration of bottom water and macrophyte biomass in the southern basin of Lake Biwa, Japan. *Japanese Journal of Limnology* **2006**, *67*, 23–27.
57. Haga, H.; Ohtsuka, T.; Matsuda, M.; Ashiya, M. Echosounding observations of coverage, height, PVI, and biomass of submerged macrophytes in the southern basin of Lake Biwa, Japan. *Limnology* **2007**, *8*, 95–102.

58. Ishikawa, K.; Haga, H. Ecological Regime Shift in the South Basin of Lake Biwa : Focus on Algal Blooms and Submerged Macrophyte Overgrowth. In *UNESCO International Symposium on Scientific, Technological and Policy Innovations for Improved Water Quality Monitoring in the Post-2015 SDGs Framework*; Kyoto, Japan, 2015; pp. 1–3.
National Institute for Environmental Studies, Japan (https://www.nies.go.jp/biodiversity/invasive/index_en.html

Chapter 2

LITERATURE REVIEW

2.1 Limnologic Background

An inland water body surrounded by land (apart from rivers and streams that serves to feed or drain the lake), larger than ponds with quiet or slow moving water and not a part of ocean is defined as lakes. Currently, there is no internationally accepted definition of lakes that distinguish between lakes and pond. Thus a definition of lake frequently supported by the size of the water body, while limnologists describe the water body of size > 8 hectares, and others > 40 hectares as the lake [1]. The complex aquatic ecosystem of lakes is distinctively classified based on the differences in water chemistry, productivity, water depth, light availability, temperature and flow [2]. However, a typical lake comprises three distinct zones (Figure 2.1) as follows

a) *Littoral Zone* - extends from the near shore area to the depth where sunlight penetration is 1% of the incident surface light (i.e. photic zone) and provisions photosynthesis by the aquatic macrophyte. This zone has high biodiversity of flora and fauna with interactions often occurring between species.
b) *Limnetic (Pelagic Zone)* – zone farther from the shore and lies near to the water surface. Unlike littoral zone light does not penetrates to the bottom in this zone.
c) *Profundal Zone* – the deepest zone found below the light penetration level and relevant only in extremely deep lakes. Whereas the transition between littoral and profoundal zone is term as sublittoral zone which is the deepest zone for the plant growth.

The part of the lake which receives < 1% of the light is also called as the aphotic zone. The thermal stratification in lakes occurs due to the change in temperature result in the mixing of the dense cold and warm layers of water and thereby result in three distinct layers namely,

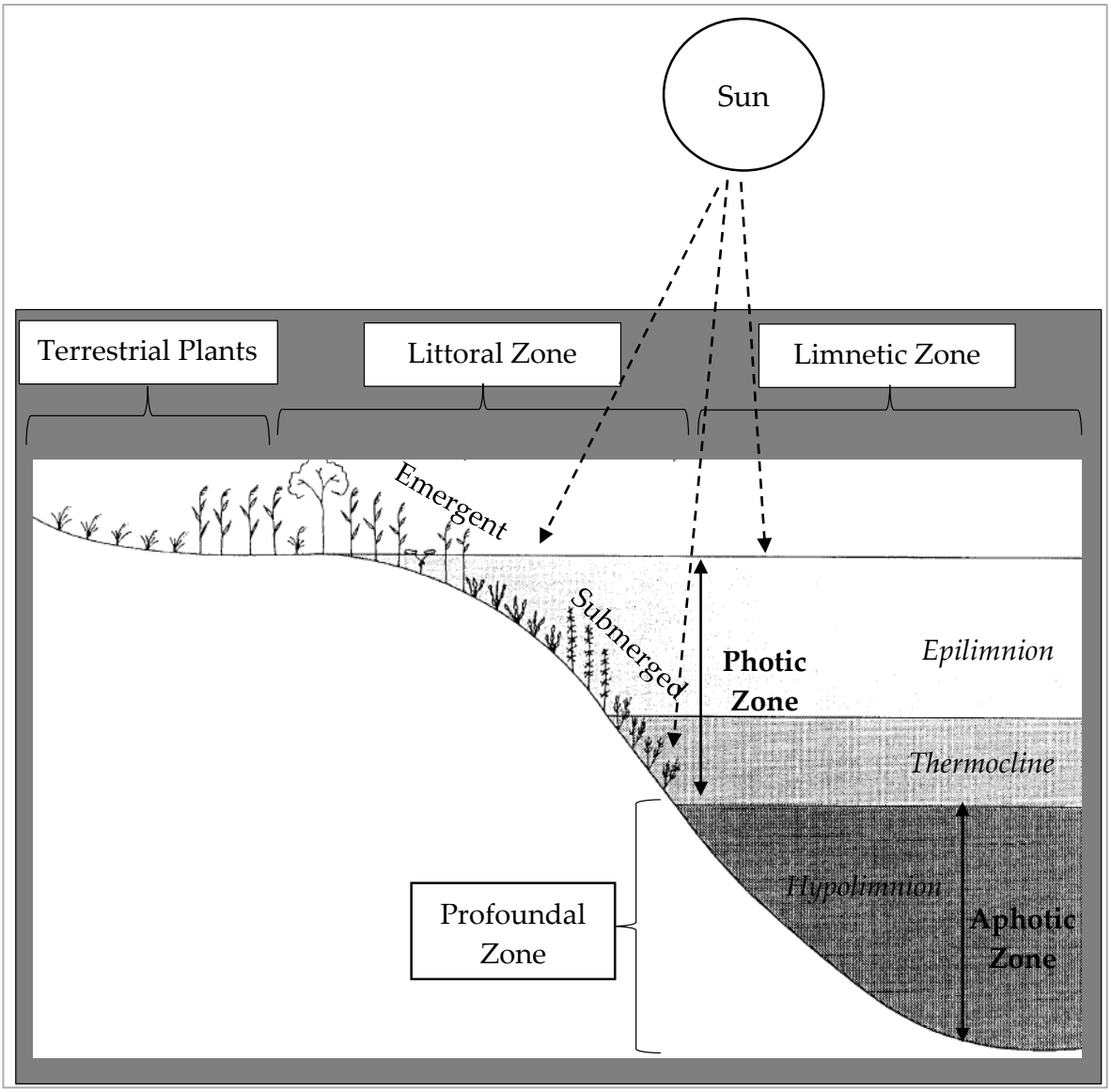

Figure 2.1. Schematic of Lake Zones and Ecosystem.

a) the Epilimnion - which is the top most warm layer with high dissolved oxygen; b) the Hypolimnion - the dense bottom layer in a thermally stratified lake, isolated from the wind mixing; and c) the Thermocline - is the transitional layer between Epilimnion and Hypolimnion where the temperature changes more quickly with water depth [2]. In the shallow lakes, usually defined as lakes where the sunlight reaches to the bottom corresponds to the water depth of < 3 – 4 m, the water mixing occurs more frequently in all season due to warming of the lake water. Whereas, in deep lakes the mixing usually occurs in spring and fall and the bottom of the lakes remain cold and dark as the sunlight cannot reach the bottom [3]. Thus shallow lakes have rich and productive ecosystem and are the valuable habitat for aquatic flora and fauna (http://www.dnr.state.mn.us/wildlife/shallowlakes/index.html).

The productivity and the nutrients richness mainly nitrogen and phosphorus, define the trophic state index (TSI) of the lake, which further classified the lake in to four main categories they are:

a) Oligotrophic – deep and very clear lakes with low primary productivity due to low nutrient content.
b) Mesotrophic – clear lakes with intermediate level of productivity and medium level of nutrients. Often have the submerged macrophyte beds.
c) Eutrophic – high nutrient content with high biological productivity usually have macrophyte-dominated clear water state or phytoplankton-dominated turbid water state.
d) Hypereutrophic – Excessive nutrient content followed by frequent nuisance algal blooms and low transparency. Low light penetration restricts the aquatic plants to grow in such lakes.

Generally, mesotrophic and eutrophic lakes can have abundant photosynthetic communities [2–5].

2.2 Submerged Aquatic Vegetation in Lakes

2.2.1. Ecological Function of Submerged Aquatic Vegetation in Lakes

Submerged aquatic vegetation are defined as plants that are usually rooted in the bottom soil of the lake with the vegetative parts predominantly submerged. They are commonly found in the shallow stagnant waters or sometimes in flowing water, with sufficient light for photosynthesis and nutrient availability to grow. Macrophytes grow between the shoreline and open waters dominated by plankton, and can potentially intercept or modify material flows from land to the pelagial zone. The life cycles of macrophytes are intermediate in length, much longer than those of plankton but generally shorter than those of fish. In temperate lakes, the production--decomposition cycle of macrophytes, and the associated biogeochemical fluxes, follow an annual cycle. Nutrient cycling by plankton has a turnover time of days, whereas the residence time of nutrients in fishes is many years. In general, the macrophyte nutrient pool, which is often quite large cycles at an intermediate rate at the interfaces of water with sediment, and terrestrial ecosystems with freshwater ecosystems.

In aquatic food web SAV are the primary producers and thus significantly influence the productivity and biogeochemical cycles in the freshwater ecosystems [2,6,7]. Figure 2.2, explains the ecological state in lake where the energy flow from the primary producers mainly macrophyte and algae to tertiary and secondary consumers (i.e. humans and large fish). The flow of both energy and nutrient normally begins with sunlight driven photosynthesis and respiration. Respiration (the oxidation of organic material) releases energy that was originally captured from sunlight through photosynthesis. Decomposers are sinks for plant and animal wastes, but also recycle nutrients for photosynthesis. Oxygen released during photosynthesis adds to oxygen supplied by the atmosphere. Cold water can hold more oxygen than warm water. During periods of stratification, the only potential source of oxygen to the deeper lake is photosynthesis[6].

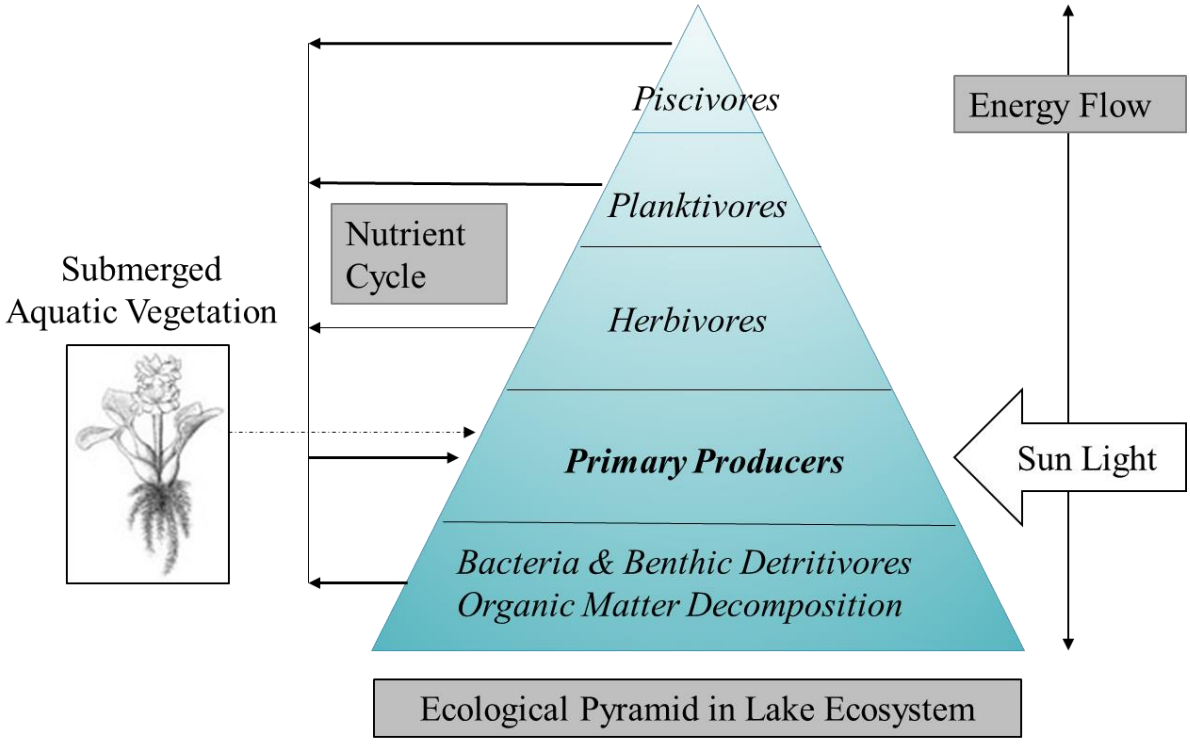

Figure 2.2. Ecological Pyramid in Lake Ecosystem.
(Source: Limnology-http://wgbis.ces.iisc.ernet.in/energy/monograph1/Limpage4.html)

2.3 Description of Submerged Aquatic Vegetation in the Lake

In shallow waters, the presence of SAV is possible to the maximum water depth of 6 m , while for deeper waters in a given water body, the SAV can grow to the water depth ranges

between 15 m to 20 m, approximately [8]. The characteristic of some of the rooted perennial plants found in the Lake Biwa are given below:

2.3.1 Tall Growing Submerged Plants

1. *Potamogeton Maackianus*: (Native SAV specie domianant in the Lake Biwa) a perennial plant, submerged in fresh water with has high stem density and a dense subterranean root stem. Growth height minimum 0.3 m to >3 m. Stems creeping at base or even to lower part, slender, terete to slightly compressed, richly branched; turions absent. Spikes usually few flowered, with only 2 or 3 whorls of contiguous or shortly distant opposite flowers; peduncles 1–4 cm. This plant is shade tolerance thas grown in deep waters by elongating its stem[9].

Potamogeton Maackianus

2. *Egeria Densa*: (Allien SAV specie dominant in the Lake Biwa) a rooted and submerged perennial plant with a growth height range 0.2 m to 5 m. The leaves and stems are generally bright green with the short internodes. Leaves which are minutely serrated and linear, are 1-3 cm long, up to 5 mm broad, and found in whorls of four to eight. The lowest leaves may be opposite or in whorls of 3; middle and upper leaves are in whorls of 4 to 8. Stems are erect, cylindrical, and grow until they reach the surface of the water where they form dense mats. Flowers have three petals which are white (18-25 mm) and float on or rise just above the water's surface. It can be distinguished from related species by the absence of turions (shoots from underground stems) and by the presence of showy white flowers that float on the water [9–12].

(https://nas.er.usgs.gov/queries/greatlakes/FactSheet.aspx?SpeciesID=10&Potential=Y&Type=2&HUCNumber=)

Egeria Densa

3. *Ceratophyllum Demersum*: A submerged plant which is sometimes rooted but mostly non-rooted and derive nutrients from the water column for its growth. Its stand height range between 1 m to 4.5 m. It is also called as hornwort and coontail because of its appearance. The serrated, forked leaves of coontail are arranged on the stems in whorls, with usually 5-12 leaves in each whorl. It can float free in the water column, and sometimes forms dense mats just below the surface. Because this plant gets nutrients from the water, it grows best where these nutrient levels are high. It can also tolerate a wide range of water hardness.

Ceratophyllum Demersum

(http://www.ecy.wa.gov/programs/wq/plants/native/coontail.html), (http://www.lakeandwetlandecosystems.com/plants/aquatic-plants-emergent-submergent-floating-leaf/submergent-plants/coontail-ceratophyllum-demersum/).

4. *Ellodea Nuttallii*: (Allien SAV specie was dominant in the Lake Biwa) an invasive perennial and submerged plant native to North America. It has long slender and branched stem. Its leaf mostly arranged in whorls of 3 and this plant often does not produce flowers. Leaves very finely toothed along the edges [13].

Ellodea Nuttallii

(http://www.ecy.wa.gov/programs/wq/plants/plantid2/descriptions/elocan.html)

5. *Myriophyllum Spicatum*: Also called as Eurasian watermilfoil, a submerged perennial plant with finely dissected feather-like leaves. Leaves are arranged in whorls of 4 (rarely 5) around the stem (usually red) at each node, and has 12 or more leaflet pairs. It is an extremely adaptable plant, able to tolerate and even thrive in a variety of environmental conditions. It grows in still to flowing waters, and rooted in water depths from 1 m to 10 m (regularly reaching the surface while growing in water 3 to 5 meters deep).

Myriophyllum Spicatum

(http://www.ecy.wa.gov/programs/wq/plants/weeds/aqua004.html).

6. *Hydrilla Verticillata*: (Native SAV specie dominant in the Lake Biwa) a submerged and perennial plant rooted to the depth of 6 m in water. *Hydrilla* adversely impacts aquatic ecosystems by forming dense canopies and shade out the native species. Its dense mats alter the water quality by raising pH, decreasing oxygen, and increasing temperature. This plant is highly adaptive to changing environmental conditions. For instance, it can grow in low-light areas. And absorbs carbon from the water more efficiently than other species. It is very tolerant to both standing and flowing water with as growth rate of an inch per day. This plant produce tubers that grow from the roots can persist, in a viable state, in the lake bottom for several years [13].

Hydrilla Verticillata

(http://msue.anr.msu.edu/news/hydrilla_verticillata_status_of_the_perfect_aquatic_weed_in_and_around_the).

2.3.2 Short Growing Submerged Plants

1. *Vallisneria Asiatica*: (Native and endemic SAV species in the Lake Biwa)) A submerged short growing rooted plant, native to China and Japan. Grows in the shallow water of 1 m to 2 m, usually in sandy or gravel bottom of the lakes. With spiral shaped twisted leaves of 10 – 80 cm long.

Vallisneria Asiatica

2. *Vallisneria Denseserrulata*: (Native and endemic SAV species in the Lake Biwa) A submerged short growing rooted plant, native to China and Japan. Leaf Margin with tooths and projection, similar to *Vallisneria Asiatica* but have rough leaves without twist, Leaf length 10-60 cm, and usually grow in shallow water depth of 1 m to 3 m. Usually grow near waterways. It stand height in water ranges between of 0.5 m to 1.3 m [13].

Vallisneria Densesrrulata

2.4 Monitoring and Mapping Requirements

The water column signal is of major concern when mapping submerged vegetation with remote sensing techniques. In contrast to the remote sensing of terrestrial vegetation, there is practically no signal returning from the water or the substrate at wavelengths beyond 680 nm, due to absorption by pure water ([5,14]). As a result of the physical properties of pure water and its optically active constituents, the remotely sensed optical signal is thus limited to the visible or optical part of the spectrum. With increasing depth of the water, the signal is rapidly attenuated and diminished as it is filtered through the water column. All remotely sensed measurements of reflected radiance over submersed species will be similarly influenced by water column effects, ultimately affecting the accuracy with which spectral classification of individual species can be performed [14]. Strong light attenuation gradients may be caused by a combination of water depth and also by factors that affect water color and clarity, such as dissolved organic matter, suspended matter and phytoplankton content.

The spectral differences between the benthic substrates and attenuation of light by a water column above the substrate, are the main factors limiting the ability of remote sensing techniques for monitoring or to detect the macrophyte species. Generally, submerged vegetation has low absolute reflectance, and increasing wavelengths normally results in decreased reflectance. In the turbid waters, where bottom albedo is not as high as that of carbonate sand and the diffuse attenuation in the water column is very large, the benthic albedo can contribute less than 10% of the total measured surface reflectance signature [15]. However, removing the effects of the water column and water depth may help in distinguishing the spectral signatures associated with benthic substrate. Within the spectral

signature lies the potential for interpretation of complex substrate composition from albedo [7,14–20].

2.5 Optical Remote Sensing and Water

The knowledge of distribution and abundance of submerged aquatic vegetation is essential in studying aquatic environments and is an important facet of water quality and resource management. Therefore, recent years have seen increasing interest and research in remote sensing of water quality of inland and coastal waters to map vegetation distributions, algal blooms, and substrate types, among other variables (Pinnel, 2007; Zhang *et al.*, 2016; Takamura *et al.*, 2003). The first assumption in mapping benthic vegetation using the satellite remote sensing is that of optically shallow water. If there is a measurable reflectance contribution from the plants or bottom substrate in the water column then the water is optically shallow.

Optically shallow waters are a special case in remote sensing of aquatic systems, without measurable bottom influence on the remotely sensed reflectance, the water is optically deep. As the spectrum of light emanating from the water surface in shallow waters contains information on the optical properties of the water constituents and the benthic substrate, the challenges for extracting substrate composition from surface reflectance lie in the removal of the water column reflectance and in the interpretation of the substrate into constituent areal coverage. The degree of the difficulty in these challenges depends, in part, on the instrumental spectral resolution, but more importantly on the spectral uniqueness and relative strengths of the signals arising from the water and the substrate [5,14,20,22–29].

2.6 Remote Sensing of Submerged Aquatic Vegetation

Light availability is predominantly an important factor determining the structure and distribution of macrophyte in the lake ecosystems. Absolute reflectance of submerged species (e.g. *Potamotegon pectinatus*) are generally low, often lower than reflectance from deeper or background open water areas. Absorption of light by plants are controlled by leaf biochemical properties (e.g. water, chlorophyll pigments) whereas the magnitude of reflectance of light from plant leaves depends mainly on leaf morphology (e.g. cell wall thickness, air space) , leaf surface quality and leaf internal structure. Whereas, the internal structure of leaves controls

the magnitude of reflectance and transmittance across the whole spectrum. Spatial and temporal variations in light nutrient availability, water temperature, and water movement are the other factors which influence growth and photosynthetic rate, and therefore also influence the spectral reflectance of macrophyte [2,29].

A number of techniques exist for mapping and monitoring the benthos of shallow waters. The Hydroacoustic Eco sounder, have been used successfully [30] to monitor the biomass of the SAV species in the lakes however not widely applicable due to the hardware and software limitation. Nevertheless, due to the large area coverage, ease of data acquisition and low cost associated with the medium resolution satellite image (e.g. Landsat TM/ETM/OLI, Spot, Terra/Aster) they are widely used for mapping SAV along with other limnologic parameters [31–33]. Several remote sensing techniques have been used for SAV spectral analysis and bottom mapping such as vegetation presence frequency, Vegetation Indices , linear mixture model, radiative transfer model, modular inversion program, submerged aquatic vegetation mapping algorithm, Water Color Simulator (WASI) and HYDROLITE [2,16,21,34–37].

References

1. Elton, C. S.; Miller, R. S. The Ecological Survey of Animal Communities: With a Practical System of Classifying Habitats by Structural Characters. *The Journal of Ecology* **1954**, *42*, 460.
2. Pinnel, N. A method for mapping submerged macrophytes in lakes using hyperspectral remote sensing, Technical University of Munich, 2007.
3. Kevern, N. R.; King, D. L.; Ring, R. Lake Classification Systems – Part 1 2011, 1–5.
4. Nishino, M. Biodiversity of Lake Biwa. In *Lake Biwa: Interactions between Nature and People*; Kawanabe, H.; Nishino, M.; Maehata, M., Eds.; 2012; pp. 1–732.
5. Kirk, J. T. O. *Light and photosynthesis in aquatic ecosystems*; 3rd ed.; Cambridge University Press, 2011.
6. Carpenter, S. R.; Lodge, D. M. Effects of submersed macrophytes on ecosystem processes. *Aquatic Botany* **1986**, *26*, 341–370.
7. Takamura, N.; Kadono, Y.; Fukushima, M.; Nakagawa, M.; Kim, B. Effects of aquatic macrophytes on water quality and phytoplankton communities in shallow lakes. *Ecological Research* **2003**, *18*, 381–395.
8. Watanabe, F. S. Y.; Imai, N. N.; Alcântara, E. H.; Rotta, L. H. da S.; Utsumi, A. G. Signal Classification of Submerged Aquatic Vegetation Based on the Hemispherical-Conical Reflectance Factor Spectrum Shape in the Yellow and Reg Regions. *Remote Sensing* **2013**, *5*, 1856–1874.
9. *Lake Biwa: Interactions between Nature and People*; Kawanabe, H.; Nishino, M.; Maehata, M., Eds.; Springer Dordrecht Heidelberg New York London, 2012.
10. Yarrow, M.; Marín, V. H.; Finlayson, M.; Tironi, A.; Delgado, L. E.; Fischer, F. The ecology of egeria densa planchon (liliopsida: Alismatales): A wetland ecosystem engineer. *Revista Chilena de Historia Natural* **2009**, *82*, 299–313.
11. Of, S.; Marion, I. N. L. QUIESCENCE , GROWTH AND SENESCENCE OF EGERIA DENSA Pheno-morphological determination Biomass determination. **1984**, *20*, 329–338.
12. Matthews, J.; Koopman, K. R.; Beringen, R.; Odé, B.; Pot, R.; Velde, G. Van Der; Valkenburg, J. L. C. H. Van; Leuven, R. S. E. W. Knowledge document for risk analysis of the non-native Brazilian waterweed (Egeria densa) in the Netherlands. **2014**.
13. Zehnsdorf, A.; Hussner, A.; Eismann, F.; Rönicke, H. Limnologica Management options of invasive Elodea nuttallii and Elodea canadensis. *Limnologica* **2015**, *51*, 110–117.
14. Mumby, P. J.; Green, E. P.; Edwards, A. J.; Clark, C. D. Measurement of seagrass standing crop using satellite and digital airborne remote sensing. *Marine Ecology Progress Series* **1997**, *159*, 51–60.
15. Silva, T. S. F.; Costa, M. P. F.; Melack, J. M.; Novo, E. M. L. M. Remote sensing of aquatic vegetation: Theory and applications. *Environmental Monitoring and Assessment* **2008**, *140*, 131–145.
16. Heege, T.; Bogner, a; Pinnel, N.; Bostater, C. R.; Santoleri, R. Mapping of submerged aquatic vegetation with a physically based process chain. *Remote Sensing of the Ocean and Sea Ice 2003* **2004**, *5233*, 43–50.
17. Nelson, S. A. C.; Cheruvelil, K. S.; Soranno, P. A. Satellite remote sensing of freshwater macrophytes and the influence of water clarity. *Aquatic Botany* **2006**, *85*, 289–298.
18. Zou, W.; Yuan, L.; Zhang, L. Analyzing the spectral response of submerged aquatic vegetation in a eutrophic lake, Shanghai, China. *Ecological Engineering* **2013**, *57*, 65–71.
19. Curcio, J. A.; Petty, C. C. The near infrared absorption spectrum of liquid water. *J. Opt. Sos. Am. A* **2011**, *41*, 302–304.
20. Doerffer, R.; Fischer, J. Concentrations of chlorophyll, suspended matter, and gelbstoff in case II waters derived from satellite coastal zone color scanner data with inverse modeling methods. *Journal of Geophysical Research* **1994**, *99*, 7457–7466.
21. Zhang, Y.; Liu, X.; Qin, B.; Shi, K.; Deng, J.; Zhou, Y. Aquatic vegetation in response to increased eutrophication and degraded light climate in Eastern Lake Taihu: Implications for lake ecological restoration. *Scientific Reports* **2016**, *6*, 23867.
22. Mobley, C. D. Radiative Transfer in the Ocean. *Encyclopedia of Ocean Sciences: Second Edition* **2008**, 619–628.

23. Babin, M. Variations in the light absorption coefficients of phytoplankton, nonalgal particles, and dissolved organic matter in coastal waters around Europe. *Journal of Geophysical Research* **2003**, *108*, 3211.
24. Dierssen, H. M.; Kudela, R. M.; Ryan, J. P.; Zimmerman, R. C. Red and black tides: Quantitative analysis of water-leaving radiance and perceived color for phytoplankton, colored dissolved organic matter, and suspended sediments. *Limnology and Oceanography* **2006**, *51*, 2646–2659.
25. Hale, G. M.; Querry, M. R. Optical Constants of Water in the 200-nm to 200-μm Wavelength Region. *Applied Optics* **1973**, *12*, 555.
26. Kou, L.; Labrie, D.; Chylek, P. Refractive indices of water and ice in the 0.65 to 2.5 μm spectral range. *Applied Optics* **1993**, *32*, 3531.
27. Gordon, H. R.; Morel, A. Y. *Remote Assessment of Ocean Color for Interpretation of Satellite Visible Imagery A Review*; Barber, R. T.; Mooers, C. N. K.; Bowman, M. J.; Zeitzschel, B., Eds.; Springer-Verlag New York Berlin Heidelberg Tokyo, 1983.
28. Reinart, A.; Paavel, B.; Tuvikene, L. Effect of coloured dissolved organic matter on the attenuation of photosynthetically active radiation in Lake Peipsi. *Proc. Estonian Acad. Sci. Biol. Ecol.* **2004**, *53*, 88–105.
29. Terrel, M. M.; Fukushima, T.; Matsushita, B.; Yoshimura, K.; Imai, A. Long-term light environment variability in Lake Biwa and Lake Kasumigaura, Japan: Modeling approach. *Limnology* **2012**, *13*, 237–252.
30. Haga, H.; Ohtsuka, T.; Matsuda, M.; Ashiya, M. Echosounding observations of coverage, height, PVI, and biomass of submerged macrophytes in the southern basin of Lake Biwa, Japan. *Limnology* **2007**, *8*, 95–102.
31. Brooks, C.; Grimm, A.; Shuchman, R.; Sayers, M.; Jessee, N. A satellite-based multi-temporal assessment of the extent of nuisance Cladophora and related submerged aquatic vegetation for the Laurentian Great Lakes. *Remote Sensing of Environment* **2015**, *157*, 58–71.
32. Güttler, F. N.; Niculescu, S.; Gohin, F. Turbidity retrieval and monitoring of Danube Delta waters using multi-sensor optical remote sensing data: An integrated view from the delta plain lakes to the western-northwestern Black Sea coastal zone. *Remote Sensing of Environment* **2013**, *132*, 86–101.
33. Pacheco, A.; Horta, J.; Loureiro, C.; Ferreira Retrieval of nearshore bathymetry from Landsat 8 images: A tool for coastal monitoring in shallow waters. *Remote Sensing of Environment* **2015**, *159*, 102–116.
34. Shuchman, R. A.; Sayers, M. J.; Brooks, C. N. Mapping and monitoring the extent of submerged aquatic vegetation in the laurentian great lakes with multi-scale satellite remote sensing. *Journal of Great Lakes Research* **2013**, *39*, 78–89.
35. Villa, P.; Mousivand, A.; Bresciani, M. Aquatic vegetation indices assessment through radiative transfer modeling and linear mixture simulation. *International Journal of Applied Earth Observation and Geoinformation* **2014**, *30*, 113–127.
36. Oyama, Y.; Matsushita, B.; Fukushima, T.; Matsushige, K.; Imai, A. Application of spectral decomposition algorithm for mapping water quality in a turbid lake (Lake Kasumigaura, Japan) from Landsat TM data. *ISPRS Journal of Photogrammetry and Remote Sensing* **2009**, *64*, 73–85.
37. Hestir, E. L.; Khanna, S.; Andrew, M. E.; Santos, M. J.; Viers, J. H.; Greenberg, J. A.; Rajapakse, S. S.; Ustin, S. L. Identification of invasive vegetation using hyperspectral remote sensing in the California Delta ecosystem. *Remote Sensing of Environment* **2008**, *112*, 4034–4047.
(http://www.dnr.state.mn.us/wildlife/shallowlakes/index.html)

Chapter 3

DETECTION DEPTH ESTIMATION OF SUBMERGED AQUATIC VEGETATION

3.1 Submerged Aquatic Vegetation Species

3.1.1 Introduction

The satellite remote sensing is a potential tool monitoring the growth and characteristics of SAV species in fresh waters [1,2]. The principles behind aquatic vegetation and terrestrial vegetation spectral characteristics are same. Nevertheless, aquatic plants are not easily detectable due to the complex aquatic environment than its terrestrial counterparts [3]. This is largely due to the interaction of optically active components in the water column which significantly attenuates the incoming and outgoing reflectance with increase in water depth.

The detectable depth of SAV depends strongly on the spectral characteristic of SAV species and the optically active components present in the water column. The reflectance in aquatic macrophyte species attributed to the pigment concentration (chlorophyll, carotenoids), leaf morphology and vegetation density [4]. The broad leaved plants with highly branched canopies have more reflective area thereby have higher reflectance (Williams et al. 2003). Whereas, the vertically oriented plant or reduced leaf area offers less surface area to interact with the electromagnetic radiation thereby have low reflectance [5]. Thus, each SAV species with different characteristic may have different reflectance spectra.

On the other hand, water strongly absorbs the electromagnetic radiation in longer wavelengths (after 700 nm), an important optically active component in underwater light attenuation [6]. Also, the light scattering and absorption properties of phytoplankton's, cDOM and non-phytoplankton suspended solids (NPSS), substantially attenuates the water-leaving reflectance [6,7]. Therefore, in turbid water, the diffuse attenuation in the water column is very large whereas the bottom albedo is very low, which only contributes <10% of the total measured water surface reflectance [8]. Consequently, the strength of SAV signal essentially depends on the distance between the water surface and plant canopy as well as the concentration of optically active components in the water column. In his paper, Visser *et al*.

(2015) stated that for optically shallow waters obtaining SAV bathymetry for scale <1 m is difficult due to complex interaction of electromagnetic waves with the constituents in water.

Due to the changing ecological and water quality condition as well as the complex interaction of the water column components in different lakes, the effect of optically active components on the reflectance spectra of underwater plants has not been extensively studied. Furthermore, the reflectance signal from each species change with the change in plant biomass, density and variation in morphological characteristics. For that reason, it is essential to understand the influence of water depth and concentration of optically active components on SAV spectra. In addition, estimating the species detection depth in optically clear and turbid lake condition will assist in selecting the appropriate method and the application of remote sensing approach for the monitoring of the submerged vegetation species in a lake.

3.1.2 Submerged Aquatic Vegetation Species in Lake Biwa

The submerged vegetation species found in south basin of Lake Biwa are divided into two group, they are:

1) Dominant SAV species (descending order) – *Potamogeton Maackianus, Hydrilla Verticillata, Egeria Densa, Elodea Nuttallii, Myriophyllum Spicatum* and *Ceratophyllum Demersum.*

2) Endemic SAV species – *Vallisneria Asiatica (Biwaenes)* and *Vallisneria Denseserullata* (Figure 3.1).

Whereas the invasive alien species dominant in the south basin are, *Egeria Densa, Elodea Nuttallii* and *Myriophyllum Spicatum,* and other dominant SAV species are native to Lake Biwa such as *Potamogeton Maackianus*. The total biomass (g dry wt/m^2) observed for the 52 stations, in September, 2014 shows the recovery of SAV in the south basin from past years. Among all the species, the total biomass of *Potamogeton Maackianus* was significantly higher (7072 g dry wt/m^2) followed by *Hydrilla Verticillata* (4664 g dry wt/m^2) and *Egeria Densa* (2301 g dry wt/m^2). Whereas, *Elodea Nuttallii* after reduced growth in past years recovered in 2014 with 3843 g dry wt/m^2). The dominant species accounts for the 96% of the total SAV biomass in 2014 [9,10]. The *in-situ* measurement (boat survey) conducted for total 8 location south basin in September 2016 shows the dominance of *Egeria Densa* with total biomass of 1353 g dry wt/ m^2 followed by *Hydrilla Verticillata* with 484 g dry wt/ m^2.

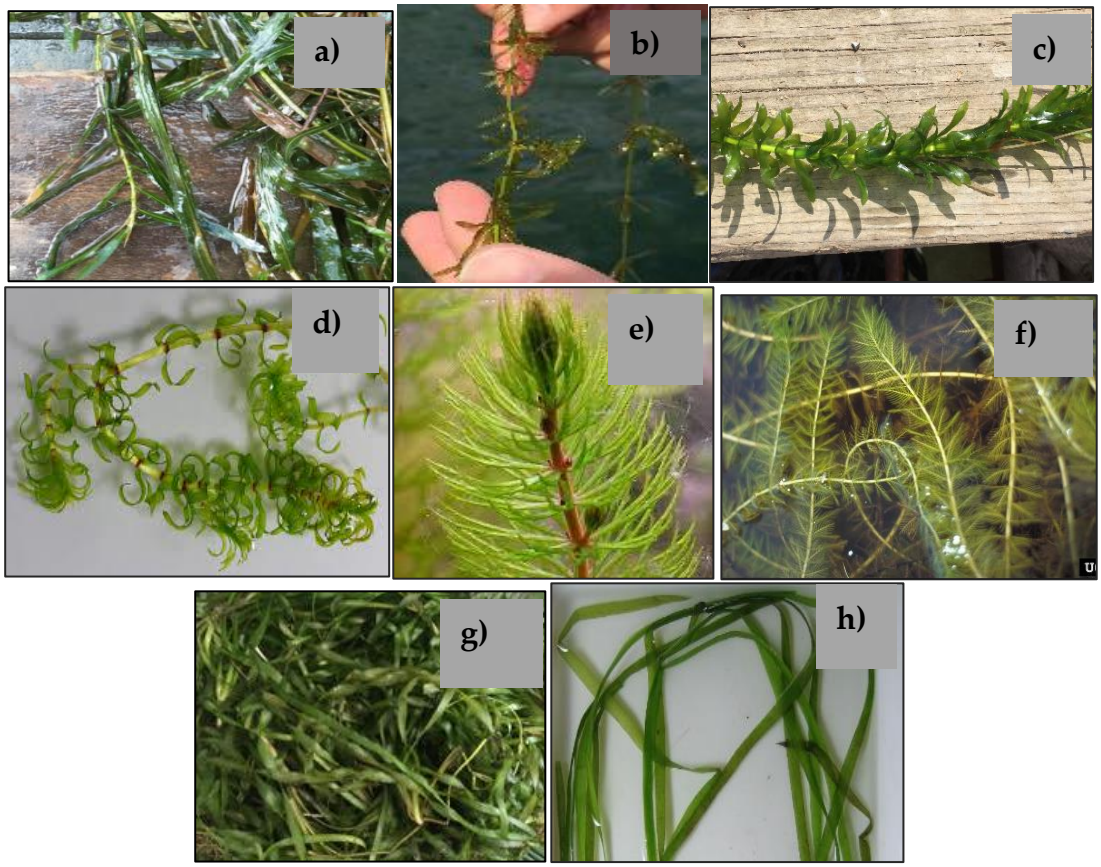

Figure 3.1 The SAV species found in the south basin of the Lake Biwa, a) *Potamogeton Maackianus* b) *Hydrilla Verticillata* c) *Egeria Densa* d) *Elodea Nuttallii* e) *Ceratophyllum Demersum* f) *Myriophyllum Spicatum* g) *Vellisneria Asiatica (Biwaenes)* and h) *Vellisneria Denseserullata*

The dominant species are mostly perennial in nature with high growth occur between May to October. Although, the stand height of these rooted SAV species can vary from < 1 m to 7 m in clear lake with sufficient light condition. However, in the south basin, the observed average stand height is in between < 1 m to 3.3 m, approximately [11,12].

Figure 3.2 and 3.3, shows the dominance of species at each observed station in the south basin for September 2014 and 2016. The large SAV biomass was observed in optically clean water with low concentration dominated by *Egeria Densa* and *Potamogeton Maackianus*. However, some species like *Hydrilla Verticillata* an invasive, aggressive plant and native species like *Vallisneria Asiatica* and *Vallisneria Denseserrulata* was most commonly seen proliferating in the turbid water of the basin.

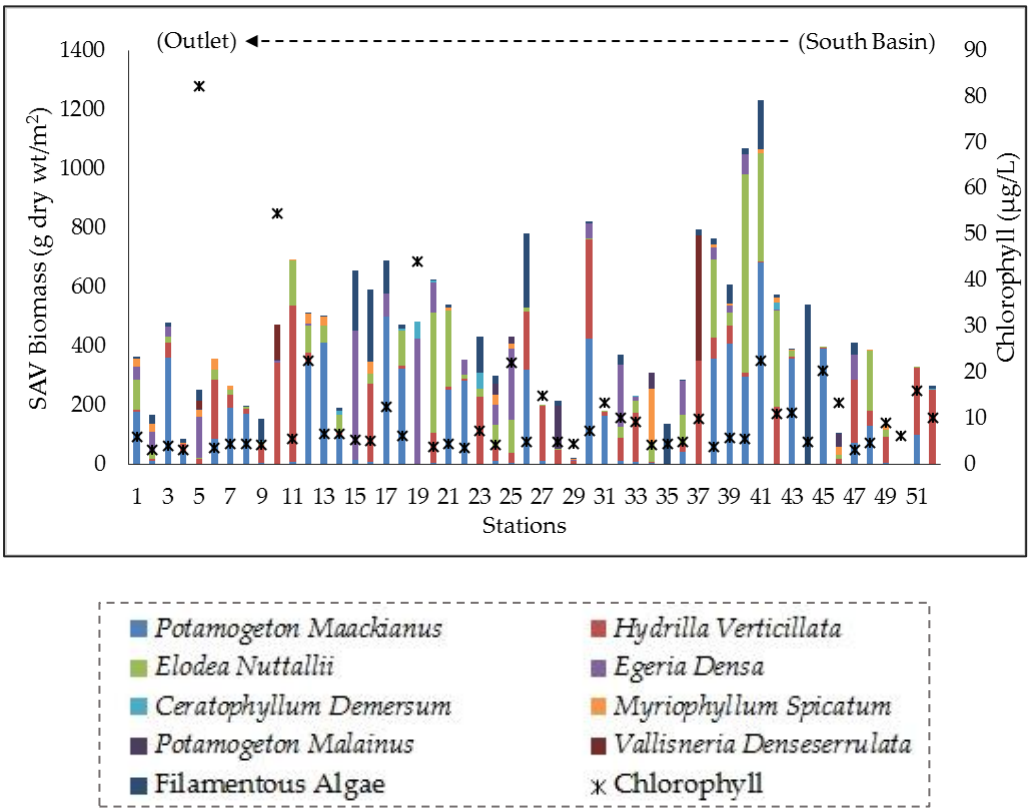

Figure 3.2 SAV biomass and chlorophyll concentration in the south basin of Lake Biwa (September 2014).

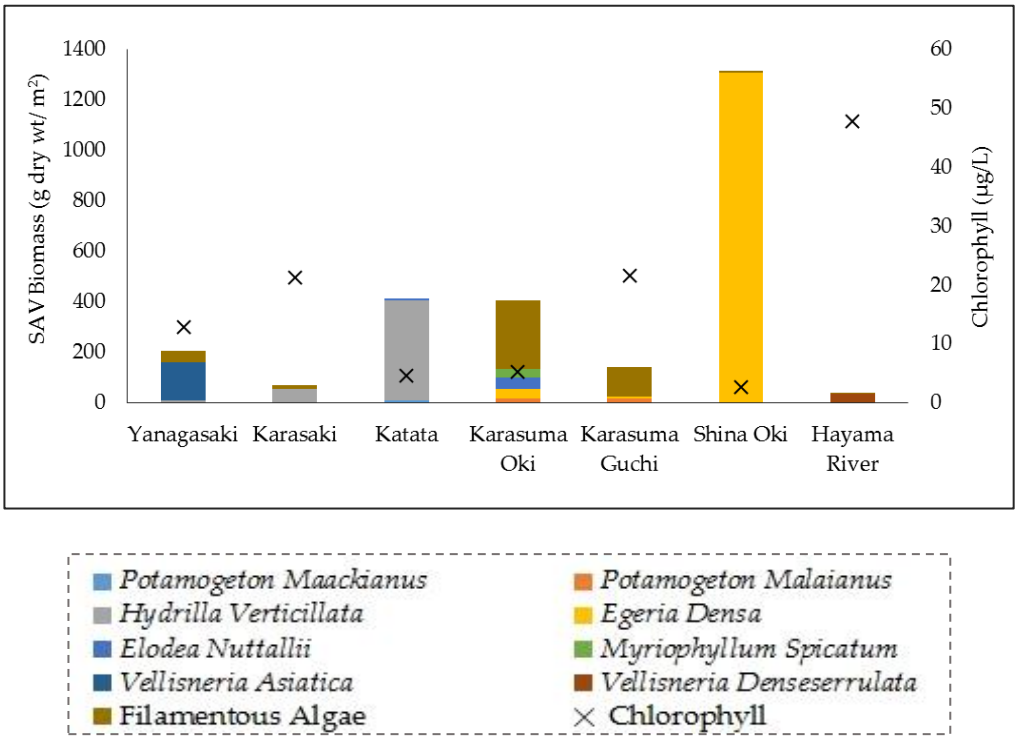

Figure 3.3 SAV biomass and chlorophyll concentration in the south basin of Lake Biwa (September 2016).

3.1.3 Methodology

Lake data collection and measurement – For this study, the two dominant SAV species in the south basin of the Lake Biwa were used for detection depth estimation, they are, a) *Egeria Densa* – the invasive alien SAV species and b) *Potamogeton Maackianus* – the naturally occurring SAV species. For September 2014, the lake data was provided by Lake Biwa Environmental Research Institute (LBERI), for 52 stations in the south basin (http://www.pref.shiga.lg.jp/). The collected and surveyed data involves the biomass of *Egeria Densa* and *Potamogeton Maackianus*, the concentration of phytoplankton, SS, DOC, and lake water depth and reflectance measurement.

On September 2, 2016, we surveyed total eight observation points located in the south basin, measuring the SAV biomass and stand height (m), Chlorophyll a, Total Suspended Solids (TSS in mg/L), DOC (mg/L) and water depth. At each location, 50*50 cm of quadrat was used (by diver survey) to measure the SAV coverage and species biomass. The position of each quadrat was recorded using a Global Position System (GPS) followed by the camera photographs of the sampled site. The fresh weight (g Wet Weight m^{-2}) of the SAV species from each quadrat was measured in the LBERI lab immediately after sampling. Afterward, the sample was dried at 60 °C for 48 hours in a drying oven, to determine the dry weight (g DW m-2) [13]. The observed data for September 2014 and 2016 is shown in Table 3.1.

Table 3.1 *In-situ* measured data of September 2016.

Locations	Water Depth (m)	Temperature (°C)	TP (mg/L)	Chlorophyll (µg/L)	TSS (mg/L)	DOC (mg/L)	SAV Biomass (g DW m^{-2})
			South Basin				
Shinaoki	4.5	27.64	0.03	2.64	5.00	1.30	2.74
Katata	5.1	28.53	0.03	5.00	8.50	1.50	1.66
Karasumaoki	1.9	28.31	0.04	13.37	11.00	1.51	13.37
Karasumaguchi	1.7	27.37	0.05	29.75	15.79	1.67	24.89
Karasaki	4.2	29.66	0.04	21.37	10.50	1.35	4.84
Yanagasaki	1.7	34.43	0.04	12.92	9.47	2.00	10.08
Hayama River	0.9	28.02	0.04	47.82	18.00	2.13	28.47

We measured the spectral radiance at each observation point using the FieldSpecTM Pro JR Field Portable Spectroradiometer with a sampling interval of 1.4 nm between 350-1000 nm and 2 nm between 1000-2500 nm. The measured on-site radiance was converted to reflectance using the white panel radiance (i.e., know 100 % radiance).The measurements were made

from a nadir position where the sensor head (i.e., 5° field of view) mounted on a fixed iron rod (extends to 1.5 m away from the boat) located 1 m above the water surface. Also, we kept the sun-sensor azimuth at 90° and the viewing zenith angle at 45° which corresponds to the minimum of sun-glint [14] whereas, simultaneously avoiding the shadows and reflections from the sampling platform. At all the locations, the reflectance measurements were taken while keeping the boat stationary and visually confirming the minimum disturbances in the water by the boat. The inappropriate measurements due to any disturbances (e.g. disturbances by the boat, viewing geometry) were removed from the data set. At each site, 5-7 measurement was taken between 10:00 and 15:00 local time under clear weather conditions. The observation points were selected based on the distribution of homogeneous patches of SAV species and their abundance (referring September 2014 SAV biomass data and LBERI expert suggestions). During sampling, we found that SAV sample from each location contains the mixture of more than one species. Therefore, we measured the reflectance of each species measured individually in the dark experiment room with 500 W halogen light using the Spectroradiometer. The reflectance spectra of each species were measured 5-6 times and averaged to eliminate any potential variation in the illumination. In this study, the reflectance calculated between 400 nm to 900 nm was used because of the low signal-to-noise ratio at the longer wavelengths. The reflectance measured using spectroradiometer shows that both species have the significant difference in their reflectance spectra, particularly in the NIR region (Figure 3.4). The methodological framework is shown in Figure 3.5.

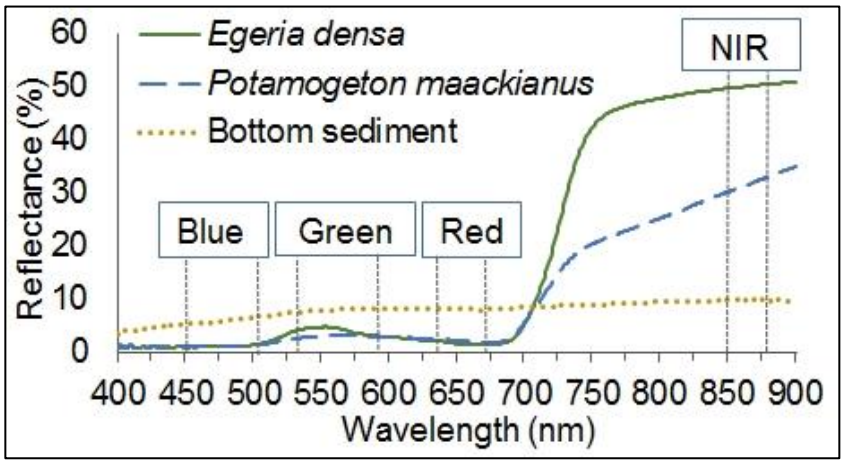

Figure 3.4 The reflectance spectra of SAV species *Potamogeton Maackianus* and *Egeria Densa* and bottom sediment reflectance measured using the portable Spectroradiometer in dark room.

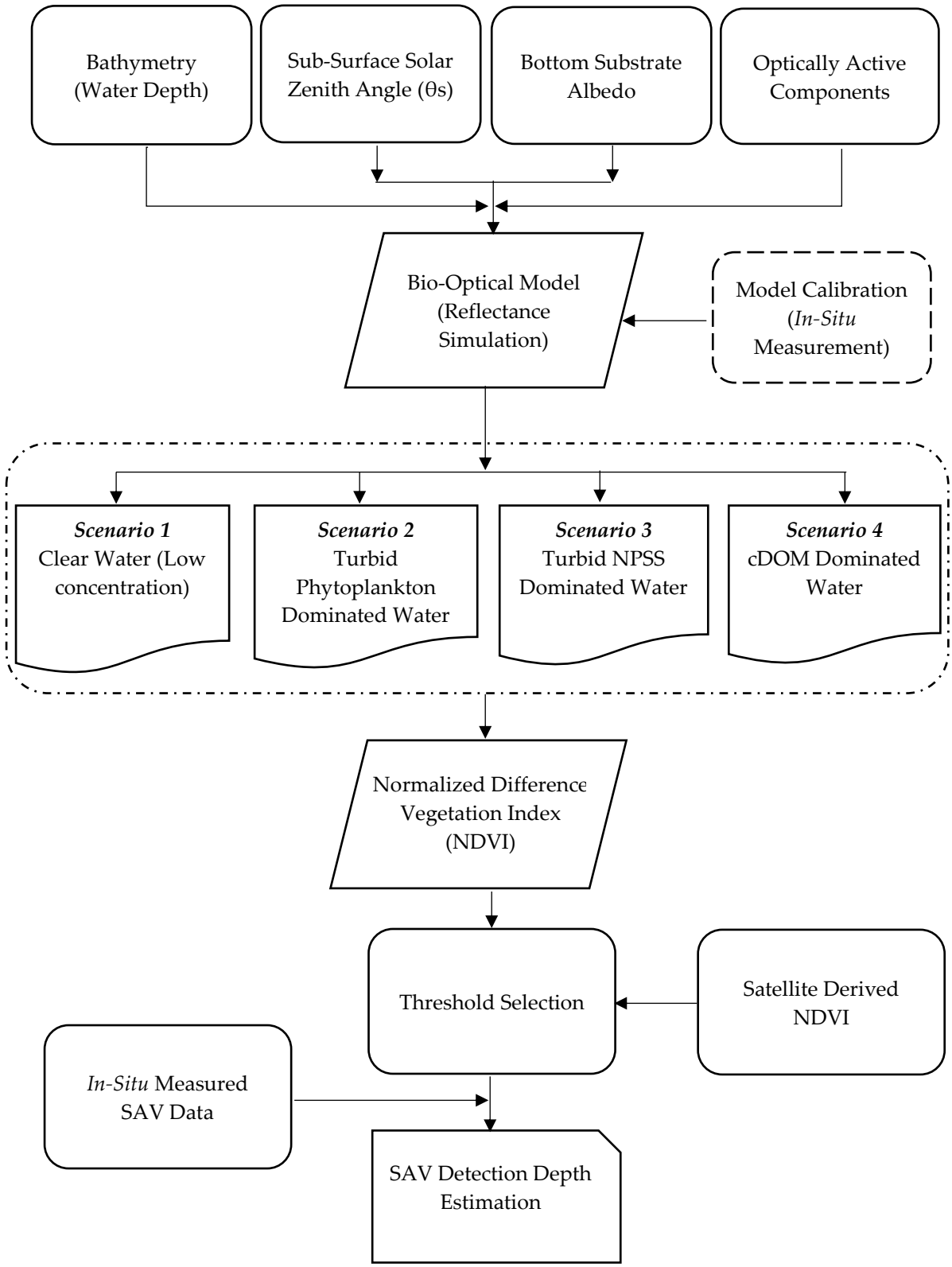

Figure 3.5. Schematic of SAV Detection Depth Estimation Methodology.

Satellite Data Acquisition and Processing - The imagery from Landsat-8 Operational Land Imager (OLI) satellite was acquired for the peak growth period of SAV in the Lake Biwa,

mainly in September (09 September 2014 and 07 September 2016). We downloaded images based on survey time, geographical extent and environmental conditions (cloud-free and wind speed < 3 m/s), obtained from U.S. Geological Survey (USGS) EarthExplorer (https://earthexplorer.usgs.gov/). Image rectification and geo-processing were achieved using ENVI 5.2 image analysis software and ArcMap 10.3.1. Apart from rescaling to Top of Atmosphere (TOA) reflectance, the images were atmospherically corrected using the mid-latitude summer atmospheric model and maritime aerosol model in the atmospheric correction module FLAASH of ENVI 5.2. Horizontal visibility of the study area was obtained from the closest stations (Kyoto and Hikone) from the Japan Meteorological Agency (http://www.jma.go.jp/jma/index.html) and also referred from the weather and climate data info website (http://www.weatherandclimate.info/), varies from 16 Km to 25 Km, for the month of September (2014 and 2016). The water area from the images was masked out for aquatic vegetation classification and mapping. The atmospherically corrected reflectance from each Landsat-8 bands was compared with the in-situ measured reflectance, as shown in Figure 3.6.

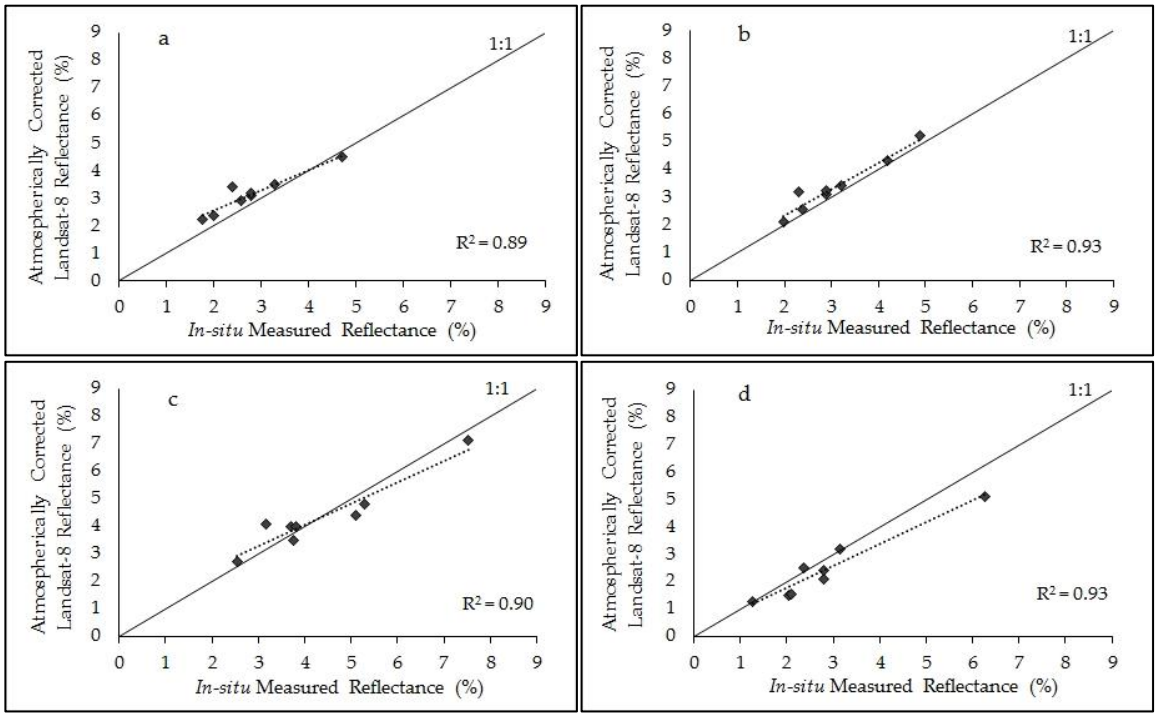

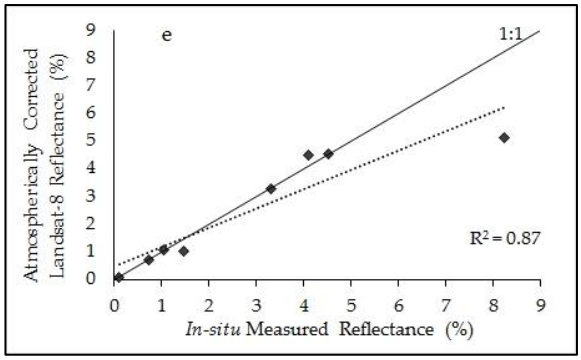

Figure 3.6. The atmospherically corrected reflectance of Landsat-8 bands (7 September 2016 image) with the *in-situ* measured reflectance using spectroradiometer in the south basin of Lake Biwa; a) band1 , b) band2 , c) band3, d) band4, and e) band5 of Landsat-8.

The reflectance of the species was then simulated using the Bio-Optical model. The model was first validated with the *in-situ* measured reflectance in the lake and then used to simulate four scenarios each species based on the water depth and concentration of optically active components. The simulated scenarios were used to calculate the vegetation index NDVI for *Egeria Densa* and *Potamogeton Maackianus*, respectively. The species detection depth was estimated using the simulated NDVI and the satellite-derived NDVI values for the location with abundance of SAV based on 2014 and 2016 data. The obtained NDVI values were used to decide the threshold for the NDVI. Subsequently, the detection depth of each species was estimated at changing concentration of optically active components and water depth. The results were validated using the *in-situ* measured data of SAV in September 2016.

3.2 Reflectance Simulation using Bio-Optical Model

3.2.1 The Bio-Optical Model

As water leaving reflectance is a function of the water column and bottom substrate reflectance. In this study, the bio-optical model used to simulate the SAV species reflectance was based on this two main component. The water column reflectance comprises the reflectance from the optically active components and the bottom albedo from sediment or SAV [15]. Since more than 90% of the south basin is covered with macrophyte bed [10,11,16]. Therefore in this study, we assumed that the bottom albedo is mainly from the SAV bed for simulation. Also, the bottom sediment reflectance often remains muted in deep water [17] than the standing SAV on the lake bottom surface. The Bio-Optical model used in this study

is given in Equation 3.1. The parameters detail can be found in Equation 3.2 to 3.5. The details of the equation can be found in Lee et al. (1998) and Oyama et al. (2009).

$$r_{rs} = (0.070 + 0.16u^{0.752})u\left(1 - 1.03 \times Exp\left\{-\left[\frac{1}{\cos(\theta_W)} + 1.2(1 + 2.0u)^{0.5}\right](a + b_b)H\right\}\right) + 0.31\rho \times Exp\left\{-\left[\frac{1}{\cos(\theta_W)} + 1.1(1 + 4.9u)^{0.5}\right](a + b_b)H\right\} \quad (3.1)$$

Where r_{rs} is defined as subsurface reflectance, u can be expressed in terms of a and b_b as in Equation (3.2). Where a and b_b are the total absorption and backscattering coefficient, respectively, contributed by the pure water, phytoplankton, NPSS and cDOM in the water column, expressed as in Equation 3.3 to 3.4. In addition, θ_w indicate the subsurface solar zenith angle, H indicateS the bottom depth (m) and ρ indicate the remote sensing reflectance of the shallow water. The absorption coefficient of pure water was taken from the literature [19,20].

$$u \equiv \frac{b_b}{a + b_b} \quad (3.2)$$

$$\alpha\ \lambda\ = \alpha_w\ \lambda\ + \alpha_p\ \lambda\ + \alpha_x\ \lambda\ + \alpha_y\ \lambda \quad (3.3)$$

$$b_b(\lambda) = b_b(\lambda) + b_{b,w}(\lambda) + B_p b_{b,p}(\lambda) + B_x b_{b,x}(\lambda) \quad (3.4)$$

Where, B_P and B_x are 0.018, taken from Mobley et al. 1993.

The water leaving reflectance above the water surface (R_{rs}) was then calculated using Equation 3.5 (Lee et al. 1998).

$$R_{rs}(\lambda) = \frac{0.518 r_{rs}(\lambda)}{1 - 1.562 r_{rs}(\lambda)} \quad (3.5)$$

The absorption and backscattering coefficients of pure water, phytoplankton, NPSS and cDOM, were based on the simple bio-optical model in Table 3.2.

Table 3.2. Bio-optical model to estimate the absorption and backscattering coefficients of pure water, phytoplankton, NPSS and cDOM.

Absorption $\alpha\ \lambda$	**Backscattering** $b_b\ \lambda$
$\alpha_w\ \lambda$; 400-700 nm [20]; 700-1000 nm [21]	$b_{b,w} = 0.00111 \times \lambda / 550^{-4.32}$ [23]
$\alpha_\rho\ \lambda = \alpha_0\ \lambda + \alpha_1\ \lambda \times \ln\left[\alpha_\rho\ 440\right] \times \alpha_\rho\ 440$ $\alpha_\rho\ 440 = 0.06 \times chl\text{-}a^{0.65}$ [15]	$b_{b,p}\ \lambda = 0.3 \times$ chl-a $^{0.62} \times 550 / \lambda$ [22]
$\alpha_x\ \lambda = 0{\cdot}041 \times$ NPSS $\times e^{-0.0123 \times \lambda - 443}$ [23]	$b_{b,x}\ \lambda = 0{\cdot}51 \times$ NPSS $\times \lambda / 555^{-0.15}$ [23]
$\alpha_y\ \lambda = \alpha_{cDOM}\ 440 \times \exp\ S_{cDOM}\ \lambda - 440$ $\alpha_{cDOM}\ 440 = \alpha\ 440 \times DOC + e$ [24–26]	-

Note: w, ρ, x, y *indicates pure water, phytoplankton, NPSS and cDOM;* α_0 *and* α_1 *coefficients are taken from* [15], S_{cDOM} *- slope of cDOM,* $\alpha\ 440$ *and* e *taken from* [26].

Before, the reflectance simulation, the Bio-Optical model was calibrated with the *in-situ* measured reflectance (September 2016) using the average reflectance of at least three stations representing the environmental conditions of the satellite acquisition day [18]. The selected stations were Shinaoki, Karasaki and Katata. The ratio of the mean simulated and observed reflectance was calculated and multiplied with the simulated standard spectra of the satellite for each endmember, which was reintegrated into Landsat-8 bands (Figure 3.7).

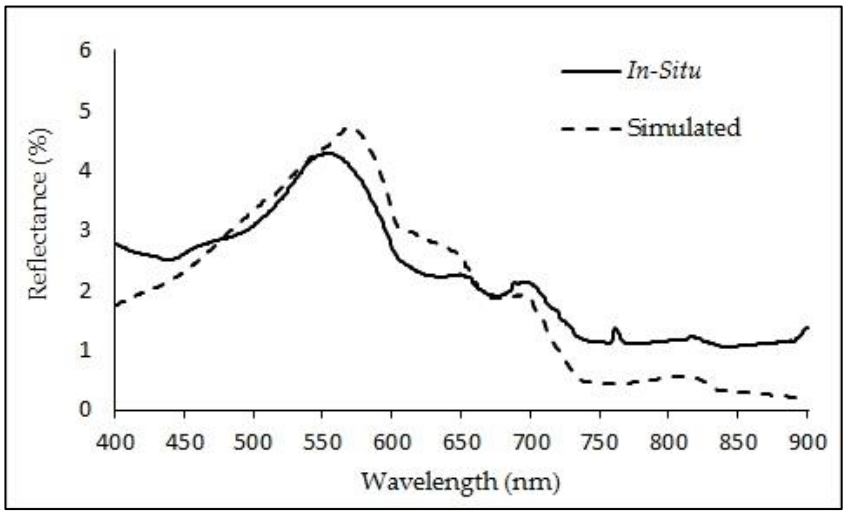

Figure 3.7. Calibration of Bio-Optical Model using the mean simulated and mean *in-situ* measured reflectance of the three stations in the south basin of Lake Biwa.

3.3 Evaluating the Influence of Optically Active Components on SAV Species

The scenarios of *Egeria Densa* and *Potamogeton Maackianus* were calculated at maximum and minimum concentration of optically active components and varying water depth. The scenarios were simulated separately for *Egeria Densa* and *Potamogeton Maackianus*, assuming the homogeneous cover of each SAV (Figure 3.8). The scenarios are:

1) *Scenario-a*: SAV reflectance at minimum concentration of phytoplankton (< 1 µg/L), NPSS (< 1 mg/L) and cDOM (1.3 mg/L of DOC).
2) *Scenario-b*: SAV reflectance at maximum phytoplankton concentration only (100 µg/L) and other parameters concentration remain minimum.
3) *Scenario-c*: SAV reflectance at maximum NPSS concentration only (100 mg/L) and
4) *Scenario-d*: SAV reflectance at maximum concentration of cDOM only (2.7 mg/L of DOC).

In this chapter, the absorption coefficient of cDOM is calculated based on the DOC concentration. For the calculation of absorption coefficient of cDOM, the equation parameters value (i.e., $a(440)$ and e) is limited for the maximum DOC of 2.7 mg/L, for Lake Biwa [26]. Therefore, the maximum concentration was taken as 2.7 mg/L for scenario-d.

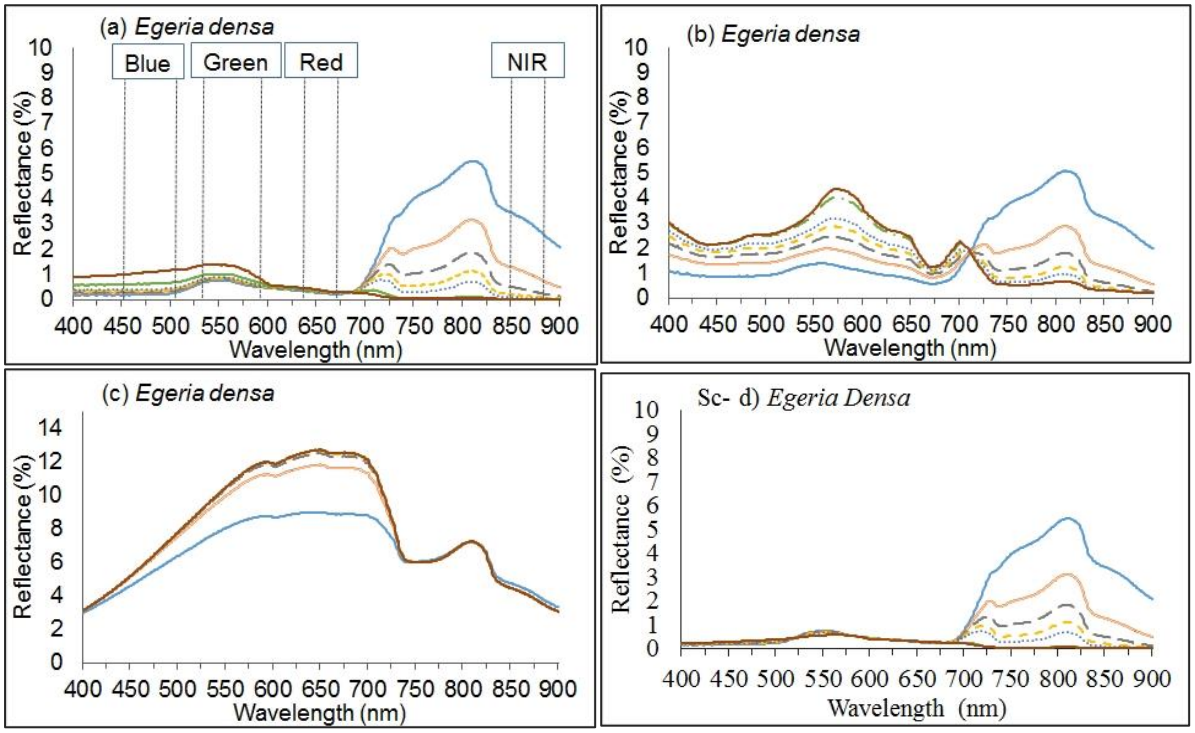

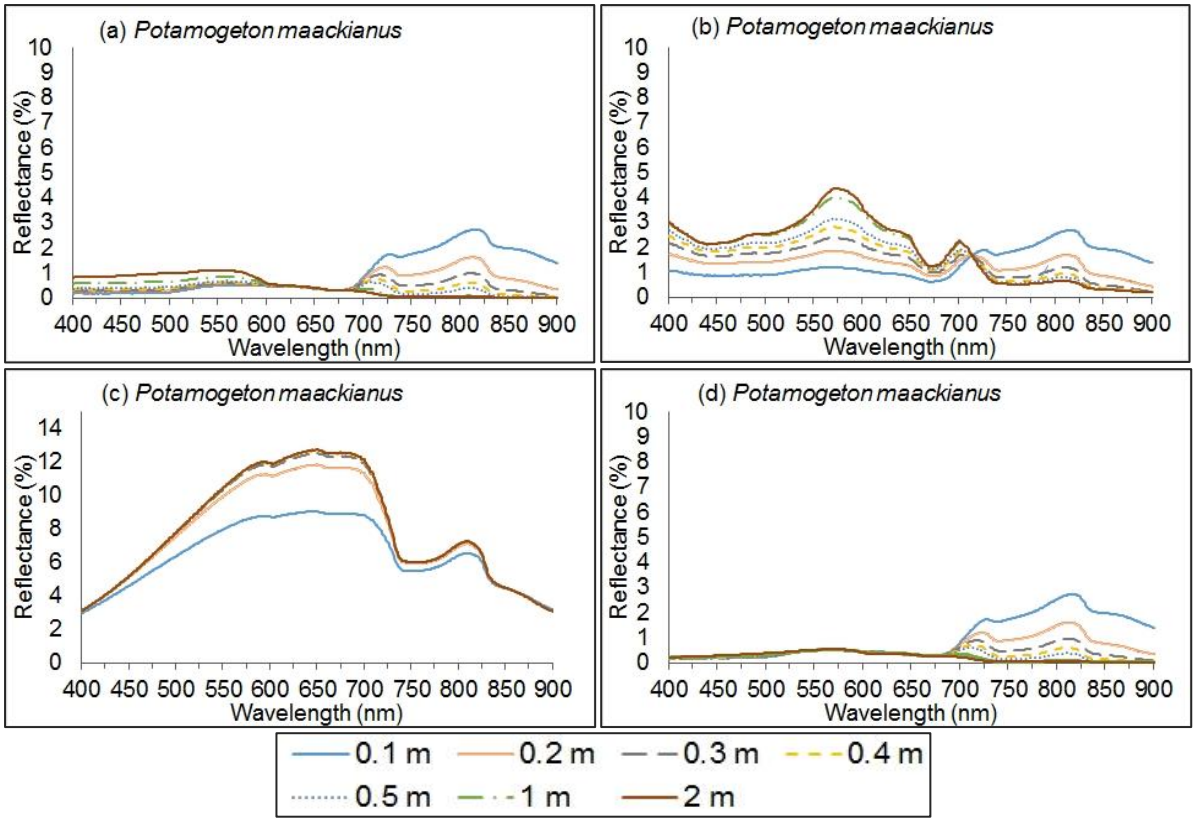

Figure 3.8 Simulated reflectance range of *Egeria Densa* and *Potamogeton Maackainus* at four scenarios and maximum (2 m) and minimum (0.1 m) water depth from the surface.The simulation was conducted taking SAV as bottom surface: (a) scenario-a at minimum concentration; (b) scenario-b at maximum concentration of chlorophyll-a only; (c) scenario-c at maximum concentration of NPSS only; and (d) scenario-d at maximum concentration of cDOM only.

The minimum concentration for scenarios was selected to understand the reflectance of SAV species in clear water without any influence of phytoplanktons and suspended sediments. On the other hand, to understand the influence of each component on SAV reflectance, the scenarios with maximum concentration taking individual OAC components was simulated. The simulated reflectance after 2 m water depth remains unchanged, therefore, to estimate the detectable depth of SAV species, each scenario was simultaneously simulated at minimum and maximum water depth of 0.1 m and 2 m, respectively (Figure 3.8). Additionally, to understand the change in water leaving reflectance when no vegetation present, the same scenarios were also simulated taking sediment only as the bottom surface (Figure 3.9).

The results highlight that for SAV identification, NIR band is significant, which at minimum concentration shows high reflectance of > 3% and >2% for *Egeria Densa* and

Potamogeton Maackianus, respectively (Figure 3.8 a). On the other hand, with increase in concentration of phytoplankton (Chl-a) and NPSS, the reflectance peak shifted from NIR to green and red region of the spectra (Figure 3.8 (b) and (c)). The result indicates the importance of visible region for phytoplankton and NPSS identification in water. In addition, scenario-d shows the negligible effect of cDOM on the SAV reflectance particularly in NIR region, whereas a decrease in reflectance occurred in blue, green and the red regions. It could be due to the higher absorption of cDOM in the visible region of the spectrum, particularly in the blue band. Additionally, the negligible effect of cDOM can also be attributed to low concentration of Dissolved Organic Carbon (DOC), as the case in Lake Biwa, which may not have significant influence on the bottom albedo reflectance. In scenario-b, the overall reflectance increased significantly for both SAV and sediment bed, in blue, green and red regions (Figure 3.8 and 3.9). Conversely, in NIR band the reflectance with SAV bed shows a slight change with increase in chl-a concentration. The result shows the dominance of SAV reflectance in NIR band. Furthermore, the dominance of SAV with high reflectance, at low water depth (< 1m) even when the chlorophyll concentration rise.

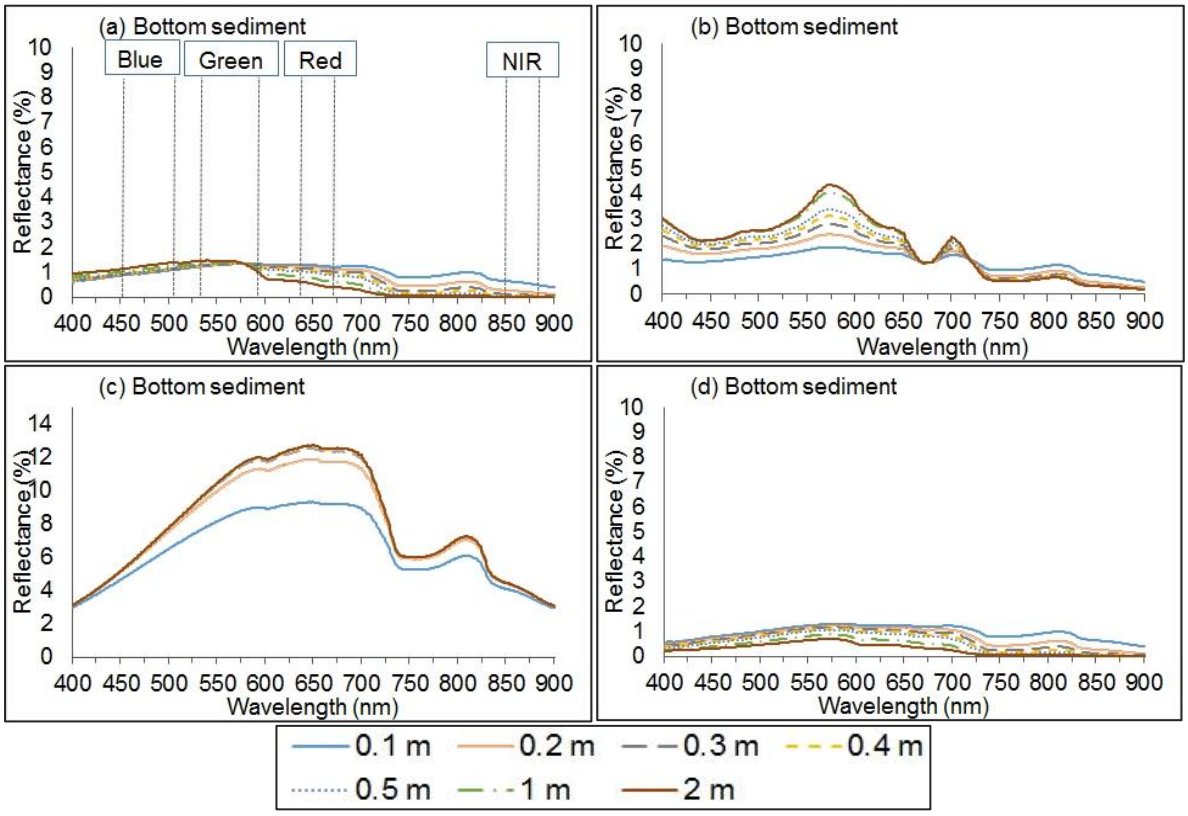

Figure 3.9 Simulated reflectance range of bottom sediment at four scenarios and maximum (2 m) and minimum (0.1 m) water depth from the surface. Taking sediment as the bottom surface, the simulated scenarios are: (a) scenario-a at the minimum concentration; (b) scenario-b at the maximum

concentration of chlorophyll-a only; (c) scenario-c at maximum concentration of NPSS only; and (d) scenario-d at maximum concentration of cDOM only.

In Figure 3.9, the simulated scenarios with sediment as the bottom surface shows high reflectance mainly in green and red bands, whereas in NIR band it shows relatively low reflectance. The bottom sediment in clear water scenarios (a and d) remains slightly low with <2% reflectance overall reflectance which decreases with increase in water depth. Furthermore, in optically turbid water, the reflectance of bottom sediment was dominated by the NPSS and phytoplankton concentration in the water column.

The reflectance peak of SAV was noted at the minimum depth (0.1 m) (Figure 3.8). However, the reflectance peaks of optically active components were noted at the maximum water depth. It could be attributed to the increase in absorption and scattering function of water constituents (phytoplankton, SS and cDOM), with increase in water depth. When compared, the scenarios with SAV bed and bottom sediment, it shows that the bottom sediment has lower contribution in water leaving reflectance with increase in concentration of optically active components and water depth. Additionally, the SAV bed which contributes substantially to overall water reflectance depending on the type of SAV species and water depth even in turbid waters.

3.4 SAV Canopy Depth Estimation

To estimate the detection depth of SAV species, we calculated the Normalized Difference Vegetation Index (NDVI), for each simulated SAV scenarios of *Egeria Densa* and *Potamogeton Maackianus* (Figure 3.10). Though, the simulated result showed the dominance of phytoplankton and NPSS on SAV reflectance at maximum concentration, but how their individual influence changes with increase in concentration were not known. With this in mind, we then calculated simulated NDVI for changing chlorophyll and NPSS concentration, to evaluate the change in SAV detection depth when influenced by optically active components, individually (Figure 3.11).

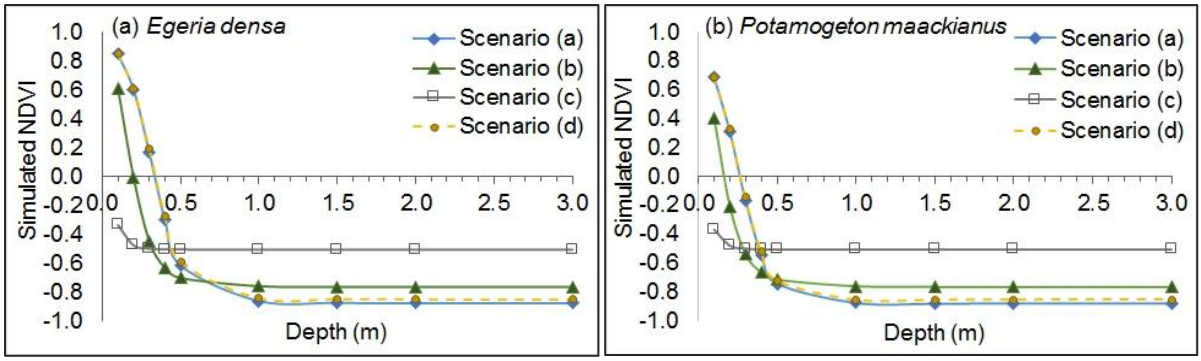

Figure 3.10 (a) Simulated NDVI for *Egeria Densa* and *Potamogeto Maackianus* at all four scenarios.

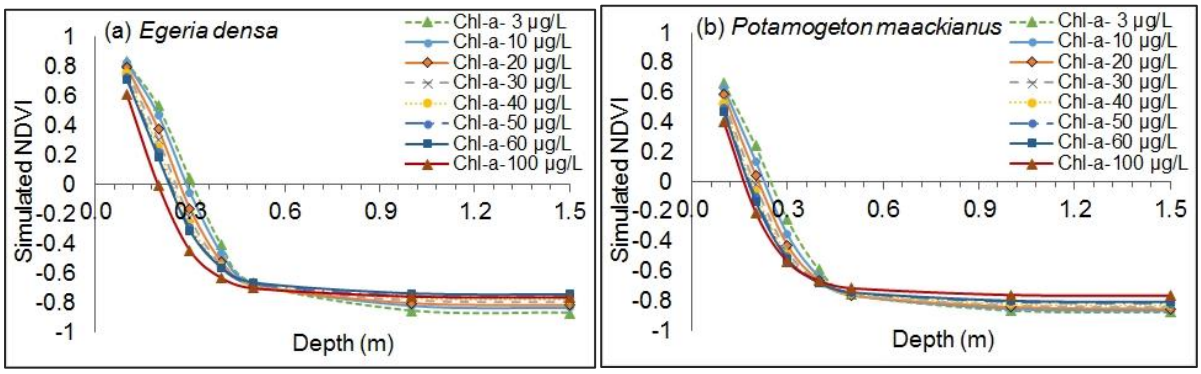

Figure 3.10 (b) Simulated NDVI for changing chlorophyll concentration for *Egeria Densa* and *Potamogeton Maackinus*

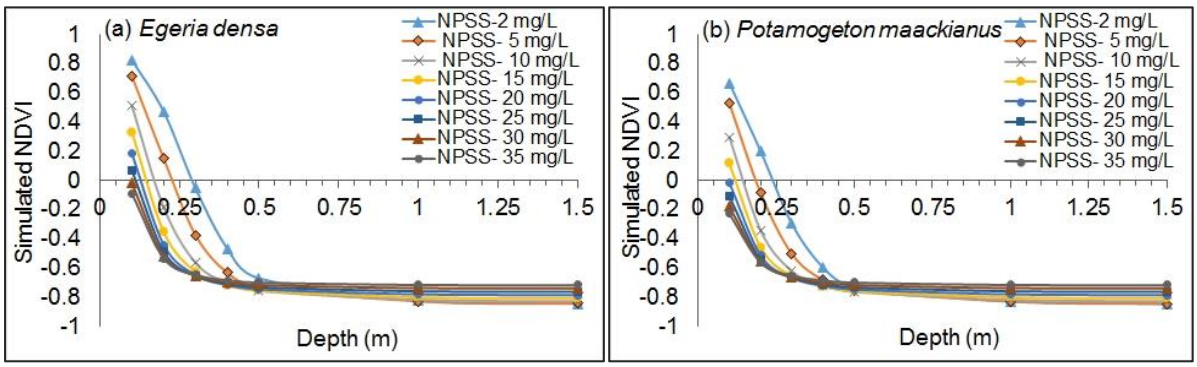

Figure 3.11. Simulated NDVI for changing NPSS concentration for *Egeria Densa* and *Potamogeton Maackianus.*

The simulated result shows a decrease in SAV detectable depth at every 10 µg/L of chlorophyll-a and every 5 mg/L concentration of NPSS (Figure 3.11 (a) and (b)). The minimum detectable depth of *Egeria Densa* and *Potamogeton Maackianus* was noted at NPSS concentration of 30 mg/L (0.06 m) and 25 mg/L (0.07 m), respectively.

Because we expect to estimate the SAV detection using the satellite data. Therefore, using the satellite-derived NDVI information, we decided the NDVI thresholds to be applied on the simulated NDVI for each species. The satellite-derived NDVI from the images of September

2014 and 2016 were extracted for the 52 observation points in the south basin of Lake Biwa (Table 3.3). The threshold for the NDVI was selected based on the observation points with the abundance of *Egeria Densa* and *Potamogeton Maackianus*, as shown in (Figure 3.2 and 3.3). According to the 2014 SAV biomass data, out of 52 observation stations we selected the stations dominated by *Egeria Densa* (i.e. station 5, 15, 19, 25, 32, 36) and *Potamogeton Maackianus* (i.e. station 13, 3, 6, 7, 8, 12, 13, 22, 26, 30, 39, 41, 45) contributing > 50% of the total biomass (Table 3.3).

Table 3.3. Satellite-derived NDVI for *Egeria Densa* and *Potamogeton Maackianus.*

SAV Species	Clear Water (Chlorophyll < 20 μg/L)			Turbid Water (Chlorophyll >20 μg/L)		
	NDVI 2014	Water Transparency (m)	Water Depth (m)	NDVI 2014	Water Transparency (m)	Water Depth (m)
Egeria Densa	-0.71 – 0.47	1.9-3.7	0.36-4.1	0.71	0.0	0.0
Potamogeton Maackianus	-0.85- -0.15	2.3-3.6	3.9-4.8	0.70	0.01	0.4

Furthermore, using the classified SAV result of Chapter 5, we extracted the NDVI threshold from the SAV classified pixels in 2014 and 2016 (Table 3.4).

Table 3.4. Satellite-derived NDVI of classified SAV pixels in 2014 and 2016 (based on the result of Chapter 5).

	Based on SAV Classified Area 2014			Based on SAV Classified Area 2016		
	NDVI	Water Transparency (m)	Water Depth (m)	NDVI	Water Transparency (m)	Water Depth (m)
SAV	-0.87 – 0.49	1.37-3.37	0.36-4.6	-0.99-0.43	1.0-2.1	0.45-2.9

Based on the satellite-derived SAV NDVI, we decided three different thresholds for detection depth estimation. The three thresholds were a) NDVI = 0, b) Minimum NDVI value of the classified SAV pixels and c) Mean NDVI of the maximum and minimum values of the classified SAV pixels. The information of calculated threshold and SAV stand height for each species and SAV as a whole is given in Table 3.5. The *in-situ* measurement conducted in September 2016 gives the maximum stand height of *Egeria Densa* observed at Shinoki station is 2.5 m, whereas, for *Potamogeton Maackianus* the maximum observed was 1.9 m at Katata station (Table 3.5 and 3.7). Overall, the minimum and maximum stand height of SAV as observed in the south basin of Lake Biwa is 0.17 m to 2.5 m, respectively. On the other hand, the maximum SAV stand height observed in 2007 using the echosouding images, in the the

south basin of the Lake Biwa was 3.3 m [12]. According to the previous work [12], the SAV stand height tends to increase in the deeper water (4 m to 6 m), whereas decrease in the shallow water near the shorelines. In shallow waters, the presence of SAV is possible to the maximum water depth of 6 m, while for deeper waters in a given water body, the SAV can grow to the water depth ranges between 15 m to 20 m, approximately [27]

Table 3.5. NDVI Thresholds based on the satellite-derived NDVI of 52 observation points and SAV classified locations in 2014 and 2016. The observed water depth (2014 and 2016) and SAV stand height (September 2016) is also shown in table.

	NDVI Threshold		SAV Stand Height - Lake Biwa Observation 2016 (m)		SAV Stand Height from Literature (m)		SAV Water Depth in Lake Biwa (m)	
	Min	Mean	Min	Max	Min	Max	Min	Max
Egeria Densa	-0.71	-0.12	-	2.5	0.2	5	1.7	2.9
Potamogeton Maackianus	-0.85	-0.5	-	1.9	0.3	4	1.9	4.9
SAV Species	-0.87- -0.99 (2014,2016)	-0.93 (2014,2016)	0.7	2.5 - 3.3 (2016, 2007)	0.2	6	1.7	5.6

To estimate the SAV species detection depth, we first calculated the SAV Canopy Depth (m.). The depth from the water surface to the top of the vegetation canopy submerged in the water is called as the canopy depth. We calculated the SAV canopy depth by subtracting the maximum SAV stand height from the maximum depth of SAV growth in water. Because of the limited observed data for SAV stand height (eight locations), we also used the species stand height (*Egeria Densa*, *Potamogeton Maackianus,* and overall SAV in Lake) from extensive literature review in Chapter 2. Thus we got the maximum species stand height from observed data in Sepetember 2016 and Literature, which is used to estimate the canopy depth for each species. The minimum and maximum canopy depth calculated for SAV (i.e., which contains the mixture of all species) ranges between -0.4 m to 2.3 m based on the minimum and maximum SAV stand height (Table 3.6). For *Egeria Densa* the maximum canopy depth calculated is 0.3 m, whereas, for *Potamogeton Maackinus* the canopy depth ranges between 0.9 m to 3 m in water, respectively.

Table 3.6. Estimated SAV species (*Egeris Densa* and *Potamogeton Maackianus*) canopy depth from the i*n-situ* measured and literature reviewed maximum SAV stand height and water depth of SAV growth locations.

	Biomass >150 g DW m^{-2})		
	Max SAV stand Height (m)	Max Water Depth (m)	SAV Canopy Depth (m)
Egeria Densa	2.5 - 5	2.8 - 4.9	0.3 - -2.2
Potamogeton Maackianus	1.9 - 4	4.9	0.9 - 3
SAV Species	3.3 - 6	5.6	-0.4 - 2.3

Furthermore, we simulated the SAV canopy depth, at all three NDVI thresholds, using the simulated NDVI of *Egeria Densa* and *Potamogeton Maackinus* (Figure 3.12). Simultaneously, the canopy depth was also estimated at the increasing concentration of each dominant optically active component, chlorophyll-a and NPSS, individually. In the case of Chlorophyll-a, the simulated results at the threshold NDVI = 0, shows that the maximum canopy depth of *Egeria Densa* and *Potamogeton Maackianus* is 0.40 m and 0.30 m, respectively. However, when chlorophyll-a concentration > 20 µg/L, the the canopy depth reduced significantly to 0.29 m and 0.21 m for *Egeria Densa* and *Potamogeton Maackianus,* respectively. Importantly, very slight change in the canopy depth (i.e. almost stable) was noticed when chlorophyll-a concentration increased to > 20 µg/L. It is because, with increase in concentration chlorophyll reflectance significantly influence the SAV reflectance, this lead to the reduction in the high NDVI value of vegetation near the water surface. At high concentration, the NDVI values are mainly because of the chlorophyll in the water column, which does not change significantly and remains almost stable with increasing concentration. Therefore, according to the simulation result, the maximum canopy depth can be achieved at the chlorophyll concentration < 20 µg/L.

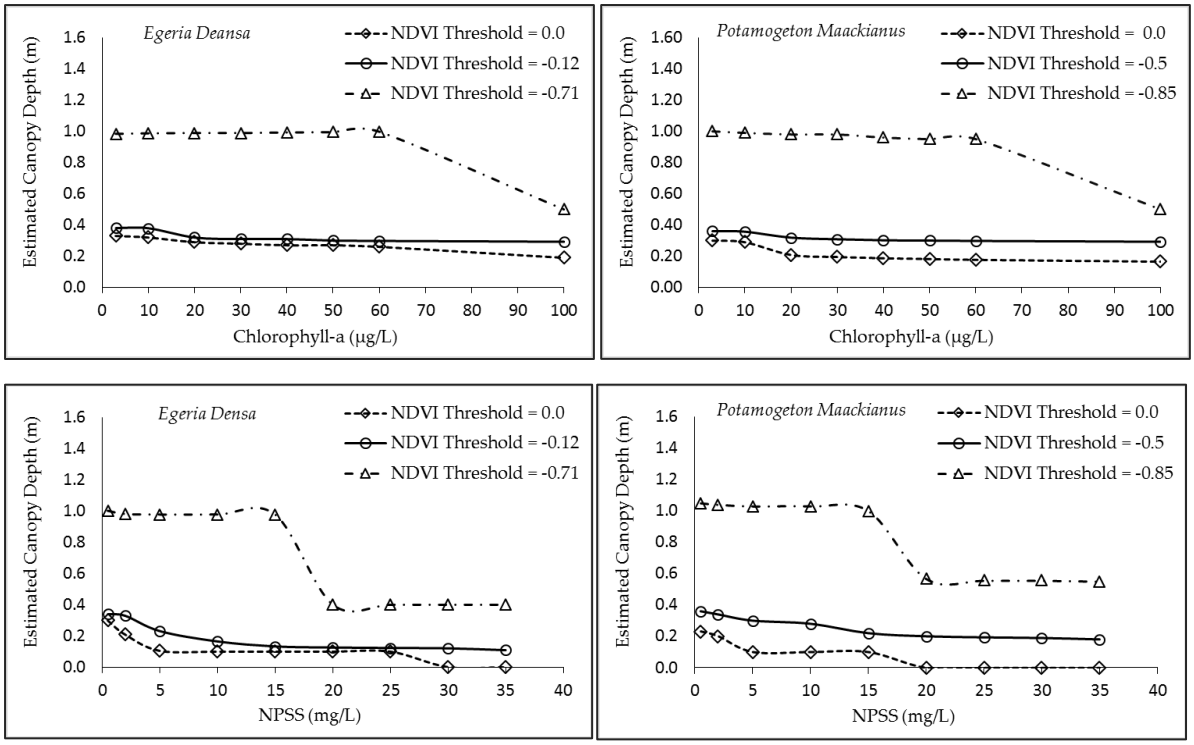

Figure 3.12 The simulated canopy depth of SAV species a) *Egeria Densa* and b) *Potamogeton Maackianus* at varying chlorophyll and NPSS concentration.

To estimate the maximum canopy depth, we simulated the species at the minimum NDVI threshold. At the minimum NDVI threshold, for *Egeria Densa* (NDVI = -0.71) and *Potamogeton Maackianus* (NDVI = -0.85), the maximum canopy depth achieved for the two species was 0.98 m and 1.0 m, respectively. The canopy depth remains stable with increasing concentration and exceptionally low at the maximum chlorophyll concentration.

At the mean NDVI threshold, for *Egeria Densa* (NDVI = -0.12) and *Potamogeton Maackianus* (NDVI = -0.5), the maximum canopy depth was 0.33 m and 0.38 m, separately. When simulated at varying chlorophyll concentration, the simulated canopy depth at all the thresholds ranges between 0.33 m to 0.98 m in *Egeria Densa* and 0.3 m to 1.0 m for *Potamogeton Maackianus*.

Similarly, we simulated the canopy depth of the two species at varying NPSS concentration for all three thresholds. At the threshold NDVI = 0, the simulated canopy depth was 0.30 m and 0.23 m for *Egeria Densa* and *Potamogeton Maackianus*, respectively. Whereas canopy depth reduced significantly for each species, at the NPSS concentration between 5 – 10 mg/L. For *Egeria Densa* and *Potamogeton Maackianus* the canopy depth reduced to 0.11 m to

0.10 m between the NPSS concentration of 5 mg/L and reduced to 0 m at the NPSS concentration 25 mg/L and 20 mg/L, respectively. The result suggests that as NPSS concentration increases (> 5 mg/L) the SAV signal reduces to below detection limit by satellite image. However, at the minimum NDVI threshold, the simulated canopy depth for *Egeria Densa* and *Potamogeton Maackianus*, is 1.0 m to 1.1 m, respectively. Whereas, at mean NDVI threshold, the simulated canopy depth is 0.34 m and 0.40 m, individually for *Egeria Densa* and *Potamogeton Maackianus*. Overall, at varying NPSS concentration the simulated canopy depth ranges between 0.11 m to 1.0 m for *Egeria Densa* and 0.11m to 1.1 m for *Potamogeton Maackianus*. The sumulation results indicate that the maximum canopy depth of the two SAV species primarily extends to 1.1 m in the water column, approximately. More importantly, the maximum canopy depth can be achieved in clear water condition with chlorophyll <20 μg/L and NPSS <10 mg/L.

To validate the simulated results, we used the *in-situ* measured data of September 2016, for the eighth location. We also used the SAV classified area 2016 (based on Chapter 5), to avoid the influence of chlorophyll and NPSS. We then estimated the canopy depth of all the in-situ measured stations, by subtracting the observed SAV stand height from the observed water depth at each location (Table 3.7).

Table 3.7. Estimated canopy depth for the in-situ measured location (September 2016).

Stations	SAV Observed Stand Height (m)	SAV Coverage Area (%)	Observed Water Depth (m)	SAV Identified-Satellite Image	Canopy Depth (m)
Yanagasaki-1	0.67 – 0.75	100	1.7	Y	0.95 – 1.03
Yanagasaki-2	0.17 – 0.18	30	0.6	Y	0.42 – 0.43
Karasaki	0.60 – 1.60	68	4.2	N	2.60 – 3.60
Karasumaoki	0.80 – 1.20	100	1.9	Y	0.70 – 1.10
Karasumaguchi	0.50 – 0.66	40	1.7	N	1.04 – 1.20
Shinaoki	2.00 – 2.50	100	4.5	N	2.00 – 2.50
Katata	0.76 – 1.90	95	5.1	N	3.20 - 4.34
Hayama River	0.40 – 0.50	40	0.9	Y	0.40 – 0.50

[3.7]Here, Y = SAV detected in satellite image; N = SAV not detected in satellite image.

The estimated canopy depth based on the *in-situ* measured data shows that the location where canopy depth is <1.1 m, were detected by the Landsat-8 satellite image. Whereas, the maximum and minimum canopy depth for SAV detection range between 0.40 m to 1.1 m. Detection depth may be more than 1.1 ±0.4 m in some lakes, depends on the biomass and type of SAV species present and variation in optically active components. However, for the south

basin of Lake Biwa, 1.1 is the maximum simulated and observed canopy depth at which the SAV can be detected using the satellite image. In addition, some high reflectance species in the lake can be detected at canopy depth > 1.1 m in Lake Biwa, but the possibility of it significantly low due to the presence of optically active components in the lake, which substantially dominates the SAV reflectance. The NDVI for 2014 and 2016 is shown in Figure 3.13.

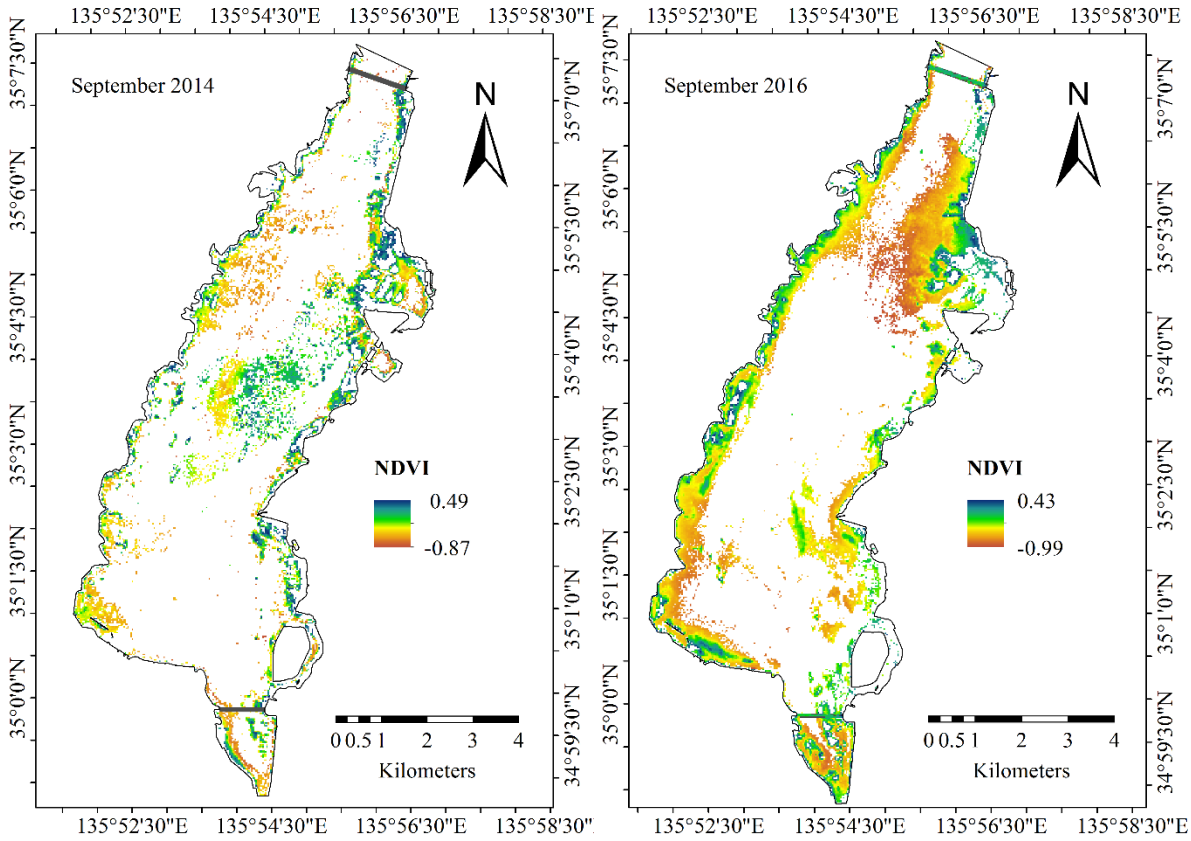

Figure 3.13. NDVI value of the classified SAV pixels in the south basin of Lake Biwa for September 2014 and 2016 (Based on classified results in Chapter 5).

3.5 Result Discussions and Conclusion

3.5.1 Discussion

The simulated SAV scenarios show the dominance of chlorophyll and NPSS on the SAV species reflectance, with increasing concentration and water depth. It could be attributed to the fact that with increase in water depth, the absorption and scattering function of the optically active components also increases. Furthermore, the reflectance of *Potamogeton Maackianus* is significantly low in almost all the scenarios. The result suggests that the influence of these components can be more dominant on low reflecting SAV species, than the

one with high reflectance. The influence of optically active components is significant in the visible region of the spectrum (blue, green and red bands). While for SAV species NIR band seems important. In addition, with increasing water depth the influence of the bottom sediment remains muted than the dense SAV bed at the bottom of the lake.

The detection depth of SAV depends on the SAV canopy depth, which is directly related its stand height and the total water depth where the plant grows in the shallow lake. Different SAV species may have different stand height in the lake depending upon several environmental factors and morphology of individual plants. Therefore, canopy depth may vary with the type of SAV species. In this study, using the simulated and satellite-derived NDVI, we estimated the canopy depth of the SAV in the eutrophic shallow basin of Lake Biwa. The canopy depth estimated for the two species, native SAV specie (*Potamogeton Maakianus*) and alien SAV specie (*Egeria Densa*) showed a maximum canopy depth of 1.1 m approximately, in clear water condition, where SAV where SAV can be detected using the satellite image. Although, there is not enough research on SAV detection depth estimation for large lakes, particularly the eutrophic shallow basin of the lake. However, some research using the hyperspectral field spectroradiometer for SAV detection in the River water gave almost the similar results [27]. The author suggested that SAV can be possibly be detected at 1 m canopy depth in clear water, however, with increase in turbidity, the SAV can be detected to maximum canopy depth of 0.46 m to 0.5 m [27].

The obtained results using Landsat-8 image is analogous to the previous work, where for turbid water, specifically when chlorophyll > 20 μg/L and NPSS > 5 – 10mg/L, the estimated canopy depth reduced to < 0.3 m, approximately. Similar results were obtained when SAV detection depth was estimated using the worldview-2 image (2 m spatial resolution), at different turbidity levels [28]. The author found that in clear water conditions (0.5 to 5 NTU turbidity), the NDVI value show good correlation with the submerged vegetation and can be distinguished in water. Whereas when the turbidity > 25 NTU, the SAV can be detected with some noise and with high turbidity (50 NTU) it is not possible to detect even at 0.5 m depth.

The obtained the results were only based on the two dominant SAV species with widespread growth in the Lake bottom. However, the results correspond well with the *in-situ* measured data for September 2016. In addition, some high reflectance species in the lake can be detected

at canopy depth > 1.1 m in Lake Biwa, but the possibility of it is significantly low due to the presence of optically active components in the lake, which substantially attenuates the SAV reflectance for canopy depth > 1 m.

3.5.2 Conclusions

The detection depth of two dominant SAV species was estimated using the Bio-Optical model, in this study. However, the detected depth may vary in different lakes. In an aquatic environment several factors influence the detection of SAV using the remote sensing approach. Some of the factors are; water depth or SAV depth in water, canopy depth, coverage area, SAV species reflectance, concentration of OAC (i.e., chlorophyll-a and non-phytoplankton suspended solids (NPSS)). This study identifies the dominance of mainly NPSS and phytoplankton on the SAV species reflectance and their detection using the satellite image. The water depth also indicated as the important parameter attenuating the bottom substrate reflectance.

The minimum and maximum canopy depth estimated at three NDVI thresholds, for *Egeria Densa* was in between 0.11 m to 1.0 m, and *Potamogeton Maackianus* was in between 0.10 m to 1.1 m, respectively. More importantly, the maximum canopy depth can be achieved in clear water condition with chlorophyll <20 μg/L and NPSS <10 mg/L. At the chlorophyll concentration >20 μg/L and NPSS >10 mg/L, the canopy depth reduced to < 0.3 m and <0.2 m. The simulated result suggests that at the canopy depth of 0.10 m to 1.1 m, the SAV can be detected by the satellite image. The result corresponds well with the in-field data of the SAV and its detection using satellite image. The study further suggests that the Bio-Optical model can be successfully used for the SAV species detailed studies in the future, for effective management efforts in the lake.

This study tried to fill the gap in depth estimation of submerged vegetation, which is limited for the lakes, specifically for eutrophic shallow lakes, due to the presence of optically active components which lead to the vertical attenuation and the misclassification of the SAV signals in a given water body.

References

1. Zhang, Y.; Liu, X.; Qin, B.; Shi, K.; Deng, J.; Zhou, Y. Aquatic vegetation in response to increased eutrophication and degraded light climate in Eastern Lake Taihu: Implications for lake ecological restoration. *Scientific Reports* **2016**, *6*, 23867.
2. Luo, J.; Li, X.; Ma, R.; Li, F.; Duan, H.; Hu, W.; Qin, B.; Huang, W. Applying remote sensing techniques to monitoring seasonal and interannual changes of aquatic vegetation in Taihu Lake, China. *Ecological Indicators* **2016**, *60*, 503–513.
3. Silva, T. S. F.; Costa, M. P. F.; Melack, J. M.; Novo, E. M. L. M. Remote sensing of aquatic vegetation: Theory and applications. *Environmental Monitoring and Assessment* **2008**, *140*, 131–145.
4. Pinnel, N. A method for mapping submerged macrophytes in lakes using hyperspectral remote sensing, Technical University of Munich, 2007.
5. Williams, D.; Rybicki, N.; Lombana, A.; O'Brien, T.; Gomez, R. Preliminary investigation of submarged aquatic vegetation mapping usingyperspectral remote sensing. *Environmental Monitoring and Assessment* **2003**, *81*, 383–392.
6. Kirk, J. T. O. *Light and photosynthesis in aquatic ecosystems*; 3rd ed.; Cambridge University Press, 2011.
7. Sváb, E.; Tyler, A. N.; Preston, T.; Présing, M.; Balogh, K. V. Characterizing the spectral reflectance of algae in lake waters with high suspended sediment concentrations. *International Journal of Remote Sensing* **2005**, *26*, 919–928.
8. Mumby, P. J.; Green, E. P.; Edwards, A. J.; Clark, C. D. Measurement of seagrass standing crop using satellite and digital airborne remote sensing. *Marine Ecology Progress Series* **1997**, *159*, 51–60.
9. Ishikawa, K.; Haga, H. Ecological Regime Shift in the South Basin of Lake Biwa : Focus on Algal Blooms and Submerged Macrophyte Overgrowth. In *UNESCO International Symposium on Scientific, Technological and Policy Innovations for Improved Water Quality Monitoring in the Post-2015 SDGs Framework*; Kyoto, Japan, 2015; pp. 1–3.
10. HAGA, H.; Ishikawa, K. Spatial Distribution of Submerged Macrophytes in the Southern Lake Biwa basin in the summer of 2014, in comparison with those in 2002, 2007 and 2012. *Japanese Journal of Limnology (Rikusuigaku Zasshi)* **2016**, *77*, 55–64.
11. *Lake Biwa: Interactions between Nature and People*; Kawanabe, H.; Nishino, M.; Maehata, M., Eds.; Springer Dordrecht Heidelberg New York London, 2012.
12. Haga, H.; Ohtsuka, T.; Matsuda, M.; Ashiya, M. Echosounding observations of coverage, height, PVI, and biomass of submerged macrophytes in the southern basin of Lake Biwa, Japan. *Limnology* **2007**, *8*, 95–102.
13. Madsen, J. D. Biomass Techniques for Monitoring and Assessing Control of Aquatic Vegetation. *Lake and Reservoir Management* **1993**, *7*, 141–154.
14. Mobley, C. D. Radiative Transfer in the Ocean. *Encyclopedia of Ocean Sciences: Second Edition* **2008**, 619–628.
15. Lee, Z.; Carder, K. L.; Mobley, C. D.; Steward, R. G.; Patch, J. S. Hyperspectral remote sensing for shallow waters. I. A semianalytical model. *Applied optics* **1998**, *37*, 6329–38.
16. Hamabata, E.; Kobayashi, Y. Present status of submerged macrophyte growth in Lake Biwa: Recent recovery following a summer decline in the water level. *Lakes and Reservoirs: Research and Management* **2002**, *7*, 331–338.
17. Hestir, E. L.; Khanna, S.; Andrew, M. E.; Santos, M. J.; Viers, J. H.; Greenberg, J. A.; Rajapakse, S. S.; Ustin, S. L. Identification of invasive vegetation using hyperspectral remote sensing in the California Delta ecosystem. *Remote Sensing of Environment* **2008**, *112*, 4034–4047.
18. Oyama, Y.; Matsushita, B.; Fukushima, T.; Matsushige, K.; Imai, A. Application of spectral decomposition algorithm for mapping water quality in a turbid lake (Lake Kasumigaura, Japan) from Landsat TM data. *ISPRS Journal of Photogrammetry and Remote Sensing* **2009**, *64*, 73–85.
19. Hale, G. M.; Querry, M. R. Optical Constants of Water in the 200-nm to 200-μm Wavelength Region. *Applied Optics* **1973**, *12*, 555.
20. Pope, R. M.; Fry, E. S. Absorption spectrum (380–700 nm) of pure water II Integrating cavity

measurements. *Applied Optics* **1997**, *36*, 8710.
21. Kou, L.; Labrie, D.; Chylek, P. Refractive indices of water and ice in the 0.65 to 2.5 μm spectral range. *Applied Optics* **1993**, *32*, 3531.
22. Gordon, H. R.; Morel, A. Y. *Remote Assessment of Ocean Color for Interpretation of Satellite Visible Imagery A Review*; Barber, R. T.; Mooers, C. N. K.; Bowman, M. J.; Zeitzschel, B., Eds.; Springer-Verlag New York Berlin Heidelberg Tokyo, 1983.
23. Ruddick, K. G.; Cauwer, V. De; Park, Y.-J.; Moore, G. Seaborne measurements of near infrared water-leaving reflectance: The similarity spectrum for turbid waters. *Limnology and Oceanography* **2006**, *51*, 1167–1179.
24. Babin, M. Variations in the light absorption coefficients of phytoplankton, nonalgal particles, and dissolved organic matter in coastal waters around Europe. *Journal of Geophysical Research* **2003**, *108*, 3211.
25. Gege, P. The water color simulator WASI: An integrating software tool for analysis and simulation of optical in situ spectra. *Computers and Geosciences* **2004**, *30*, 523–532.
26. Terrel, M. M.; Fukushima, T.; Matsushita, B.; Yoshimura, K.; Imai, A. Long-term light environment variability in Lake Biwa and Lake Kasumigaura, Japan: Modeling approach. *Limnology* **2012**, *13*, 237–252.
27. Watanabe, F. S. Y.; Imai, N. N.; Alcântara, E. H.; Rotta, L. H. da S.; Utsumi, A. G. Signal Classification of Submerged Aquatic Vegetation Based on the Hemispherical-Conical Reflectance Factor Spectrum Shape in the Yellow and Reg Regions. *Remote Sensing* **2013**, *5*, 1856–1874.
28. Liew, S. C.; Chang, C. W. Detecting submerged aquatic vegetation with 8-band WorldView-2 satellite images. In *Detecting submerged aquatic vegetation with 8-band WorldView-2 satellite images*; IEEE, 2012; Vol. 3, pp. 2560–2562.

USGS Earth Explorer (https://earthexplorer.usgs.gov/)
Japan Meteorological Agency (http://www.jma.go.jp/jma/index.html)
Weather Data (http://www.weatherandclimate.info/)

Chapter 4

MAPPING OF OPTICALLY ACTIVE COMPONENTS USING SATELLITE IMAGE

4.1 Water Quality of the South Basin of Lake Biwa

4.1.1 Introduction

In shallow lakes, the loss of submerged aquatic vegetation (SAV) is closely linked with the eutrophication [1,2]. The excessive nutrient loading primarily due the amplified anthropogenic activities adjacent to the natural environment of the lake, lead to the accelerated eutrophication eventually result in the ecological regime shift [2–4]. For instance, Lake Biwa experienced serious eutrophication problem in 1977, followed by the nutrient runoff from surrounding farmlands, man-made modification to attached lakes and the lake shores thereby resulted in degradation of natural environment in and around the lake. This elicited the significant decrease in native flora and fauna species in the lake. Following this, the Shiga Prefectural government enacted the Ordinance on Prevention of Eutrophication of Lake Biwa, which come into effect in 1980. Since then, the constant efforts has been made for pollution prevention in the lake, in cooperation with local residents [5]. Therefore, the regular long-term monitoring of the lake water quality is vital for the water quality conservation and maintaining the healthy freshwater ecosystem.

The conventional methods of water quality monitoring (e.g. boat survey) are typically time-consuming, expensive and frequently fail to account for the heterogeneity within the large water bodies [6]. Remote sensing technique constitutes an alternative means of estimating water quality, which allow the long-term monitoring and synoptic overview of the large lakes [7,8]. In the complex aquatic environment of the shallow lakes, the optical properties of water largely depend on the concentration and characteristic of suspended sediment, phytoplankton and dissolved organic carbon. The absorption and scattering characteristics of these optically active components in water, attenuates large portion of the incident light and thus restricts the light penetration to the bottom for vegetation growth [9–12]. For inland waters (Case 2 water), the water leaving reflectance is affected by the site-

specific factors mainly, the optically active components and geology of lakes. Therefore, site-specific relationships are generally developed using remote sensing for these types of water [13,14].

In this study, the water quality, primarily the dominant optically active components in the Lake Biwa were assessed and mapped using the Landsat-8 image. The parameters were mapped for the SAV growth period (September or October) from 2013 to 2016. The parameters estimated and mapped in this study are: 1) Chlorophyll-a (phytoplankton) and 2) Water Transparency

4.1.2 Water Quality of the Lake Biwa

On September 2, 2016 we surveyed total 13 observation points (only 8 located in south basin) along with LBERI, measuring the SAV biomass and stand height, Chl-a, Total Suspended Solids (TSS), DOC (mg/L) and water depth. The position of each survey points were recorded using a Global Position System (GPS) followed by the camera photographs of the sampled site. The experiment setup and equipment's used are shown in Figure 4.1.

Water samples were collected in the polyethylene bottle (at 0.2 m depth), and stored in the dark and cold box with ice while sampling. Samples were filtered immediately in the laboratory within 18 hours of sampling using 0.47μm of Whatman GF/F glass fiber filters. The samples were preserved with acid, for the measurements after 18 hours.

Before chlorophyll extraction, the samples were protected from the direct sunlight. The samples were filtered using glass filter at low pressure (<0.3 bar). For the extraction of the chlorophyll-a, the filters were immersed in the 94 % ethanol (C_2H_6O) into the extraction tube. The extraction tubes were left overnight in a dark and cold (refrigerator, temperature 4 °C). Next day the contents were mixed well and filtered again into a clean extraction tube. The 10 mm was used to measure the absorbance of chlorophyll at five different wavelengths, 630 nm, 645 nm, 663 nm, 665 nm, and 750 nm using the Spectrophotometer (Photolab® 6100 VIS Series) [15].

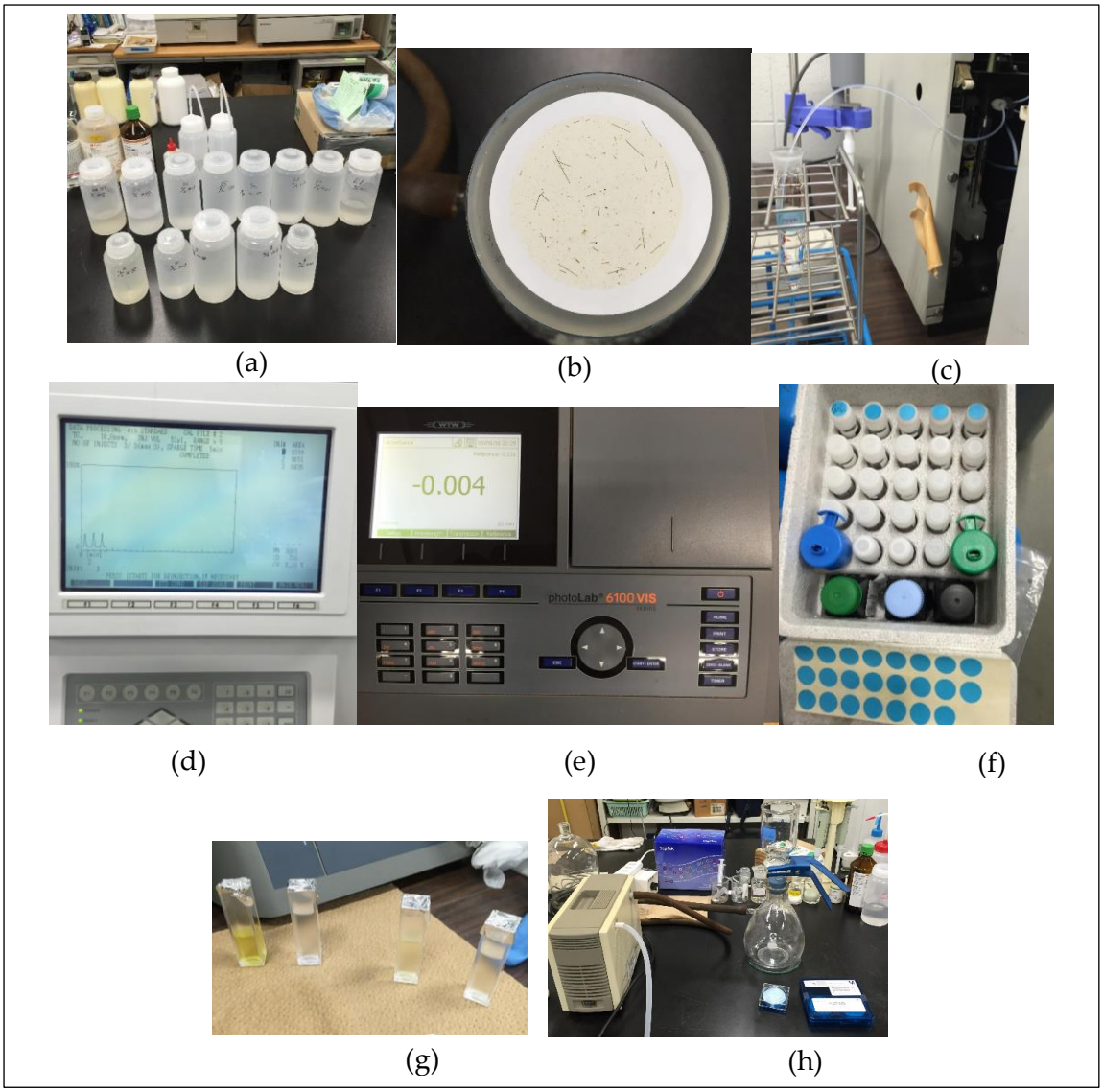

Figure 4.1. The experimental setup and equipment's used for the water quality samples collected in September 2016. The equipment's from top left: a) Water samples (2 L from each location), b) Suspended particulate matter after filtration (0.47µm of Whatman GF/F glass fiber filters), c) Measurement of DOC from TOC Meter, d) TOC Meter - Total Organic Carbon Analyzer, e) Spectrophotometer, f) Test kit for TP measurement, g) Cuvettes (10 mm) with extracted chlorophyll using ethanol, to measure using spectrophotometer, and h) Glass Filter.

Subsequently, TSS concentration was determined gravimetrically, by drying the Whatman GF/F filters at 103-104 °C for three hours. And subtracting the dried filter weight containing residue (200 ml of water sample) from the original filter weight. In addition, the DOC concentration was measured using the Total Organic Carbon (TOC) Analyzer (TOC-5000A, Shimadzu Kyoto, Japan) (Figure 4.2).

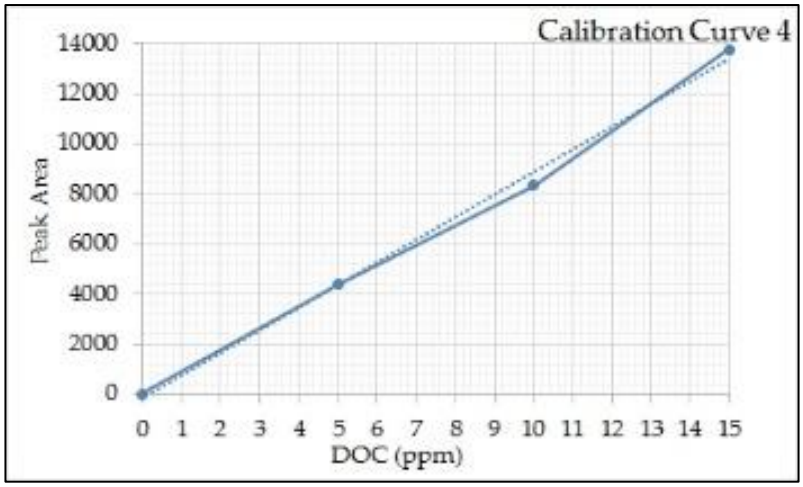

Figure 4.2. The DOC Calibration curve from the TOC Meter.

In September 2016, the observation data includes the deep north basin and the shallow eutrophic south basin (Table 4.1).

Table 4.1 Field observation of water quality parameters in the Lake Biwa for September, 2016

Locations	Water Depth (m)	Temperature (°C)	TP (mg/L)	Chlorophyll (μg/L)	TSS (mg/L)	DOC (mg/L)	Turbidity (NTU)
			South Basin				
Shinaoki	4.5	27.64	0.03	2.64	5.00	1.30	2.74
Katata	5.1	28.53	0.03	5.00	8.50	1.50	1.66
Karasumaoki	1.9	28.31	0.04	13.37	11.00	1.51	13.37
Karasumaguchi	1.7	27.37	0.05	29.75	15.79	1.67	24.89
Karasaki	4.2	29.66	0.04	21.37	10.50	1.35	4.84
Yanagasaki	1.7	34.43	0.04	12.92	9.47	1.35	10.08
Hayama River	0.9	28.02	0.05	47.82	18.00	2.13	28.47
			North Basin				
N4	90.0	-	-	1.26	0.50	1.20	0.63
HY90	88.0	-	-	0.15	0.20	1.20	0.58
N6	100.0	-	-	0.00	0.50	1.30	0.66
Ie	72.0	-	-	0.56	1.11	1.30	1.10
WN50	47.0	-	-	0.00	0.00	1.20	0.60

In addition, Non-Phytoplankton Suspended Sediment (NPSS) was calculated by subtracting concentration of phytoplankton suspended sediment (PSS) from TSS, whereas, PSS can be estimated by calculating the Organic suspended sediment (OSS) directly from the chlorophyll concentration, thus a relation between the two (PSS and Chlorophyll) were established and the NPSS was calculated [14]. The estimated NPSS concentration for the sampled locations in September 2016 is given in Table 4.2.

Table 4.2. The estimated PSS and NPSS concentration from the sampled locations in September, 2016.

Station	PSS	NPSS
Shinaoki	0.887	4.113
Katata	1.508	6.992
Karasumaoki	1.95	9.049
Karasumaguchi	2.80	12.988
Karasaki	1.863	8.637
Yanagasaki	1.681	7.438
Hayama River	3.193	14.807

As of September 2014 (the peak growth period of SAV), the average concentration of chlorophyll-a (Chl-a), suspended sediment (SS) and dissolved organic carbon (DOC) measured in the south basin is 10.9 µg/L, 1.1 mg/L and 1.5 mg/L, respectively. In the south basin, the phytoplankton dominated turbid water is commonly observed. The stations in the deep water area of the south basin (> 4 m) are mostly clear with low chlorophyll concentration (< 10 µg/L). Whereas, for shallow stations (< 3 m) located towards the outlet of the south basin and near the shore area, receiving the large nutrient loads from the draining rivers joining the basin. Thereby result in turbid water with high phytoplankton concentration (Figure 4.3).

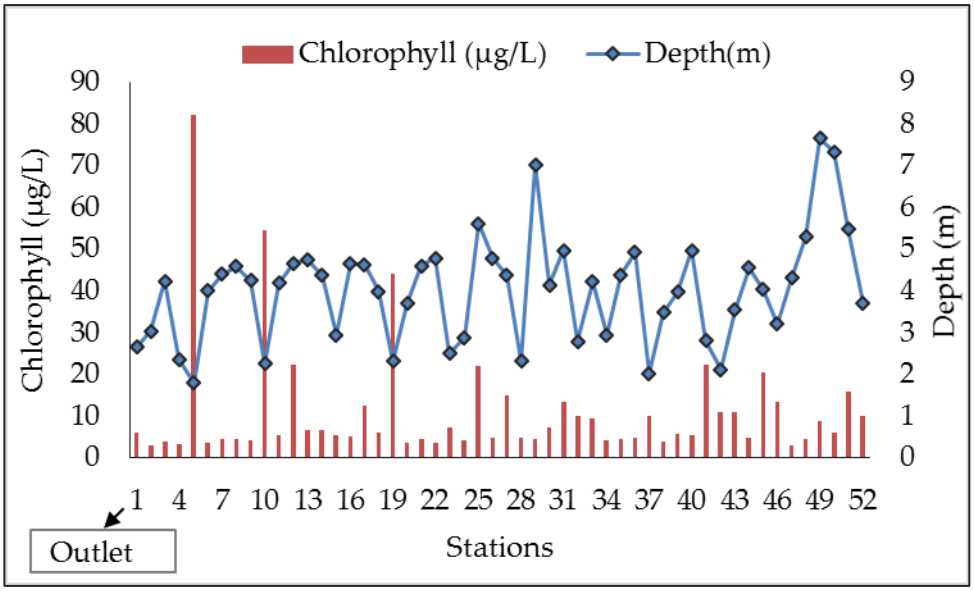

Figure 4.3. The chlorophyll concentration and water depth of 52 observation station located in the south basin (September, 2014).

In order to have greater clarity in terms of water quality parameters and growth of SAV, we performed a Principal Component Analysis (PCA) using the statistical software R, on the September 2016, observation data. PCA is the non-parametric method of classification which

makes no assumption about the underlying distribution of data [16]. The first two components in PCA explains 95% of total variation, where the first principal component (SAV) explain the clear and SAV dominated stations and second principal component represent the stations with chlorophyll and TSS dominated turbid water (Figure 4.4).

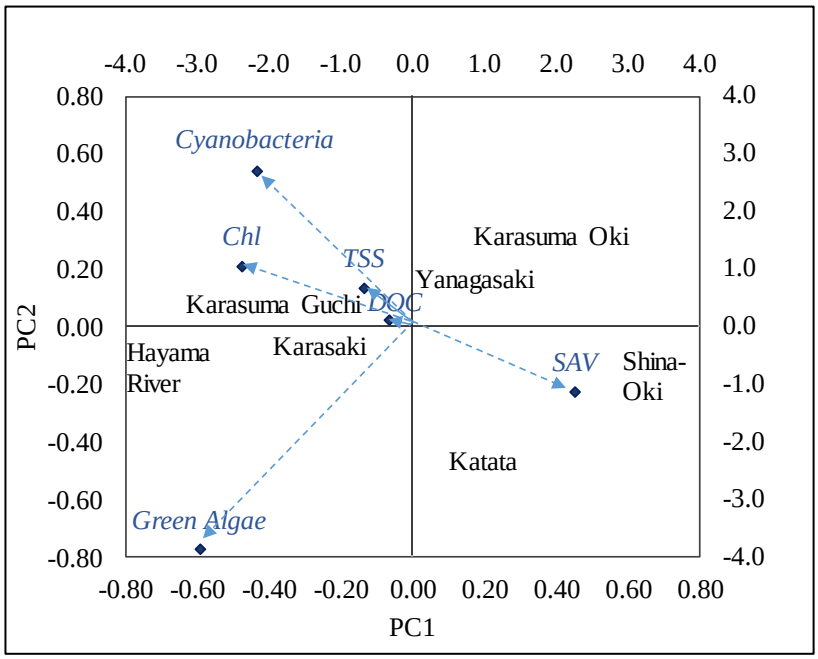

Figure 4.4. PCA loadings of based on the five water quality parameters and SAV in the south basin (September, 2016).

In addition, the stations with high SAV biomass mainly positively explained by the PC1, such as Shinaoki and Katata. On the other hand, the turbid water stations are mainly explained by PC2. In contrast, the stations, such as Hayama River is highly turbid, however not positively explained by PC2, this is because of the presence of Green Algae and some floating vegetation at Hayama River. The floating vegetation was also noted during the sampling in September 2016 (Figure 4.5).

Figure 4.5 The floating vegetation at the Hayama River station during September 2016 sampling.

Furthermore, the nutrient richness and shallow depth of the south basin also supports the prolific growth of SAV species. In recent years, the SAV in the basin recovered and this result in the stable-state of macrophyte-dominated clear water [3,17–19]. In addition the rapid invasion by the alien SAV species was also noted in the basin [18]. In particular, the abundance of SAV is commonly appear in clear deep waters of south basin, with some aggressive and tolerant species also found in turbid water area. Recently, the prolific growth of SAV resulted in the expanded coverage area of 90% of the south basin with increased biomass [18]. The SAV biomass with water depth in the south basin as measured in September, 2014 in shown in Figure 4.6. Figure 4.6 shows clearly shows that at the deeper water the growth of SAV significantly reduces, except in the case where the deep water stations are located near the shoreline, such as station 40 and 41.

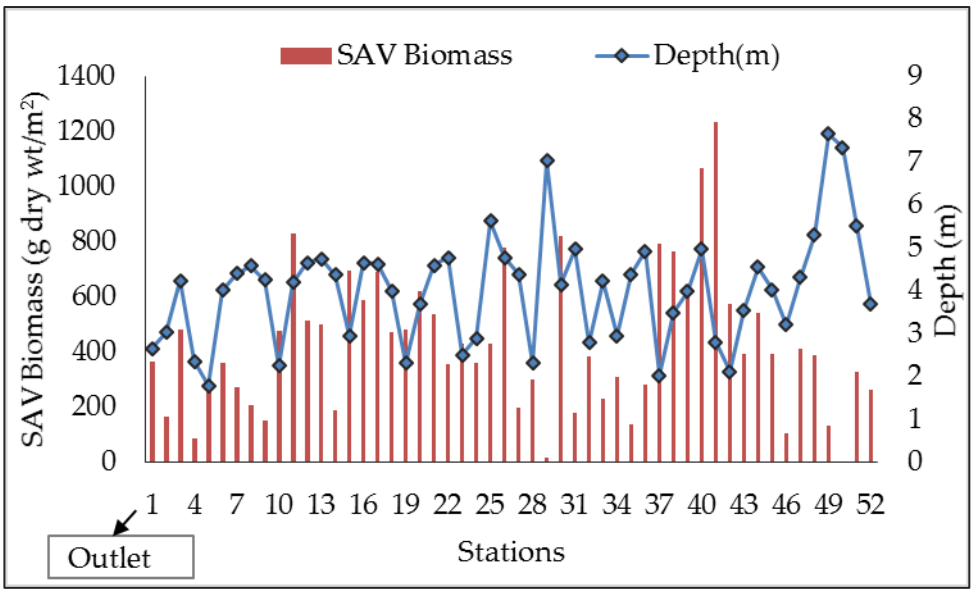

Figure 4.6 The SAV biomass and water depth of 52 observation station located in the south basin (September, 2014).

4.2 Satellite Image Processing and Rectification

The imagery from Landsat-8 Operational Land Imager (OLI) satellite was acquired for the peak growth period of SAV in the Lake Biwa, mainly in September or October each year (2013-2016). Because a cloud-free image for September 2013 was not available therefore 1st October 2013 image was used as an image representing the SAV growth period, in this study. Downloaded images were essentially based on survey time, geographical extent and environmental conditions (cloud-free and wind speed < 3 m/s), obtained from U.S. Geological Survey (USGS) EarthExplorer (https://earthexplorer.usgs.gov/). Image rectification and geo-processing were achieved using ENVI 5.2 image analysis software and ArcMap 10.3.1. Apart from rescaling to Top of Atmosphere (TOA) reflectance, the images were corrected for radiometric distortions (mainly atmospheric correction) using the mid-latitude summer atmospheric model and maritime aerosol model in the atmospheric correction module FLAASH of ENVI 5.2. Horizontal visibility of the study area was obtained for the closest stations (Kyoto and Hikone) from the Japan Meteorological Agency (http://www.jma.go.jp/jma/index.html) and also referred from the weather and climate data info website (http://www.weatherandclimate.info/), varies from 16 km to 25 km, for the month of September (2013-2016). The water area from the images was masked for aquatic vegetation classification and mapping. In addition, due to the changes in the sensor and atmospheric conditions over time, the satellite images of the different time period may result

in different pixel values. To account for these changes, and to apply the developed technique to other satellite data, the image normalization was performed for 2013, 2015 and 2016 images (September 2014 atmospherically corrected image as the reference image), using the relative radiometric normalization technique following Elvidge *et al*. 1995 and Oyama *et al*. 2009.

4.3 Development of Chlorophyll-A Estimation Model using Satellite Image

Owing to the limited data availability for the water quality parameters matching with satellite acquisition time, in the south basin of Lake Biwa. In this study, we tried to develop the model based on the new spectral decomposition algorithm, to estimate the water quality parameters, mainly chlorophyll. The algorithm is taking into account the bottom albedo, as south basin has > 90% of the basin (the bottom substrate) covered with SAV bed [19]. More importantly, to classify the submerged vegetation in the lake water, the water quality information is essential to distinguish between the turbid and clear water pixels. Therefore, we first estimated the chlorophyll using the September 2014 (52 observation points), for the year 2013, 2015 and 2016. Since, in September 2016, we have only eight locations surveyed in the south basin, therefore, we tried to calculated chlorophyll for the whole image in the same. The NPSS could not be estimated using the satellite image because of insufficient NPSS data available for any of the year under analysis, to develop a NPSS estimation model. Nevertheless, the average monthly TSS data for few location was available, which is not sufficient but the data along with the September 2016 data was used to confirm the range of suspended sediment and NPSS concentration in the south basin of the Lake Biwa. The details of the spectral decomposition algorithm is given below.

4.3.1 Spectral Decomposition Algorithm (SDA)

In order to estimate the concentration of optically active components, a new spectral decomposition algorithm (SDA) was developed in the shallow basin of the Lake Biwa. This approach is based on the similar work done by Oyama et al., 2009, 2007. In SDA approach, the mixed reflectance spectra of a given pixel is conceptualize as a linear combination of key endmembers substantially contributing to the pixel reflectance. For this study, the four main endmembers were selected based on the dominance of the endmembers in the lake, they are: a) phytoplankton (i.e., Chl-a concentration); b) Non-phytoplankton suspended solids (NPSS);

c) water and d) SAV. Since, the observed concentration of DOC at the stations in the lake Biwa is < 3 mg/L, we assumed it's effect significantly low and hence not been considered as a potential endmember in this study. Furthermore, the shallow south basin of Lake Biwa has over 90% of the bottom covered with SAV along with their large biomass, which can potentially affect the pixel reflectance, and is likely to be confused with the other algae reflectance, therefore unlike previous studies where the bottom substrate reflectance was neglected, we included SAV as an important endmember for this study. The mixed pixel spectra can be expressed as in Equation 4.1.

$$R(\lambda) = a_p \times R_p(\lambda) + a_n \times R_n(\lambda) + a_v \times R_v(\lambda) + a_w \times R_w(\lambda) \quad (4.1)$$

Where a and R indicates the decomposition coefficient and standard reflectance spectra (spectral signature) of potential endmember. While, indexes p, n, v and w represents phytoplankton, NPSS, SAV and water, respectively. Respective decomposition coefficients were directly related to the concentration of relative endmember or the endmember biomass (for endmember SAV). The four decomposition coefficients were calculated by selecting four Landsat-8 bands (Equation 4.2 to 4.5).

$$R(\lambda_1) = a_p \times R_p(\lambda_1) + a_n \times R_n(\lambda_1) + a_v \times R_v(\lambda_1) + a_w \times R_w(\lambda_1) \quad (4.2)$$

$$R(\lambda_2) = a_p \times R_p(\lambda_2) + a_n \times R_n(\lambda_2) + a_v \times R_v(\lambda_2) + a_w \times R_w(\lambda_2) \quad (4.3)$$

$$R(\lambda_3) = a_p \times R_p(\lambda_3) + a_n \times R_n(\lambda_3) + a_v \times R_v(\lambda_3) + a_w \times R_w(\lambda_3) \quad (4.4)$$

$$R(\lambda_4) = a_p \times R_p(\lambda_4) + a_n \times R_n(\lambda_4) + a_v \times R_v(\lambda_4) + a_w \times R_w(\lambda_4) \quad (4.5)$$

The equations were solved using the above four equation in R statistical computing software. Each decomposition coefficients were used independently along with their respective endmember, to develop a chlorophyll estimation model using regression analysis. The algorithm thus separates the information of each endmember in two parts, which is the mass and spectral signature of endmembers. Therefore, to estimate the chlorophyll, a relation between the endmember decomposition coefficients and their respective mass was established as shown in Equation 4.6 and 4.7.

$$C_p = f(a_p) \quad (4.6)$$

$$C_n = f(a_n) \quad (4.7)$$

Where, C_p and C_n correspond to the mass information of the endmembers (i.e. concentration) of the phytoplankton and NPSS, respectively.

4.3.2 Standard Reflectance Spectra (SRS) Simulation for Endmembers

The standard reflectance spectra (SRS) is the unique spectral signature or characteristic of the individual endmember. In order to prepare the satellite SRS several different methods have been proposed such as, tank experiment for SRS measurement using the spectroradiometer for individual components [21]. However, the reflectance spectra measured by the tank experiment does not truly represent the reflectance spectra from the actual lake environment primarily due to the limitation of the experimental boundary conditions (e.g. tank size, variability of a natural environment and effect of illumination condition). On the other hand, the manual selection of endmember SRS from spectrally pure pixels identified from the MNF (minimum noise fraction) transformed bands of the satellite image suggested by Tyler et al., 2006. However, in spectrally complex and eutrophic shallow basin of the Lake Biwa, where the bottom reflectance significantly influence the pixel reflectance, it was difficult to identify the spectrally pure pixel with confidence.

To apply the spectral decomposition algorithm to satellite image, initially, we also tried to derive the SRS of each endmember from the image itself. However, due to the mixed pixel reflectance, particularly in shallow turbid water, identifying the spectrally pure pixel for phytoplankton and NPSS reflectance was not possible. Because the turbid water area with high phytoplankton concentration often has high suspended solids concentration (as is the case in the south basin of Lake Biwa). Therefore, for this study, we simulated the endmember spectra using the Bio-Optical model proposed by Lee et al., 1998, similar to the work of Oyama et al., 2009. The details of the Bio-Optical model is given in Chapter 3.

The Satellite SRS for the respective endmembers were simulated using the Bio-Optical model based on the following conditions;

a) Chlorophyll SRS: when NPSS = 0 mg/L, cDOM = 0 mg/L and chlorophyll = 120 μg/L;

b) NPSS SRS: when NPSS = 100 mg/L, cDOM = 0 mg/L and chlorophyll = 0 μg/L and different water depth using Bio-Optical model (Figure 4.7).

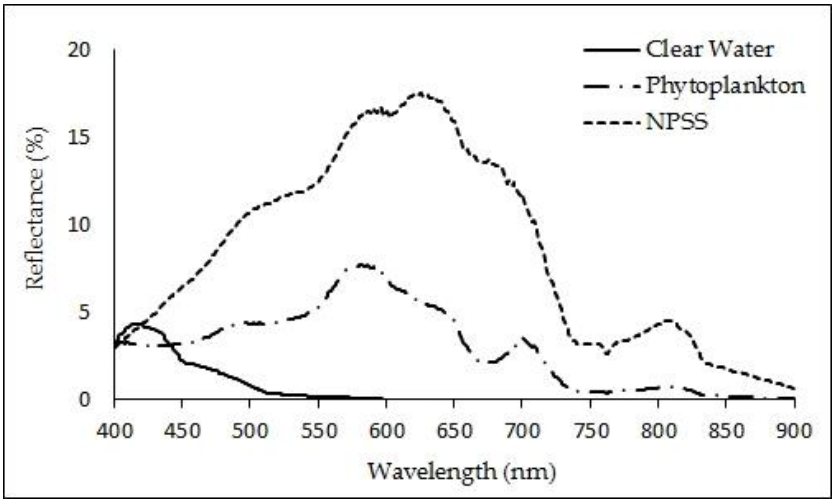

Figure 4.7. Simulated standard spectra of optically active components using the Bio-Optical model.

The SAV reflectance (measured without water using Spectroradiometer in lab) was then simulated at different water depths (0.1 m to 2 m) using Bio-Optical model, before selecting the standard reflectance spectra. However, the SAV spectra simulated at minimum water depth (0.1m) was chosen as the standard reflectance spectra for SAV, as the water attenuation at 0.1 m is significantly lower than other (>0.1 m) water depths (Figure 4.8).

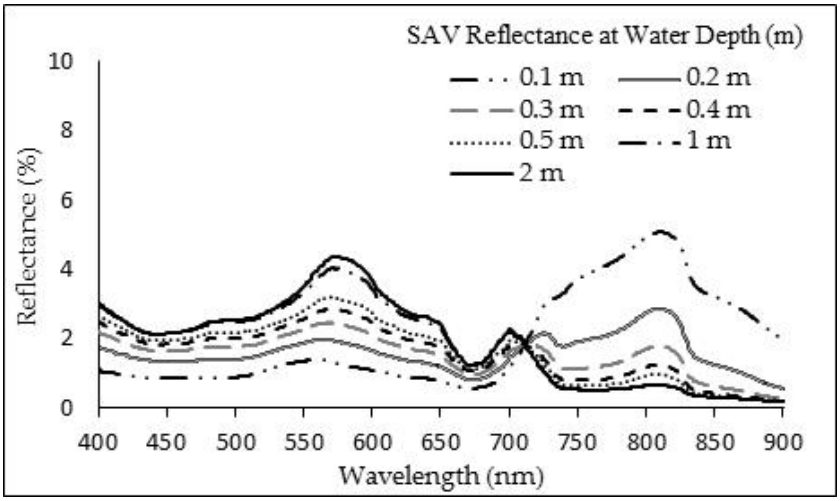

Figure 4.8. Simulated standard spectra of SAV at different depth, using the Bio-Optical model.

The chlorophyll estimation model developed using the different Landsat-8 OLI band combination is shown in Table 4.3. The relation between the observed chlorophyll and decomposition coefficient of chlorophyll (a_p) is shown in Figure 4.9. The chlorophyll model gave the best result (R^2 = 0.83, significance at p <0.001) is given in Equation 4.8.

$$C_{chl} = 35.143 - 80.334 * a_p + 54.172 * a_p^2 \quad (4.8)$$

Table 4.3 Chlorophyll estimation model obtained from different band combination based on Spectra Decomposition Algorithm.

OLI Bands	Chlorophyll - Model	R^2	p	F	SE	RMSE
1234	-34.38443 + 51.52432* a_p	0.57	<0.01	52.37	4.55	
	121.68358 - 295.541*a_p +187.546*a_p^2	0.89	<0.01	118	2.63	9.34
1245	-17.069 + 30.790* a_p	0.64	<0.01	72	4.13	
	35.143 -80.334 * a_p + 54.172 *a_p^2	0.83	<0.01	124	2.58	**8.71**
	0.671*$e^{0.0195*a_p}$	0.51	<0.05			
1345	51.524 * a_p -12.860	0.57	<0.01	52	4.55	
	30.951 -138.847 * a_p + 187.546 * a_p^2	0.80	<0.01	118	2.63	8.86
2345	4.898 + 1.215 * a_p	0.74	<0.01	294	2.39	
	5.291 + 0.664 * ap + 0.020 * a_p^2	0.81	<0.01	158	2.32	9.87
	0.258*$e^{0.1192*a_p}$	0.52	<0.01			

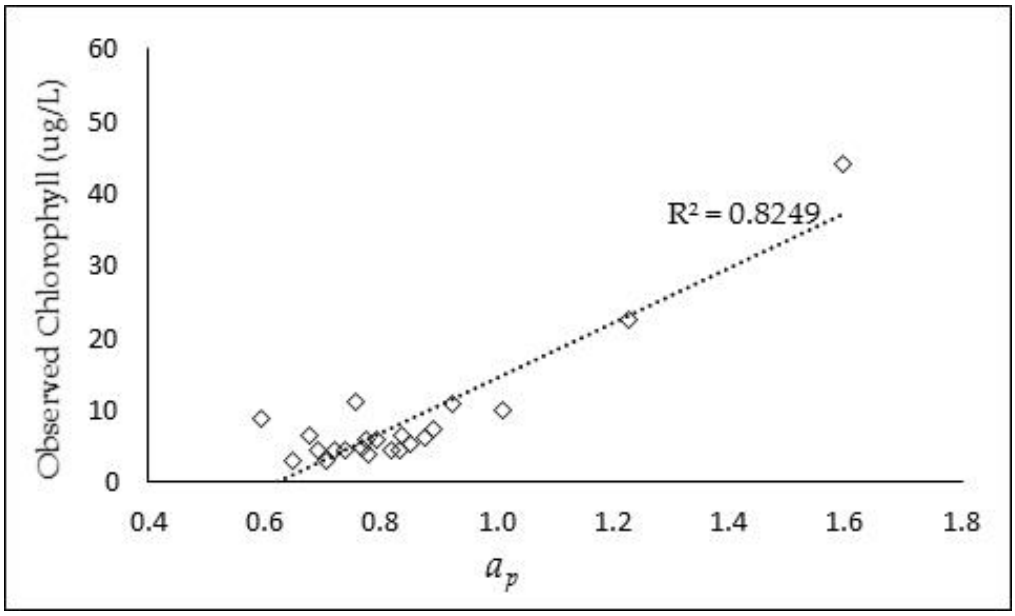

Figure 4.9 Relationship between chlorophyll and a_p .The data includes September, 2014 (N = 23).

The chlorophyll was estimated using the SDA- based approach was then validated using the in-situ measured chlorophyll for September, 2014. The Landsat-8 band 1, 2, 4, and 5 gave the best result (R^2 of 0.78) when compared between the observed and simulated chlorophyll

(Figure 4.10). The model results were evaluated with the Root Mean Square Error (RMSE) value which is 8.71, for this model.

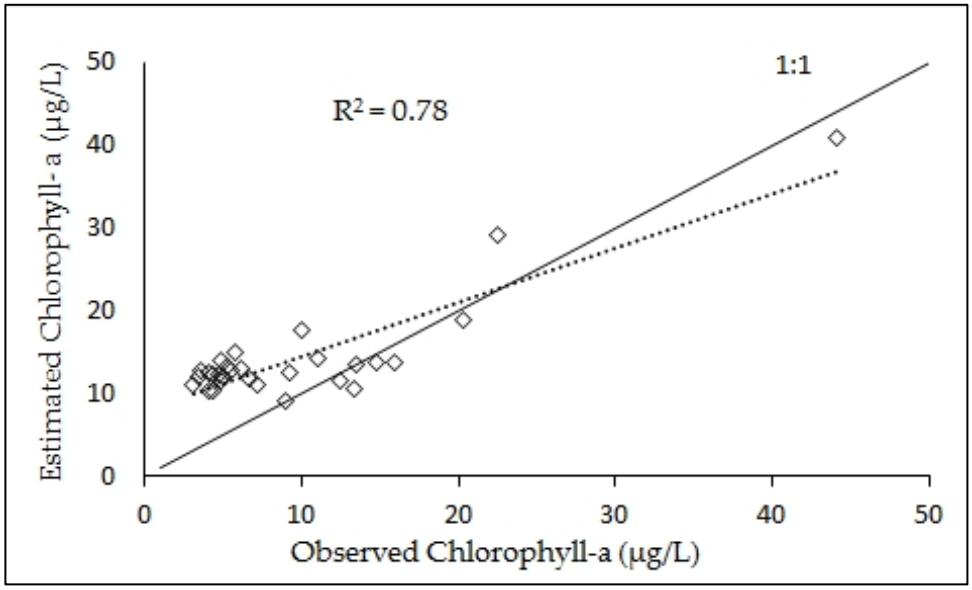

Figure 4.10 The comparison between SDA-based estimation of the chlorophyll and *in-situ* measured chlorophyll (N = 29) for September, 2014.

The calculated RMSE for the range of chlorophyll concentration estimated for September 2014 is shown in Table 4.4.

Table 4.4. Estimated RMSE between observed and satellite-derived chlorophyll for September 2014.

Chlorophyll	Absolute Error	RMSE	N
0 – 10 (µg/L)	6.78	7.12	20
10 – 20 (µg/L)	12.94	1.30	6
20 – 40 (µg/L)	2.60	2.02	2
40 – 60 (µg/L)	3.32	3.32	1

The calculated results indicate slight overestimation at low chlorophyll concentration with the overall RMSE of 7.12 µg/L. And slightly underestimated at high concentration with an RMSE of 3.32 µg/L. However, the overall RMSE obtained was 6.15 µg/L.

The validated chlorophyll model was then applied on the normalized Landsat-8 satellite image for September 2016, to estimate the chlorophyll. The estimated chlorophyll for September 2016 was than compared with the *in-situ* measured data in the south basin. The overall RMSE of 6.28 is achieved for the measured locations are shown in Table 4.5.

Table 4.5. Estimated RMSE between observed and satellite-derived chlorophyll for September 2016.

Sampled locations (September 2016)	Observed Chlorophyll (μg/L)	Satellite-Derived Chlorophyll (μg/L)	Absolute Error	Relative error (%)
Shinaoki	2.64	3.43	0.79	29.9
Katata	5.00	1.64	3.35	18.7
Yanagsaki	12.915	14.26	1.34	10.4
Karasaki	21.37	24.34	0.99	4.6
Karasumaguchi	29.75	24.35	5.40	18.1
Hayama River	47.82	33.48	14.34	45.6
Karasumaoki	13.37	8.16	5.20	38.9
Overall RMSE				6.28 μg/L

The model gave the good result for the September 2016 image. Afterwards the chlorophyll model was applied to October 2013 and September 2015 image for chlorophyll estimation. The generated chlorophyll maps from four images of different year (2013-2016) using chlorophyll estimation model are shown in Figure 4.11.

The satellite-derived chlorophyll map shows that the year 2014 was relatively clear water where most of the basin area has chlorophyll concentration < 30 μg/L whereas 2013 and 2016 appears to be comparatively turbid than other years, particularly towards the eastern shoreline and the outlet of the basin (> 30 μg/L).

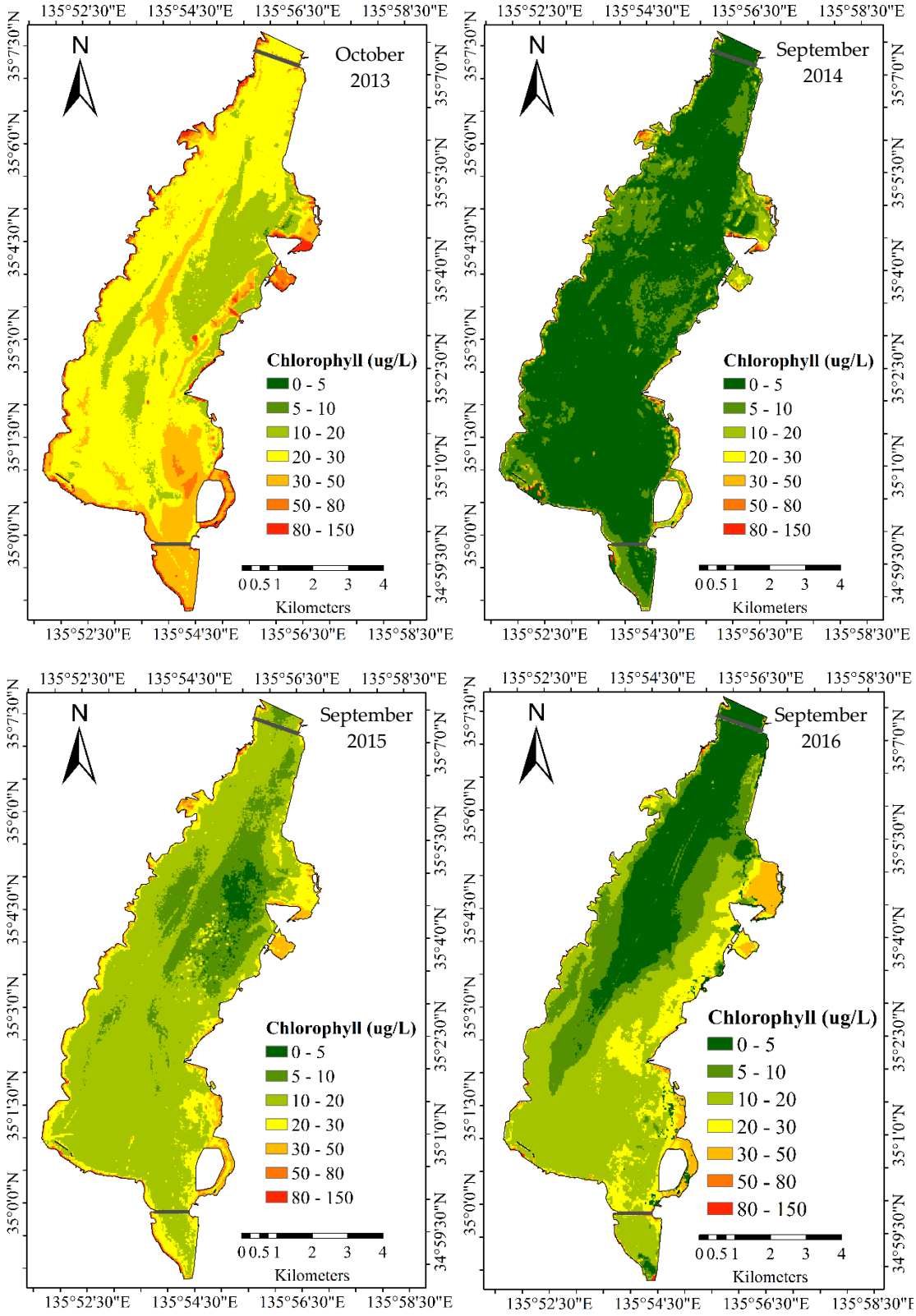

Figure 4.11 The distribution map of chlorophyll for 2013 (October), 2014 (September), 2015 (September) and 2016 (September).

4.4. Development of Transparency Estimation Model using Satellite Image.

After chlorophyll estimation, we tried to identify or map the water transparency depth, to understand the water clarity of the south basin before SAV classification. To map the extent of SAV, their reflectance must cross the air-water interface which is often hindered by the absorption and scattering processes of the OAC in the water column and the depth from water surface to the plant canopy. In addition, the presence of OAC potentially diminish the Water Transparency (WT), in shallow lakes. Nevertheless, if SAV lies within the optical depth range and significantly contributing to the water leaving reflectance, then it is likely to map the distribution of SAV using satellite image [24,25]. Therefore, in this paper, we first generated the water transparency map before estimating the SAV coverage and biomass for the eutrophic south basin of the Lake Biwa.

4.4.1 Water Transparency Retrieval Algorithm

The relation between shallow and deep water radiance can provide the optical depth information in a lake [26]. Whereas, the combination of two or more bands can contribute to the bottom albedo correction as well as in determining the water depth [27,28]. Therefore, to estimate the water clarity, using the similar approach a linear relation between the observed water transparency (October 2013) and the depth invariant reflectance of Landsat-8 bands was established, which is given by Equation (4.9) and (4.10):

$$Z_{WT} = a + b_i(X_i) + b_j(X_j) \tag{4.9}$$

Where,

$$X = ln[R_C(\lambda) - R_\infty(\lambda)] \tag{4.10}$$

In this study, the two band combination gave the best result. The indices i and j represents green and red band; a, b_i and b_j are the constants determined by multiple linear regression whereas, R_C and R_∞ imply the Landsat-8 corrected water leaving reflectance and optically deep water reflectance, respectively. To obtain the deep water reflectance we identified the pixel (minimum pixel value) located in relatively clear and deep water area based on the bathymetry map and the survey information. Subsequently, the minimum pixel value using the Near-Infrared (NIR) and Shortwave-Infrared (SWIR) reflectance bands were also

confirmed for the same area. [26,28,29]. The multiple regression model with the band combination that gave the good fit (R^2 = 0.72, significance at p <0.001, standard error = 0.38 m) with the observed water transparency data is given in Equation (4.11):

$$Z_{WT} = -2.890 + 0.183 * ln\left[\left(R_{green} - R_{\infty}\right)\right] - 1.299 * ln[R_{Red} - R_{\infty}] \quad (4.11)$$

Out of 95 observed water transparency points, we used 54 for the result validation. The observed and satellite-derived water transparency appears to be in good agreement with R^2 = 0.77 significance at p <0.001 with an overall RMSE of 0.38 and relative error of 11% (Figure 4.12).

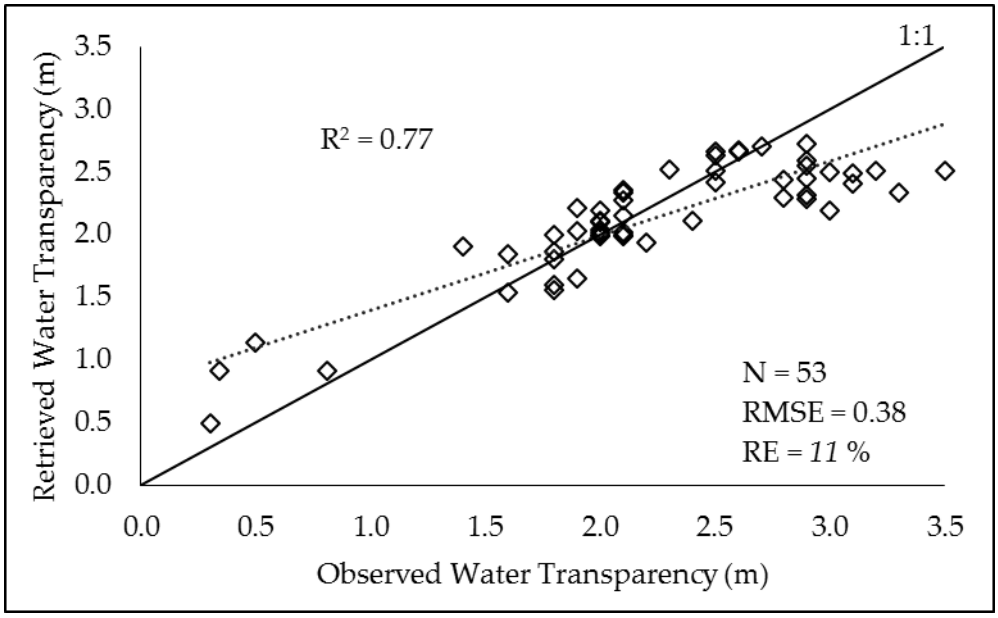

Figure 4.12 Observed and retrieved (satellite-derived) water transparency in the south basin of Lake Biwa (October 1, 2013).

The validated model was then used to retrieve the water clarity information from other satellite images, September 2014, 2015 and 2016 (Figure 4.13). The satellite-derived water transparency maps indicate the improved water clarity in the year 2014 and 2015.

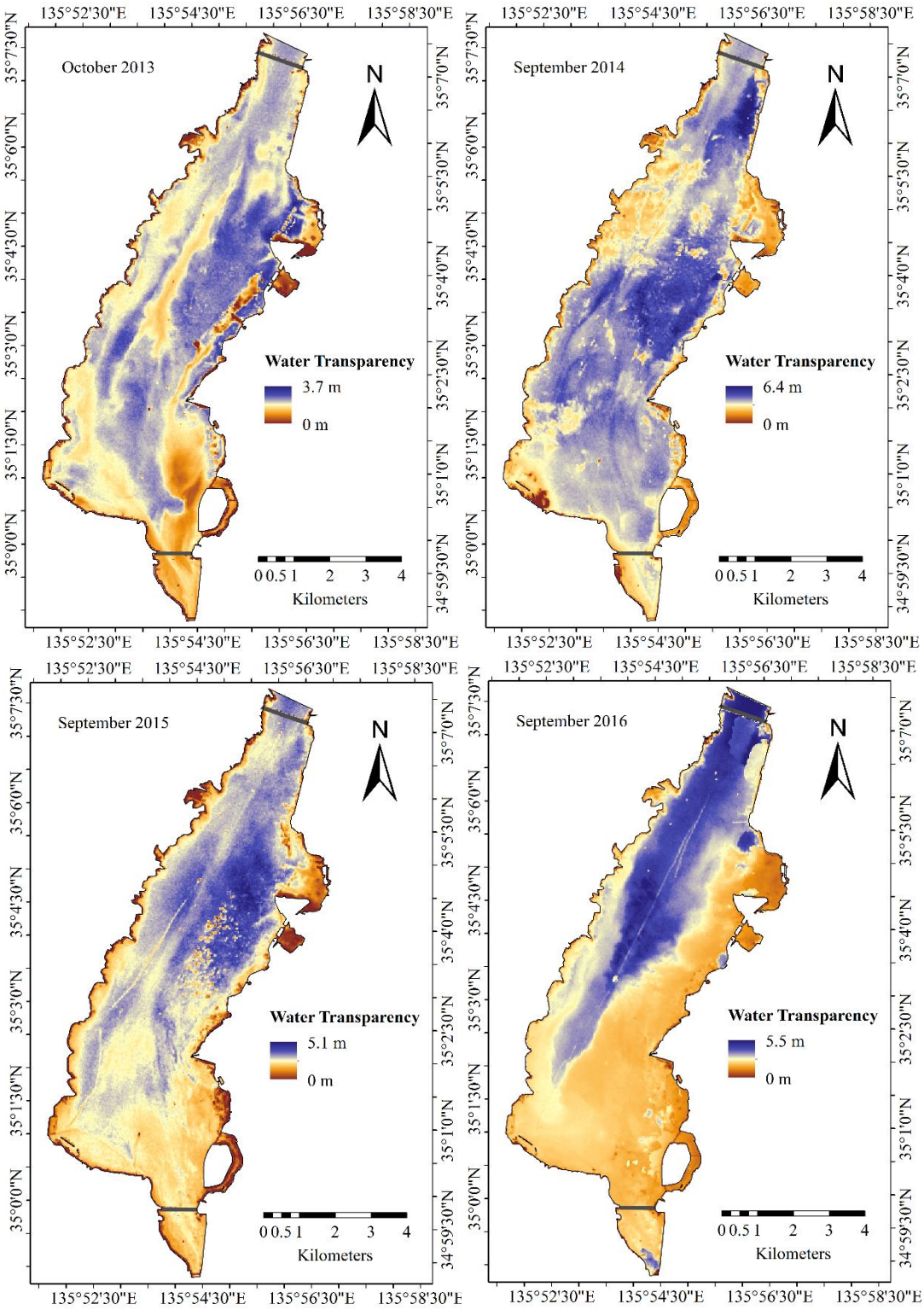

Figure 4.13 Satellite-derived water transparency map of the south basin, for October 2013, September 2014, 2015 and 2016.

In 2013, based on the ground truth data the overall RMSE and absolute error estimated for the 54 validation points in the south basin was 0.38 m and 0.28 m, respectively. Table 4.6

show the accuracy assessment for the range of water transparency derived from the satellite image, in the south basin.

Table 4.6 Accuracy assessment of satellite-derived water transparency with *in-situ* data (October, 2013), for the south basin of Lake Biwa.

Water Transparency (m)	RMSE	Absolute Error	N
< 1	0.44	0.38	4
1 - 2	0.24	0.20	11
2 - 3	0.25	0.19	32
>3	0.77	0.75	7

Furthermore, we calculated the area with water transparency <=1.5 m, between >1.5 m to <3.0 m, and => 3.0 m. In 2016 and 2013, the area with water transparency > 3.0 m is only 15% (8 km^2) and < 1% (1 km^2) respectively, whereas in 2014 it is 54% (28 km^2) of the basin area (Table 4.7). Moreover, the area with water transparency < 1.5 m increased in 2016 (14 km^2), when compared with the remaining years (i.e., only 3 km^2). Although, 92% of the basin area in 2013 has the water transparency between 1.5 m to 3 m, the maximum water transparency retrieved is the lowest with 3.7 m than 2014 (6.4 m), 2015 (5.1 m) and 2016 (5.5 m). In 2014 and 2015, more than 30% of the basin area has water transparency >3 m which indicates a relatively clear water state [30] when compared with other years. A slight overestimation of water transparency was noted particularly for the area with water transparency < 1 m. However, in almost all the years, the reduced water clarity was obtained in two particular conditions, the location with high turbidity and where the vegetation emerge out of the water surface. The estimated average water transparency for all years based on 52 stations are 2.2 m (October 2013), 2.9 m (September 2014), 2.6 m (September 2015) and 2.0 m (September 2016).

Table 4.7. Satellite-derived water transparency of the south basin of Lake Biwa (2013-2016).

Water Transparency (m)	Area (km^2)			
	2013	2014	2015	2016
(<= 1.5)	3	3	3	14
(> 1.5 to < 3.0)	48	21	31	30
(=> 3.0)	1	28	18	8

4.5. Result Discussion and Conclusion

4.5.1 Discussion

This study explained the water quality condition of the south basin of the Lake Biwa, based on the *in-situ* measurements and empirical model estimation. The recent observation in September 2016 indicates shows that the basin has increased turbidity (mainly chlorophyll-a and TSS) near the shoreline in the east. Mostly SAV species in the basin grow in the locations with optically clear water, and at the water depth where the light penetration is sufficient (Figure 4.3 and 4.6). For inland waters (Case 2 water), the water leaving reflectance is affected by site-specific factors mainly the optically active components and geology of lakes. Therefore, site-specific relationships are needed between satellite image reflectance and the optically active components

The satellite-derived chlorophyll is in good agreement with the observed chlorophyll in September 2016 and 2016, with an overall RMSE of 6.15 and 6.28 µg/L, respectively. The result indicate the turbid water condition in 2013 and 2016 when compared with 2014 and 2015. The result correspond well with the available data from LBERI data. Furthermore, the estimated chlorophyll match well with the water clarity information for all the year (2013-2016) using the water transparency retrieval algorithm (Figure 4.14).

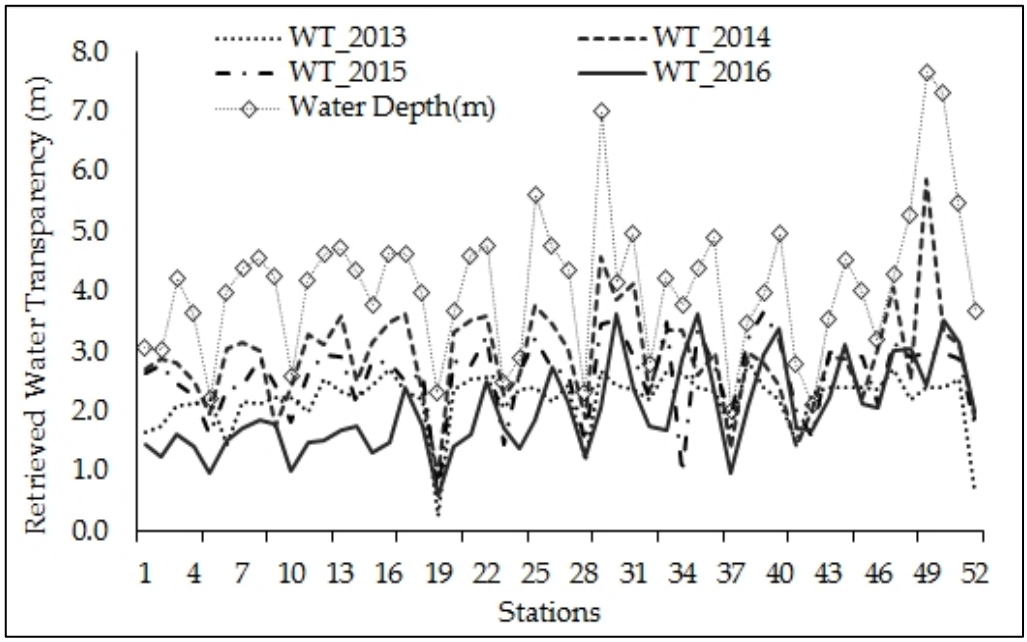

Figure 4.14. Retrieved water transparency from 52 locations (2013-2016) in the south basin of Lake Biwa.

The estimated water transparency for each year confirm the turbid water condition in 2013 and 2016 with decreased water transparency data. Whereas, the water transparency increased in 2014 and 2015 indicates relatively clear water condition than other years.

Owing to the time difference of ±5 days in the observed water transparency data and Landsat-8 image acquisition time, a good agreement between the two was not expected. However, the verified result seems acceptable with $R^2 = 0.77$ using band 3 (532-590 nm) and band4 (635-673 nm) (Table 4.5). The result correspond to the previous work where the wavelength range of 520-600 nm was determined as most suitable for water transparency monitoring in inland waters [32]. According to the previous work [19], the average water transparency estimated for July, August and September of 2003, in the south basin was 2.3 m, 3.3 m, and 3.1 m, respectively. The average water transparency derived from satellite image (Figure 4.13) in this study ranges between 2.0 m to 2.9 m for September (2014-2016), which is analogous to the aforementioned work for the same basin. The developed algorithm are successfully applied to estimate the water transparency and chlorophyll.

4.5.2 Conclusions

The in-field water quality (2016) data of the southern basin of Lake Biwa was collected and measured in the laboratory and then used for the analysis. The new spectral decomposition algorithm which is taking in to account the bottom albedo, was successfully applied to estimate the chlorophyll-a concentration ($R^2 = 0.78$) from the Landsat-8 satellite image, for the peak SAV growth month (i.e., September, October). Which also suggests that bottom reflectance is an important endmember contributing to the water leaving reflectance in a shallow lake. The algorithm was used to develop a chlorophyll estimation model using the satellite image. The estimated chlorophyll using the satellite image corresponds well with the observed data (2014 and 2016) which gives the overall RMSE of 6.15 and 6.28 μg/L. The satellite-derived chlorophyll map shows the increased chlorophyll concentration in the 2013 and 2016, indicating the turbid water condition (> 30 μg/L), particularly towards the eastern shoreline and the outlet of the basin.

Furthermore, the water transparency retrieval algorithm developed using the depth-invariant reflectance of the satellite image (RMSE = 0.38, RE = 11%), also suggests the decreased water clarity in the eastern and southern side of the basin in 2013 and 2016 (Figure

4.14). The satellite-derived maximum water transparency, 6.1 m and 5.1 m for 2014 and 2015 indicate a clear water condition, whereas the opposite was true for 2013 and 2016. The average water transparency derived from satellite image range between 2.0 m to 2.9 m, for September (2014-2016), correspond well with the LBERI research for the same basin.

The developed new spectral decomposition algorithm can be applied for water quality monitoring for a shallow lake, if the appropriate endmembers are selected and their absorption and scattering properties are known specific to a study area. On the other hand, the developed model compared to the conventional model is less sensitive to geographical and environmental variability, since the optical properties are simulated using the Bio-Optical model validated with *in-situ* measurement. However, sufficient *in-situ* measured data matching the satellite overpass time is essential for the robust application of the developed model. However, this study gives the clear picture of the changing water quality condition of the basin indicating the turbid and less turbid areas. The obtained results are informative and are useful to distinguish the turbid and water pixels from clear water and SAV, before mapping the SAV using satellite image.

References

1. Phillips, G.; Willby, N.; Moss, B. Submerged Macrophyte decline in shallow lakes : What have we Learnt in the Last Forty Years ? *Aquatic Botany* **2016**, *135*, 37–45.
2. Scheffer, M.; Carpenter, S.; Foley, J. A.; Folke, C.; Walker, B. Catastrophic shifts in ecosystems. *Nature* **2001**, *413*, 591–596.
3. Ishikawa, K.; Haga, H. Ecological Regime Shift in the South Basin of Lake Biwa : Focus on Algal Blooms and Submerged Macrophyte Overgrowth. In *UNESCO International Symposium on Scientific, Technological and Policy Innovations for Improved Water Quality Monitoring in the Post-2015 SDGs Framework*; Kyoto, Japan, 2015; pp. 1–3.
4. Zhang, S. Y.; Liu, A. F.; Ma, J. M.; Zhou, Q. H.; Xu, D.; Cheng, S. P.; Zhao, Q.; Wu, Z. Bin Changes in physicochemical and biological factors during regime shifts in a restoration demonstration of macrophytes in a small hypereutrophic Chinese lake. *Ecological Engineering* **2010**, *36*, 1611–1619.
5. *Lake Biwa: Interactions between Nature and People*; Kawanabe, H.; Nishino, M.; Maehata, M., Eds.; Springer Dordrecht Heidelberg New York London, 2012.
6. Khorram, S.; Chishire, H.; Geraci, A. L.; Rosa, G. LA Water quality mapping of Augusta Bay, Italy from Landsat-TM data. *International Journal of Remote Sensing* **1991**, *12*, 803–808.
7. Hellweger, F. L.; Schlosser, P.; Lall, U.; Weissel, J. K. Use of satellite imagery for water quality studies in New York Harbor. *Estuarine, Coastal and Shelf Science* **2004**, *61*, 437–448.
8. Liu, Y. S.; Islam, M. a; Gao, J. Quantification of shallow water quality parameters by means of remote sensing . *Progress in Physical Geography* **2003**, *27*, 24–43.
9. Babin, M. Variations in the light absorption coefficients of phytoplankton, nonalgal particles, and dissolved organic matter in coastal waters around Europe. *Journal of Geophysical Research* **2003**, *108*, 3211.
10. Reinart, A.; Paavel, B.; Tuvikene, L. Effect of coloured dissolved organic matter on the attenuation of photosynthetically active radiation in Lake Peipsi. *Proc. Estonian Acad. Sci. Biol. Ecol.* **2004**, *53*, 88–105.
11. Doerffer, R.; Fischer, J. Concentrations of chlorophyll, suspended matter, and gelbstoff in case II waters derived from satellite coastal zone color scanner data with inverse modeling methods. *Journal of Geophysical Research* **1994**, *99*, 7457–7466.
12. Sváb, E.; Tyler, A. N.; Preston, T.; Présing, M.; Balogh, K. V. Characterizing the spectral reflectance of algae in lake waters with high suspended sediment concentrations. *International Journal of Remote Sensing* **2005**, *26*, 919–928.
13. Zhang, Y.; Ma, R.; Duan, H.; Loiselle, S.; Xu, J. A Spectral Decomposition Algorithm for Estimating Chlorophyll-a Concentrations in Lake Taihu, China. **2014**, 5090–5106.
14. Oyama, Y.; Matsushita, B.; Fukushima, T.; Matsushige, K.; Imai, A. Application of spectral decomposition algorithm for mapping water quality in a turbid lake (Lake Kasumigaura, Japan) from Landsat TM data. *ISPRS Journal of Photogrammetry and Remote Sensing* **2009**, *64*, 73–85.
15. Salonen, K.; Sarvala, J. *Field manual for the determination of chloropyhll and primary production in Lake Tanganyika Research.*; 1995; Vol. 18.
16. Parinet, B.; Lhote, A.; Legube, B. Principal component analysis: An appropriate tool for water quality evaluation and management - Application to a tropical lake system. *Ecological Modelling* **2004**, *178*, 295–311.
17. Ritchie, J. C.; Zimba, P. V.; Everitt, J. H. Remote Sensing Techniques to Assess Water Quality. *Photogrammetric Engineering & Remote Sensing* **2003**, *69*, 695–704.
18. HAGA, H.; Ishikawa, K. Spatial Distribution of Submerged Macrophytes in the Southern Lake Biwa basin in the summer of 2014, in comparison with those in 2002, 2007 and 2012. *Japanese Journal of Limnology (Rikusuigaku Zasshi)* **2016**, *77*, 55–64.
19. Hamabata, E.; Kobayashi, Y. Present status of submerged macrophyte growth in Lake Biwa: Recent recovery following a summer decline in the water level. *Lakes and Reservoirs: Research and Management* **2002**, *7*, 331–338.

20. Elvidge, C. D.; Yuan, D.; Weerackoon, R. D.; Lunetta, R. S. Relative Radiometric Normalization of Landsat Multispectral Scanner (MSS) Data Using an Automatic Scattergram-Controlled Regression. *Photogrammetric Engineering & Remote Sensing* 1995, *61*, 1255–1260.
21. Oyama, Y.; Matsushita, B.; Fukushima, T.; Nagai, T.; Imai, A. A new algorithm for estimating chlorophyll-a concentration from multi-spectral satellite data in case II waters: a simulation based on a controlled laboratory experiment. *International Journal of Remote Sensing* **2007**, *28*, 1437–1453.
22. Tyler, A. N.; Svab, E.; Preston, T.; Présing, M.; Kovács, W. A. Remote sensing of the water quality of shallow lakes: A mixture modelling approach to quantifying phytoplankton in water characterized by high-suspended sediment. *International Journal of Remote Sensing* **2006**, *27*, 1521–1537.
23. Lee, Z.; Carder, K. L.; Mobley, C. D.; Steward, R. G.; Patch, J. S. Hyperspectral remote sensing for shallow waters. I. A semianalytical model. *Applied optics* **1998**, *37*, 6329–38.
24. Pinnel, N. A method for mapping submerged macrophytes in lakes using hyperspectral remote sensing, Technical University of Munich, 2007.
25. Zou, W.; Yuan, L.; Zhang, L. Analyzing the spectral response of submerged aquatic vegetation in a eutrophic lake, Shanghai, China. *Ecological Engineering* **2013**, *57*, 65–71.
26. Lyzenga, D. R. Passive remote sensing techniques for mapping water depth and bottom features. *Applied Optics* **1978**, *17*, 379.
27. Lyzenga, D. R.; Malinas, N. P.; Tanis, F. J. Multispectral bathymetry using a simple physically based algorithm. *IEEE Transactions on Geoscience and Remote Sensing* **2006**, *44*, 2251–2259.
28. Pacheco, A.; Horta, J.; Loureiro, C.; Ferreira Retrieval of nearshore bathymetry from Landsat 8 images: A tool for coastal monitoring in shallow waters. *Remote Sensing of Environment* **2015**, *159*, 102–116.
29. Bierwirth, P. N.; Lee, T. J.; Burne, R. V Shallow sea-floor reflectance and water depth derived by unmixing multispectral imagery. *Photogrammetric Engineering and Remote Sensing* **1993**, *59*, 331–338.
30. Haga, H.; Ohtsuka, T.; Matsuda, M.; Ashiya, M. Echosounding observations of coverage, height, PVI, and biomass of submerged macrophytes in the southern basin of Lake Biwa, Japan. *Limnology* **2007**, *8*, 95–102.
31. Zhu, L.; Wang, S.; Zhou, Y.; Yan, F.; Zhou, W. Water quality monitoring in Taihu Lake using MODIS image data. *IEEE Geoscience and Remote Sensing Symposium, IGARSS'04* **2004**, *4*, 2314–2317.
32. Domínguez Gómez, J. A.; Chuvieco Salinero, E.; Sastre Merlín, A. Monitoring transparency in inland water bodies using multispectral images. *International Journal of Remote Sensing* **2009**, *30*, 1567–1586.

Chapter 5

MAPPING OF SUBMERGED AQUATIC VEGETATION USING SATELLITE IMAGE

5.1 Introduction

5.1.1 Remote Sensing of Submerged Aquatic Vegetation

In an aquatic environment the submerged aquatic vegetation (SAV) reacts slowly and progressively to the changes in the nutrient conditions and thus can be used as the long-term limnologic indicators in lakes [1]. Monitoring and mapping the abundance and distribution of SAV is thus essential for effective management of the lake ecosystem. Historically, SAV distribution and abundance data has been acquired through exhaustive filed sampling programs including a boat survey. For such studies permanent transects or stations are defined and SAV is monitored using periodic site visit (HAGA and Ishikawa, 2016; Silva et al., 2008; Madsen, 1993).

More recently, aerial photographs and high resolution airborne hyperspectral images have been used for vegetation mapping to overcome the spatial heterogeneity in the optically complex aquatic environment [5–7]. The Hydroacoustic Eco sounder, have been used successfully [8] to monitor the biomass of the SAV species in the lakes however not widely applicable due to the hardware and software limitation. Nevertheless, due to the large area coverage, ease of data acquisition and low cost associated with the medium resolution satellite image (e.g., Landsat TM/ETM/OLI, Spot, Terra/Aster) they are widely used for mapping SAV along with other limnologic parameters [9–11]. Several remote sensing techniques have been used for SAV spectral analysis and bottom mapping such as vegetation presence frequency, Vegetation Indices , linear mixture model, radiative transfer model, modular inversion program, submerged aquatic vegetation mapping algorithm, Water Color Simulator (WASI) and HYDROLITE [5,12,7,13–16]. A satellite-based spectral decomposition algorithm used to map and estimate the water quality of optically shallow lakes by disaggregating the spectra into the optically active components [16]. However, the influence of the bottom substrate has not been accounted.

Water along with other optically active components, significantly attenuates the incoming and out-going radiations in water bodies [17–20]. In addition, the bottom reflectance (SAV or bottom sediment) is an important component when interpreting the radiometric signal for shallow waters. Ackleson and Klemas (1987) studied the signal interaction between the three main components (water, bottom substrate and plants) contributing to the water leaving reflectance. The showed that in shallow waters, the overall reflectance signal is determined by the vegetation density. Furthermore, with increase in depth, the dominance of reflectance is shifted to the water column components[21]. This suggests that bottom substrate reflectance is an important component when mapping the SAV in shallow waters.

5.1.2 Research Objectives

1) Classification and mapping of SAV distribution using Landsat-8 satellite image for the eutrophic south basin of Lake Biwa, mainly for the peak growth period of SAV (i.e., September or October) 2013 to 2016.
2) Development of SAV biomass estimation model and its application in the south basin for the classified SAV area.
3) Classification of the dominant SAV species in the south basin, using the Landsat-8 satellite image.

5.1.3 Methodological Framework

In this study, the SAV distribution and biomass was monitored and mapped using the Landsat-8 satellite image. The binary decision tree was used in ENVI 5.2 image processing software to map the SAV for the excessive growth period of September and October (2013 2016). The developed biomass model was used to estimate the biomass of the SAV classified area.

The methodological framework for this study is shown in Figure 5.1. The data used in this study is shown in Table 5.1.

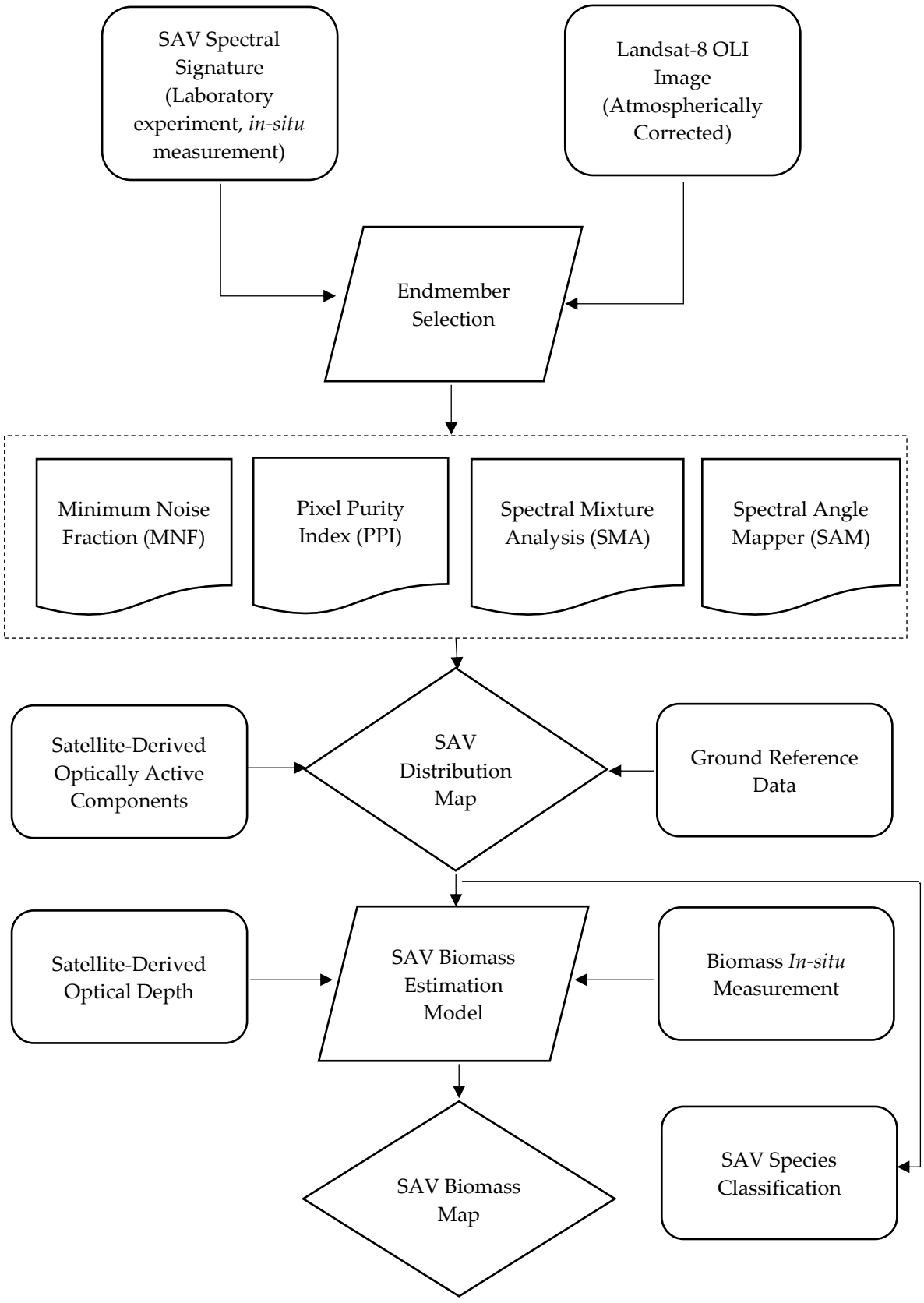

Figure 5.1 Schematic of the methodology framework.

Table 5.1. Available data information for the south basin of Lake Biwa (2013-2016).

Data Collected	Data Sources	Available Data/Locations/Time				Training Locations/ Points	Validation Locations/ Points	Methods/ Algorithms
		2013 (Sep-Oct)	2014 (Sep)	2015 (Sep)	2016 (Sep)			
Water Depth (m)	LBERI	-	52	-	8	-	-	-
Water Transparency (m)	JWA	95	-	-	-	42	53	Water Transparency Retrieval Algorithm
Water Quality (Chl, TSS, DOC)	LBERI	-	52	-	8	-	-	-
SAV Biomass and stand height (Diver Survey)	*In-situ* Survey, LBERI	-	52 (1 location for emerged vegetation was excluded)	-	8	23	17 (2014) and 8 (2016)	Spectral Decomposition Algorithm – Biomass Estimation Model
(Training and validation points): SAV Turbid Water Clear Water Emergent-V Floating-V Soil (from Imagery, Photographs & Field data)	LBERI, JWA, *In-Situ* Survey	 30 10 6 6 5 8	 27 22 18 2 3 8	 27 12 7 6 3 8	 25 12 8 3 4 8	[2013,14,15,16] 13, 10, 10, 8 4, 7, 5, 5 3, 6, 3, 3 3, 1, 3, 1 2, 1, 1, 2 4, 3, 3, 3	[2013,14,15,16] 17, 17, 17,17 6, 15, 7, 7 3, 12, 4, 5 3, 1, 3, 2 3, 2, 2, 2 4, 5, 5, 5	Binary Decision Tree (NDVI, NIR, SWIR, SMA, SAM)
Spectral Reflectance (Spectroradiometer)	*In-situ* Survey	-	-	-	8	-	-	-
Satellite Images (Landsat-8 OLI)	USGS-Earth-Explorer	1 Oct	9 Sep	28 Sep	7 Sep	-	-	-
Horizontal Visibility (Km)	JMA, Weather and climate data	2	2	2	2	-	-	-

[1] Oct and Sep in the data means October and September months.

5.2 Endmember Selection

The stand height of under water plants can vary from < 1 m to > 7 m, depending on the bathymetric variability, species characteristic and suitable light and environment condition [22]. In lake Biwa, SAV stand height tend to increase at the water depth of 4-6 m and decrease in relatively shallower (< 3 m) turbid water area [8]. However, as the water depth increases the remote sensing signal of SAV largely attenuated by the water and the increased concentration of OAC in the water column. Additionally, in turbid water the SAV reflectance

substantially dominated by the reflectance from the suspended sediment, phytoplankton and cDOM. Thus, it often leads to mixed pixel effect and becomes difficult to identify the SAV in the complex and dynamic aquatic environment. In order to map the SAV, it is essential to isolate the SAV signal from the confounding influences in the lake water. We therefore used Linear spectral mixture analysis (SMA), which can divide each pixel into the representative fraction of selected endmember spectra, where each endmember consists of the spectra of key components on the ground [23]. In order to find the best combination of endmembers for the mixed pixel reflectance, a matrix inversion was performed using Equation (5.1).

$$R_{Ci} = \sum_{j=1}^{n} f_j RE_{ij} + \varepsilon_i \tag{5.1}$$

And

$$0 \leq \sum_{j=1}^{n} f_j \leq 1$$

Where, R_{Ci} is corrected pixel reflectance of band; f_j the fraction of endmember j in the image; RE_{ij} is the endmember j reflectance at band i ; n the number of endmembers: ϵ_i and the residual error of band i. Whereas, the number of possible endmembers will always be less than the number of bands.

The Minimum noise fraction (MNF) transformation was applied to the Landsat-8 images before SMA, to select the appropriate band and exclude the band with negligible information [24]. Importantly, before applying these techniques we explicitly removed the undesired pixels such as terrestrial pixels by water mask. However, to remove the other sources of confusion (e.g. the bridge across lake in the south basin) which may not have been removed by the water mask, we performed the SMA using the prominent endmembers (Land, aquatic vegetation and water), identified by the apexes of 2-D scatter plot of four MNF images (Figure 5.2).

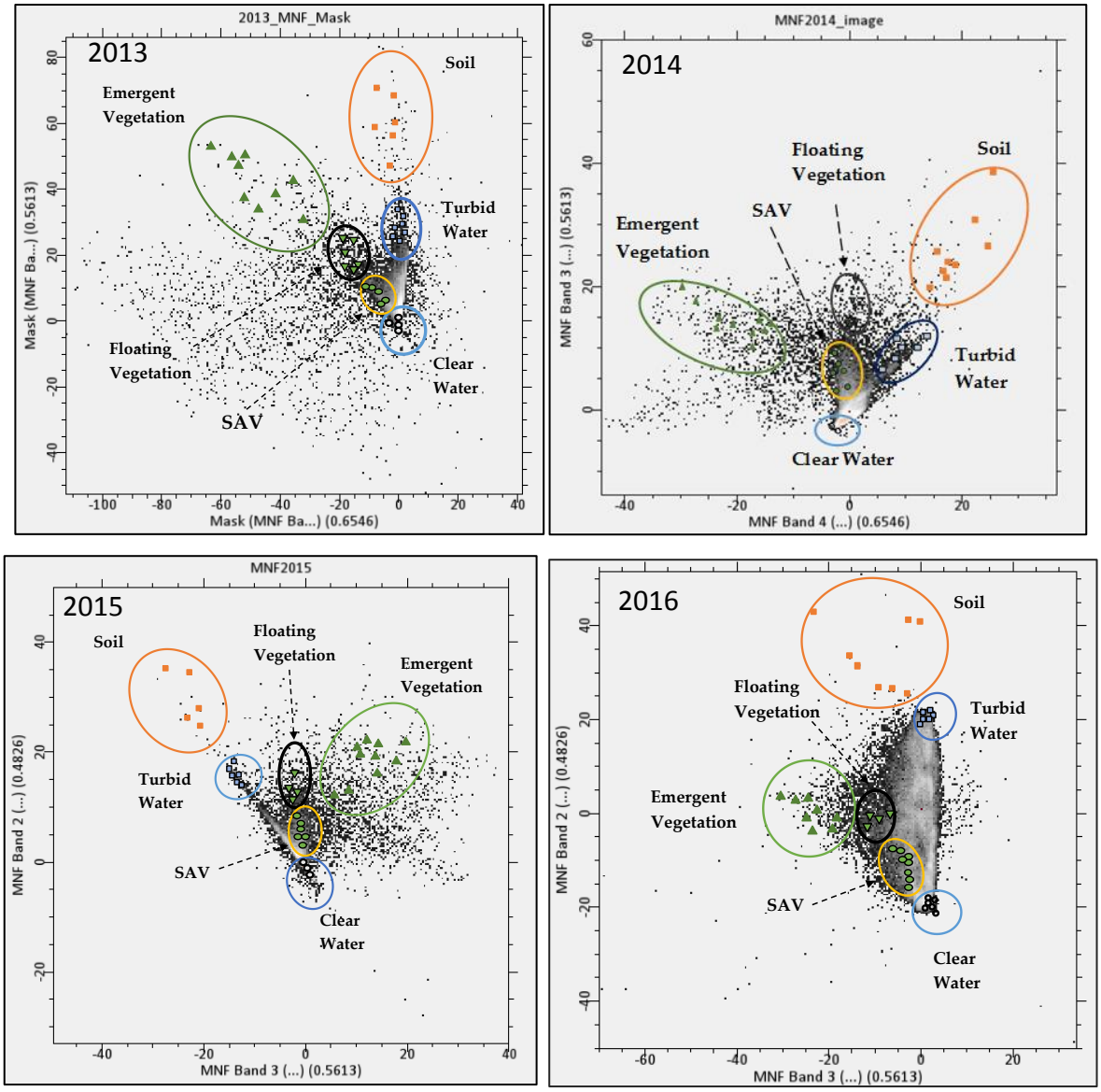

Figure 5.2 Endmember 2-D scatter plot derived from MNF transformed Landsat-8 image. The manually selected pixels extracted from the image with respect to the ground reference data points (2013-2016).

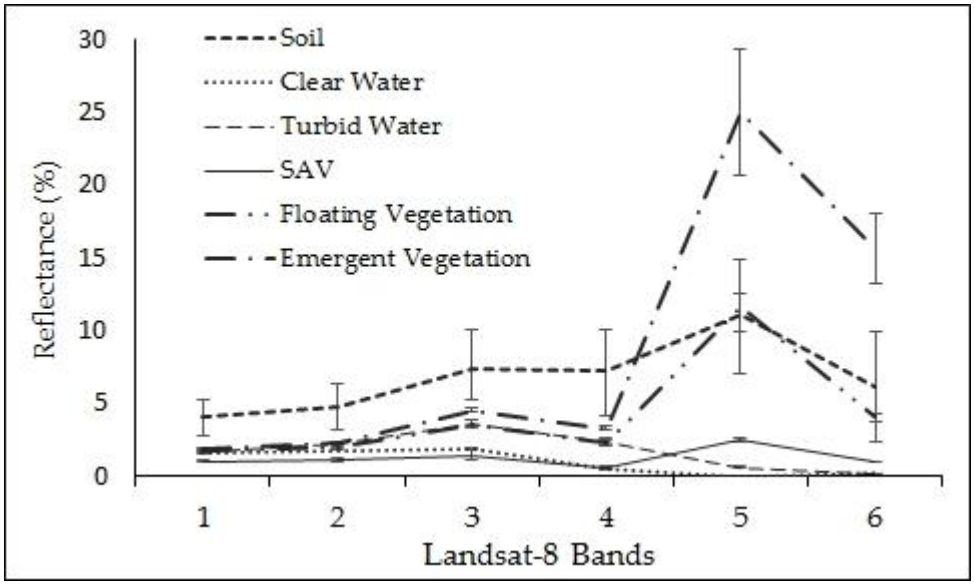

Figure 5.3 Endmembers used in spectral mixture analysis (SMA). The endmember spectra extracted from Landsat-8 imagery from the ground reference data points of September, 2014.

The endmember spectra extracted from the Landsat-8 OLI image for the September, 2014 is shown in Figure 5.3. Manual selection of the pixels was done using the 2-D scatter plot, in order to select the most spectrally pure pixel for the respective endmembers used in the spectral mixture analysis.

5.3 Development of Binary Decision Tree

A decision tree approach was used to classify and isolate the SAV pixels, where each node of the tree reduces the variance in the remaining pixels to be classified. The 2014 field data (52 observation points) was separated into training (24 points) and validation (28 points) data for the decision tree. The SMA was used in conjunction with Normalized Difference Vegetation Index (NDVI) to discriminate the emergent and floating vegetation from lake water. The emergent and floating vegetation have distinctively high albedo and NDVI than SAV, turbid and clear water in Landsat-8 SWIR and NIR bands, thus the reflectance of these bands was used in the decision tree to distinguish SAV from other emergent vegetation and turbid water. The NDVI and the reflectance of Landsat-8 SWIR and NIR bands for each class were used to decide the classification thresholds for the binary decision tree. Similarly, the classification threshold for all four images (2013-2016) was determined individually, given in Table 5.2.

Table 5.2. Classification thresholds based on the vegetation index and reflectance of NIR and SWIR bands of Landsat-8 atmospherically corrected images (2013-2016).

	2013			2014			2015			2016		
	NIR	SWIR	NDVI	NIR	SWIR	NDVI	NIR	SWIR	NDVI	NIR	SWIR	NDVI
Land (>)	0.13	0.07		0.11	0.06		0.08	0.06		0.13	0.10	
Emergent (>)	0.20	0.12	0.69	0.25	0.13	0.72	0.18	0.10	0.70	0.28	0.15	0.75
Floating (>)	0.07	0.03	0.36	0.09	0.04	0.49	0.05	0.04	0.43	0.09	0.04	0.43
SAV (< =)	0.02	0.01		0.04	0.03		0.04	0.02		0.05	0.03	
Turbid Water (>)	0.004	0.002		0.007	0.002		0.008	0.002		0.01	0.004	
Clear Water (<)	0.001	0.001		0.001	0.001		0.001	0.001		0.002	0.001	

For September 2014 image, all pixels in which the SMA soil fraction => 30% and SMA water fraction <= 10% were classified as land. Furthermore, the distinctively high NDVI value of the emergent (NDVI => 72%) and floating (NDVI => 49%) vegetation enabled us to separate them from SAV. Whereas, the pixel with SWIR reflectance <= 4% along with the SMA water fraction =>10% were classified as SAV, turbid water or clear water. The unclassified pixels were categorized as other in the decision tree (Figure 5.4).

The remaining pixels from the first SMA classification were again subjected to the second SMA classification using SAV, turbid water, and clear water as endmembers, along with the spectral angle mapper (SAM) approach to separate SAV from the lake water. SAM measures the spectral similarity between an image spectra and reference spectra (endmember spectra in this study) by treating the spectra as vectors and calculating the spectral angle between them [25]. The SMA Turbid water fraction => 30% were classified as turbid water. Whereas, the pixels with SWIR band reflectance <= 3% were used for SAV classification. Furthermore, when the SMA fraction for SAV was > 10% and the spectral angle was closest to the SAV endmember spectra we classified them as the SAV pixels. The pixels with SAV fraction from 5% to 10% with larger spectral angle were excluded from SAV classification (Figure 5.5). The similar approach was used to classify SAV for 2016 and then confirmed with the in-situ measurement (ground reference data points) and the area information.

Likewise, we generated the SAV distribution map for 2013 and 2015. Based on the area information the fixed ground control point was selected to derive the endmember spectra along with the 2-D scatter plot to confirm the distinct spectra of each endmember. For 2013 and 2015 images, the areas where the emergent, floating and SAV vegetation can commonly found in the basin was first identified using the true color image and the NDVI images. Additionally, the classified SAV maps of 2014 and 2016 were used to locate the common areas

where the occurrence of SAV, emergent, and floating vegetation is most likely. Finally, using the same approach we were able to map the extent of SAV distribution for the peak growing period of 2013.

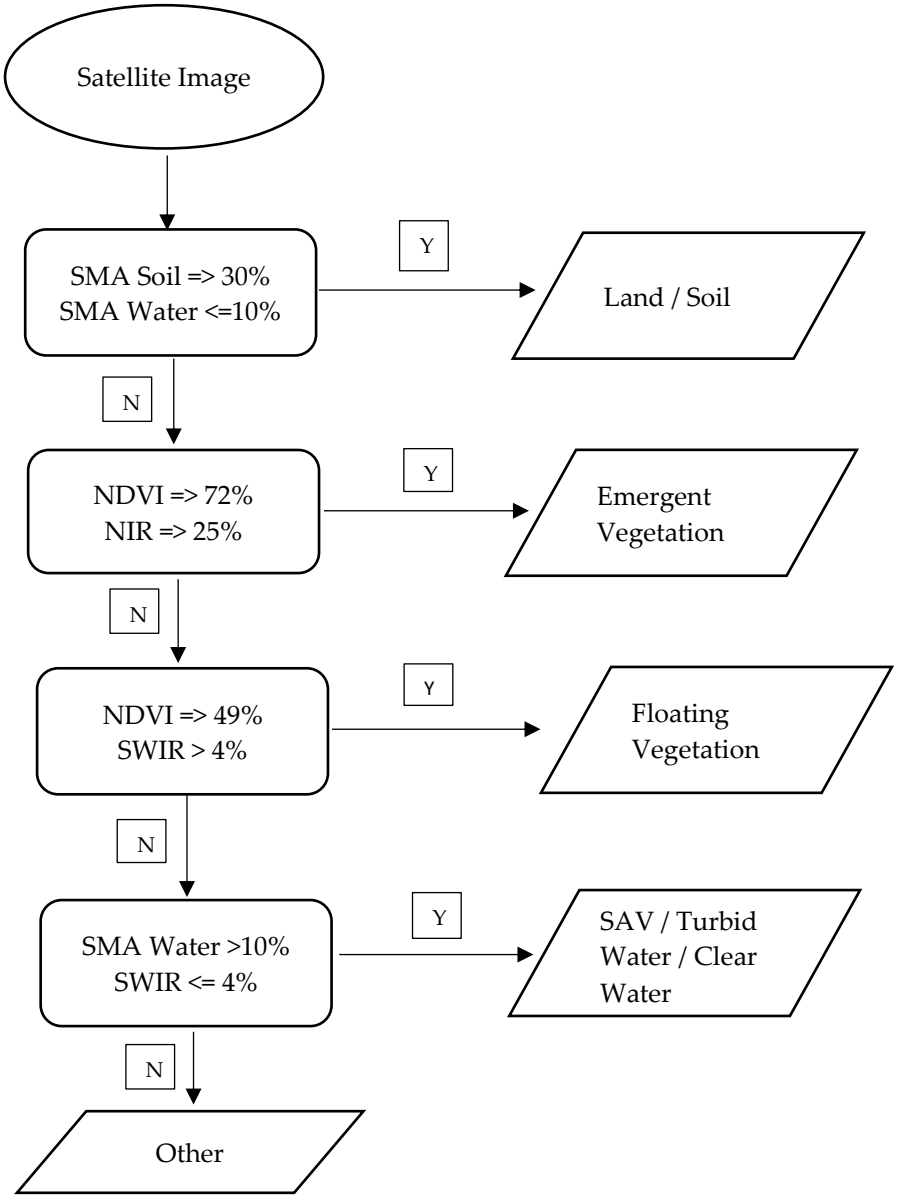

Figure 5.4. Decision tree classification developed for the extraction of land, emergent vegetation and floating vegetation from the lake water with SAV (note: Y = Yes; N = No).

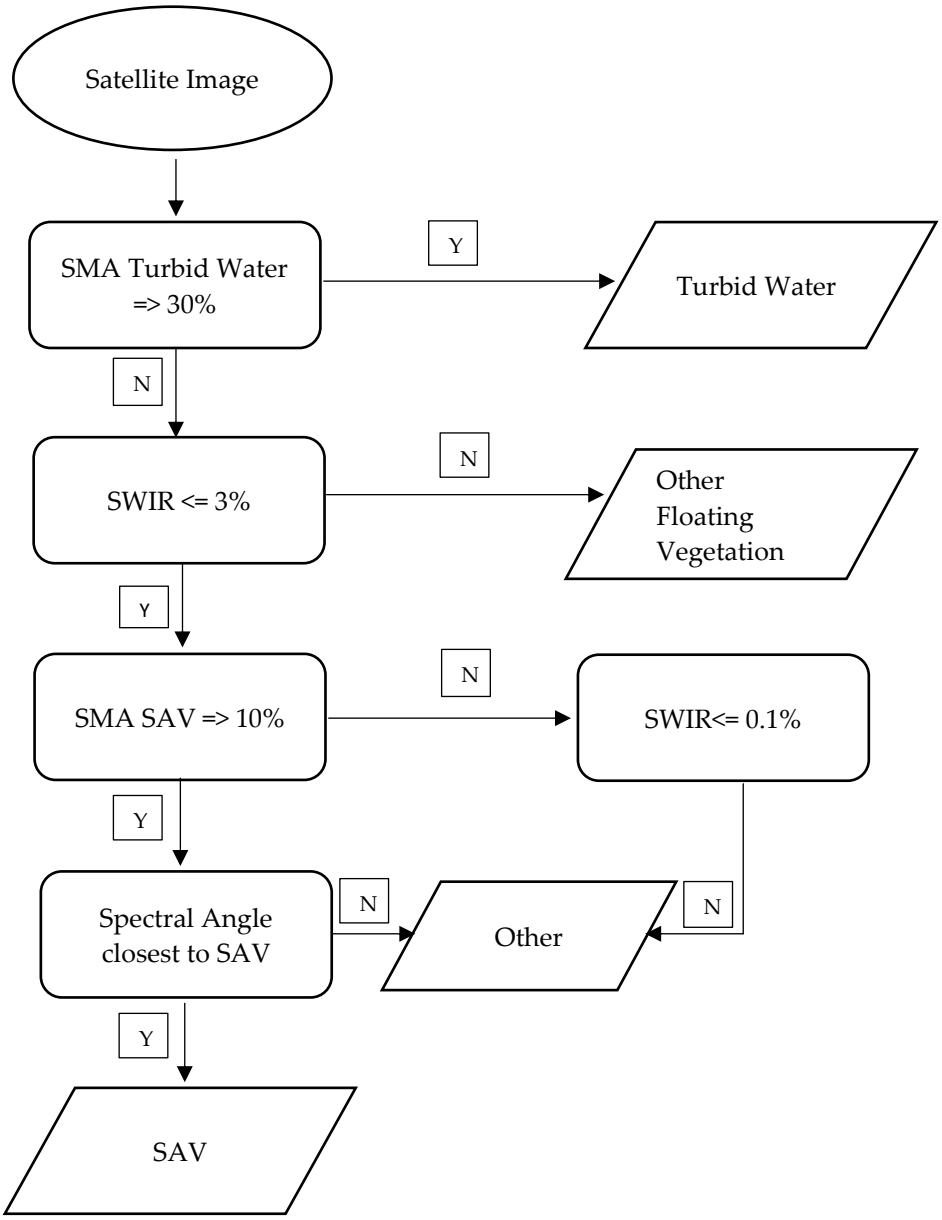

Figure 5.5 Decision tree classification developed for the extraction of SAV pixels from the turbid and clear water (note: Y = Yes; N = No).

5.4 Identifying and Mapping the Submerged Aquatic Vegetation

Using the above mentioned approach the distribution and abundance of the SAV in the eutrophic south basin of the Lake Biwa was classified using the ENVI- 5.2 Image processing software and mapped using the ArcMap 10.3.1 an image analysis software. The SAV distribution map for October 2013, September 2014, September 2015 and September 2016 is shown in Figure 5.6.

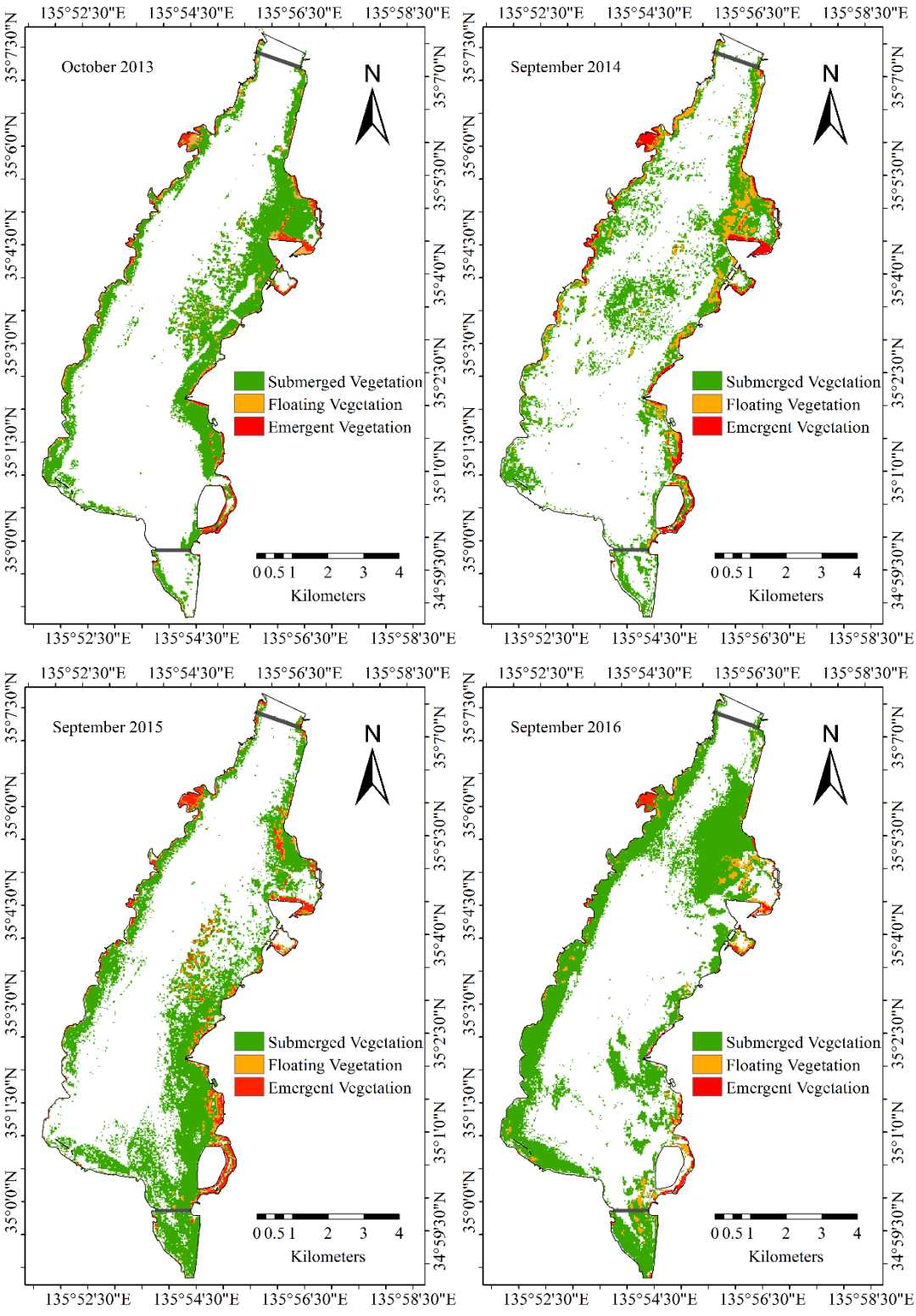

Figure 5.6 SAV distribution map of the south basin for October 2013, September 2014, 2015 and 2016.

5.5 Validation with the Ground Reference Data

5.5.1 The SAV Classification Accuracy Estimation

For the accuracy assessment of the classified SAV maps using the satellite image, we developed an error matrix. Out of 52 validation points, 44 were classified correctly, resulting in the overall accuracy of 84.6% and the kappa coefficient of 0.69. Whereas, out of 17 SAV field points 13 were correctly classified, and 3 were misclassified as other (i.e. clear water, turbid water and other unclassified) which gives the producer accuracy of 76.5% and user accuracy of 81.3%. The Kappa coefficient relative to the SAV class is 0.74 (Table 5.3), indicating the strong agreement. The SAV field points were selected based on the observed biomass in 2014, water depth and chlorophyll concentration. In addition, the locations with chlorophyll > 20 µg/L along with the site where the SAV biomass <100 g DW m^{-2} were excluded and not considered as SAV site.

Table 5.3. Error matrix produced from the field verification data of September, 2014. Of 52 stations, 44 verified correct (84.6%).

Map Class	Ground Reference						
	SAV	FV	EV	Other (Water, Turbid, Unclassified)	Total	User's Accuracy (%)	Error of Commission
SAV	13	0	0	3	16	81.3	18.8
FV	0	1	0	0	1	100	0.0
EV	0	0	1	0	1	100	0.0
Other (Water, Turbid, Unclassified)	4	1	0	29	34	85.3	14.7
Total	17	2	1	32	52		
Producer's Accuracy (%)	76.5	50.0	100.0	90.6	Overall Accuracy		
Error of Omission	23.5	50.0	0.0	9.4	84.6 %		

[4]Overall kappa Coefficient is 0.690 and Kappa coefficient relative to SAV is 0.74.

5.6 Analyzing the Change in the Distribution of Submerged Aquatic Vegetation

In 2014, 9.6 km^2 of the south basin area was infested with SAV, as detected by the Landsat-8 image. Total vegetation coverage area (i.e. SAV, floating and emergent vegetation) in the south basin increased from 15 km^2 in 2013 (October) to 23 km^2 in 2016 (September), approximately (Table 5.4).

Table 5.4. Coverage area of detected SAV estimated using the Landsat-8 OLI image.

Vegetation Area Coverage(km²)	2013	2014	2015	2016
Floating	3.47	2.42	1.31	1.12
Emergent	1.37	1.32	1.65	0.74
SAV	10.65	9.61	15.65	21.04
Total Area	15.49	13.35	18.61	22.90

The SAV distribution map generated by the satellite image showed increased SAV coverage area in recent years, particularly in 2015 (15.7 km²) and 2016 (21 km²) (Figure 5.6). The maximum water transparency at which SAV was detected in the south basin was 2.2 m, 3.7 m, 3.0 m and 3.1 m in 2013, 2014, 2015 and 2016, respectively. With increase in transparency, the maximum water depth at which the SAV was detected increased to the water depth of 5.6 m and 4.9 m in the 2014 and 2015 when compared to 4.4 m and 4.3 m in 2013 and 2016, individually. Mostly, the SAV occurrence in the eastern and northeastern shoreline was more frequent. However, in 2016, the distribution of SAV spread towards the western shoreline and the north part of the south basin.

5.7 Development of the Biomass Estimation Model

5.7.1. SAV Biomass Estimation

For the biomass estimation of the classified SAV pixels, we developed a new model based on the spectral decomposition algorithm, accounting for the bottom albedo in shallow lakes. The details of the model are given Chapter 4. In this algorithm, the mixed reflectance spectra of a given pixel are conceptualized as a linear combination of main endmembers substantially contributing to the pixel reflectance. Previously, this approach has been used to estimate the water quality parameters using the endmembers mainly from the water column of the lake [16,26]. However, in the shallow south basin of Lake Biwa over 90% of the bottom covered with SAV [6,2], which can potentially affect the pixel reflectance, and is likely to be confused with the other algae or phytoplankton reflectance, therefore we included SAV as an important endmember for this study. Therefore, SAV biomass was estimated using the spectral decomposition algorithm as expressed in Equation 5.1.

$$R(\lambda) = a_p \times R_p(\lambda) + a_n \times R_n(\lambda) + a_v \times R_v(\lambda) + a_w \times R_w(\lambda) \quad (5.1)$$

The SAV decomposition coefficient (a_v) obtained from the spectral decomposition algorithm, was used as an independent variable to estimate the SAV biomass of the classified

SAV pixels. We used regression analysis to establish the relationship between the decomposition coefficient and the SAV biomass (September 2014), gives an R^2 = 0.83 significant at $p < 0.01$, (Equation 5.2).

$$SAV_{bm} \times Exp^{-Z_{WT}} = 14.07 + 504.56 \times a_v \quad (5.2)$$

Where, SAV_{bm} indicates the SAV biomass (kg Dry Weight per pixel) and Z_{WT} is the satellite-derived water transparency. Per pixel biomass was obtained by multiplying the Landsat-8 image pixel area (30m x 30m) with the observed SAV biomass (kg DW m^{-2}) of the station.

The best model based on the in-situ measurement data and RMSE was selected to calculate the biomass (Table 5.5.)

Table 5.5 The SDA-based SAV biomass (g Dry wt. /m^2) estimation models for the south basin of the Lake Biwa.

Band Combination	SAV Biomass Model	R^2	p	F	SE	RMSE
1234	391.96 - 524.67 *a_v + 4020.79* a_v^2	0.14	<0.05	3.5	252	-
1234	157.73+ 354.0 * a_v	0.76	<0.01	176	16.4	-
	134.42 + 611.31 * a_v + 729.88 * a_v^2	0.71	<0.01	55	10.5	276
1245	3.99 + 135.12 * a_v	0.54	<0.01	52	13.21	-
	6.27 - 29.67 * a_v + 536.03 *a_v^2	0.73	<0.01	60	10	211
2345	9.44 + 247.64* a_v	0.77	<0.01	165	16.8	250
	3.95 + 523.18 * a_v - 680.07 * a_v^2	0.82	<0.01	112	7.9	198
	14.06 + 504.56* a_v	0.83	<0.01	226	14.8	130

Out of 52 observation locations, we used 17 SAV classified locations (i.e., September 2014) for the validation (Figure 5.7). The result shows the good agreement with overall R^2 of 0.79 between observed and satellite-derived SAV biomass.

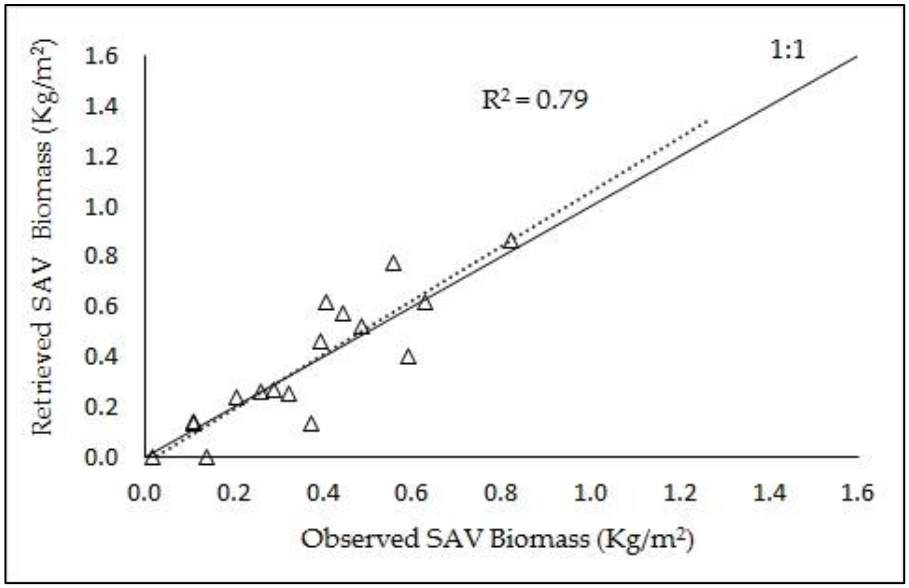

Figure 5.7. Estimated and *In-situ* measured SAV Biomass (September, 2014) in the south basin of Lake Biwa.

The satellite-derived SAV biomass of only SAV classified area in the south basin is shown in Figure 5.8. The total RMSE and mean absolute error obtained for the 17 SAV classified stations is 0.26 kg DW m^{-2} and 0.21 kg DW m^{-2}, respectively (Table 5.6). The maximum and minimum absolute error in biomass estimation are, 0.723 kg DW $m^{-2}$and 0.172 kg DW m^{-2}, respectively. The overall RMSE obtained for the eight surveyed locations (September, 2016) in the south basin is 0.28 kg DW m^{-2}, with the mean absolute error of 0.20 kg DW m^{-2}. Whereas, the maximum and minimum absolute error based on the surveyed locations are 0.667 kg DW m^{-2} and 0.013 kg DW m^{-2}, respectively. On the other hand, the total biomass estimation error obtained in 2014 and 2016 based on the SAV classified stations are, 968 kg DW m^{-2}. (1.0 T) and 332 kg DW (0.332 T), approximately.

Table 5.6. Estimated Root Mean Square Error (RMSE) of SAV Biomass using 17 SAV classified locations in the south basin (September 2014).

Biomass Range (kg DW m^{-2})	17 SAV Classified Stations	
	RMSE	N
0 – 0.1	0.17	1
0.1 – 0.3	0.30	6
0.3 – 0.5	0.20	6
0.5 – 0.7	0.20	2
0.7 – 1.0	0.33	2
1.0 – 1.4	-	0
Overall RMSE	0.26	
Mean Absolute Error	0.21	

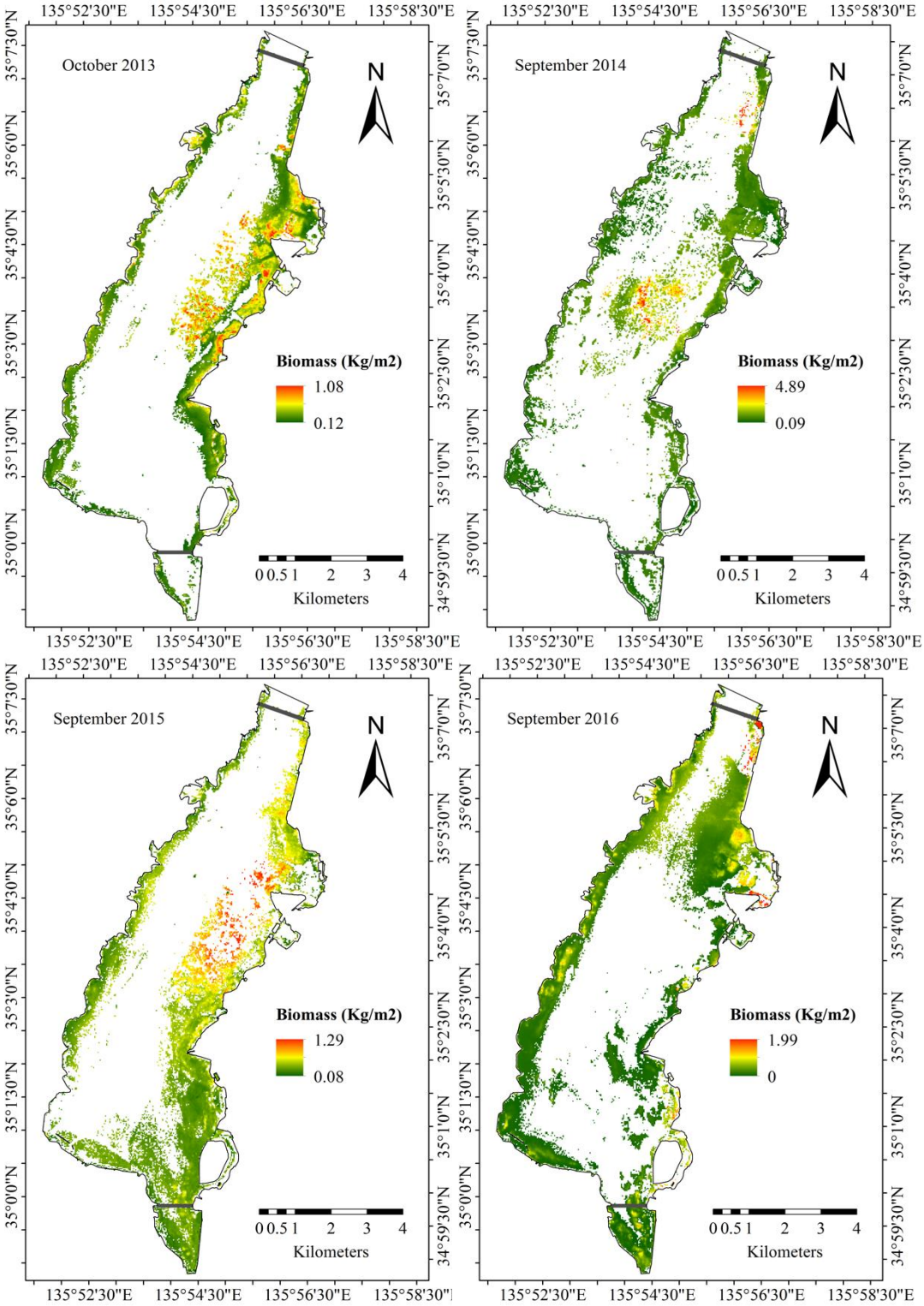

Figure 5.8. Estimated biomass (kg DW m^{-2}) of SAV and floating vegetation in the south basin of the Lake Biwa, using the spectral decomposition algorithm (for October 2013, September 2014, 2015 and 2016).

The total SAV biomass estimated for the classified area in the south basin is 3390 T, 3919 T, 5242 T and 4550 T dry weight for 2013, 2014, 2015 and 2016, respectively (Table 5.7).

Table 5.7 Estimated SAV Biomass in the south basin using new spectral decomposition algorithm for October 2013, September 2014, 2015 and 2016.

	2013	2014	2015	2016
Average Vegetation Biomass (kg DW m^{-2})	0.335	0.440	0.351	0.238
Average SAV Biomass (kg DW m^{-2})	0.318	0.408	0.335	0.216
Total Vegetation Coverage Area (km^2)	15.5	13.4	18.6	22.9
Total SAV Coverage Area (km^2)	10.7	9.6	15.7	21.0
Total Vegetation Biomass (T)	5193	5872	6530	5451
Total SAV Biomass (T)	3390	3919	5242	4550

[7]Average vegetation biomass is the average of all the stations in the south basin classified as SAV.

The four-year trend indicates the increasing SAV growth in the south basin, primarily in 2015 with 55% (1852 T) increase in the biomass than 2013, followed by 2014 and 2016 with 34 % (1160 T) and 16% (529 T) increase in SAV biomass. Additionally, an increased total vegetation biomass (i.e. SAV, floating vegetation and emergent vegetation biomass) can be seen in 2015 (6530 T) and 2014 (5872 T), which also suggests the increased growth of floating and Emergent vegetation in the years with relatively high water transparency. Despite an amplified total SAV biomass in 2015, the maximum biomass density is comparatively low (1.29 kg DW m^{-2}) than 2014 (4.89 kg DW m^{-2}) and 2016 (1.99 kg DW m^{-2}).

5.8 Submerged Aquatic Vegetation Species Classification

Since overlying water over the SAV canopy significantly affects the SAV signal detection in SAV classification. We, tried to generate a bottom albedo map to classify the SAV species present in the south basin of the Lake Biwa. However, before SAV species mapping the reflectance spectra of SAV species observed in the south basin were analyzed, to distinguish the species. The reflectance of each SAV species measured individually in the lab using the spectroradiometer. In this study, we selected the three dominant species (they are, *Potamogeton Maackianus*, *Egeria Densa*, *Hydrilla Verticillata*) and one high reflecting SAV (*Myriophyllum Spicatum*). The reflectance of each species were than reintegrated to Landsat-8 bands to be used as threshold for satellite image classification. The reflectance of dominant species is give in Figure 5.9 and in Table 5.8.

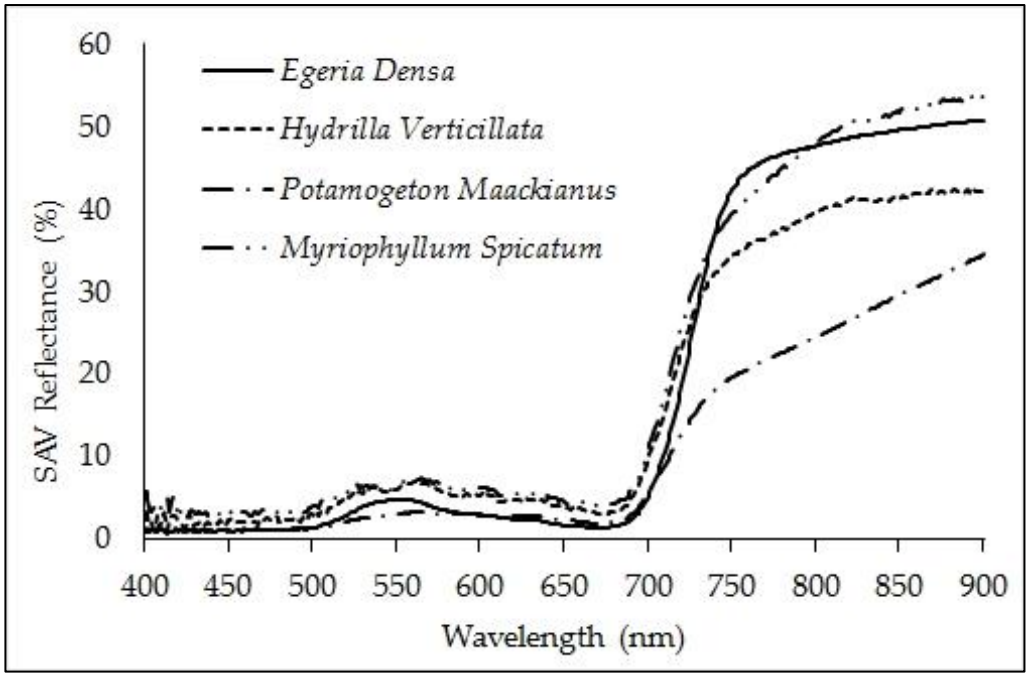

Figure 5.9. SAV species reflectance measured using the Spectroradiometer in the laboratory, for the samples collected in September 2016.

Table 5.8. SAV species reflectance at four Landsat-8 bands (Spectroradiometer measurement).

Landsat-8 Wavelength Range (nm)	Bands	*Egeria Densa*	*Potamogeton Maackianus*	*Hydrilla Verticillata*	*Myriophyllum Spicatum*
434.97 - 450.95 (442.96)	B1	1.03	1.08	1.89	3.03
452.02 - 512.06 (482.04)	B2	1.08	1.20	2.37	3.45
532.74 - 590.07 (561.41)	B3	4.55	3.20	6.96	7.26
635.85 - 673.32 (654.59)	B4	1.58	2.22	3.66	4.52
850.54- 878.79 (864.67)	B5	50.00	31.01	41.70	52.65

5.8.1 Bottom Albedo Estimation

To estimate the bottom albedo, we used physical based algorithm based on the satellite reflectance and bathymetry of the location (Lyzenga et al., 2006). The model approximately represents the radiative transfer theorem, where the water leaving reflectance is the sum of water column reflectance and the bottom albedo, in a shallow lake [27,28]. The sub-surface reflectance in a water body is thus expressed as (Equation 5.3):

$$R_i = R_w + R_b \times Exp\,(-k \times z) \tag{5.3}$$

$$R_b = r_b - R_W$$

Where R_W volume scattering over infinitely deep water (deep water reflectance in image); r_b is the bottom albedo (bottom substrate reflectance); k is sum of the diffuse attenuation coefficient for upwelling and down welling lights and; z is the water depth.

Using the inverse modeling approach through Equation 5.4, we first tried to estimate the k for the locations where the *in-situ* measurements were carried out in September 2016. Through *in-situ* measurement the type of the bottom substrate (mainly SAV) at each surveyed location was known and their reflectance was measured. In addition, the water depth at each locations was measured, the same day. The deep water reflectance measured during the survey near the north basin for deeper and clearer waters were used as the deep water reflectance. Thus we estimated the total diffuse attenuation coefficients of all the locations (Figure 5.10 and Table 5.9).

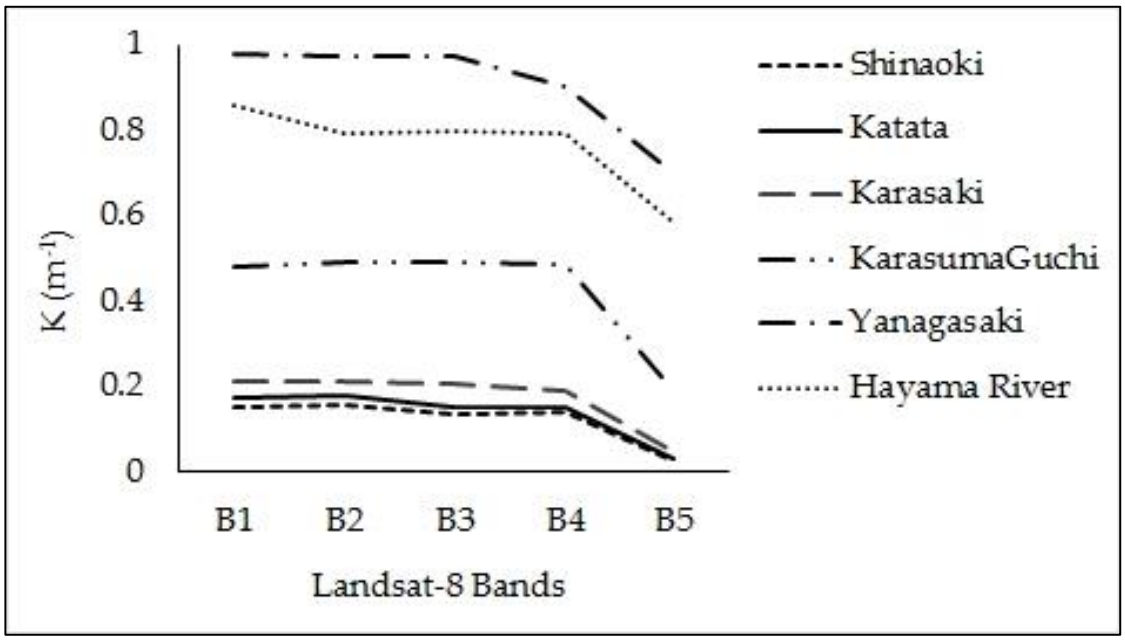

Figure 5.10. Calculated diffuse attenuation coefficient for the *in-situ* measured locations (September 2016).

Table 5.9. *In-situ* measured diffuse attenuation coefficient (K) and landsat-8 estimated K.

	B1		B2		B3		B4	
	In-situ	Satellite	*In-situ*	Satellite	*In-situ*	Satellite	*In-situ*	Satellite
Shinaoki	0.18	0.24	0.20	0.23	0.16	0.18	0.16	0.16
Katata	0.23	0.13	0.21	0.13	0.16	0.09	0.16	0.08
Karasaki	0.24	0.22	0.23	0.20	0.21	0.16	0.20	0.14
KarasumaGuchi	0.52	0.49	0.52	0.47	0.52	0.39	0.50	0.38
Yanagasaki	0.99	0.70	0.99	0.67	0.98	0.58	0.92	0.58
Hayama River	0.91	0.51	0.84	0.49	0.83	0.41	0.83	0.40

Considering the fact that the south basin of Lake Biwa has > 90% of the basin covered with SAV. We estimated the diffuse attenuation coefficient by selecting the transect points (from low depth to high depth in a straight line) in the lake near the location where the SAV coverage is > 70 %, such as near Shinaoki, Katata, Yanagasaki and karasumaoki [29].

Thus using Equation 5.3, the relation between the *K* and depth was estimated as using satellite image (Figure 5.11).

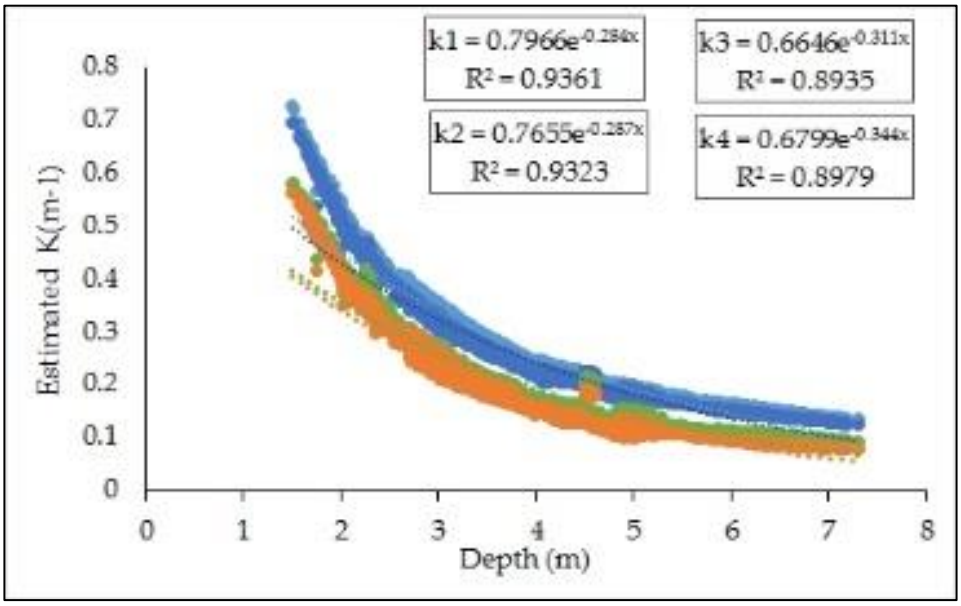

Figure 5.11. Estimated relation between satellite-derived *k* and Depth (September 2016).

Using the above relation (Figure 5.11), we estimated the diffuse attenuation coefficient for the September 2014 image for each band as shown in Figure 5.12.

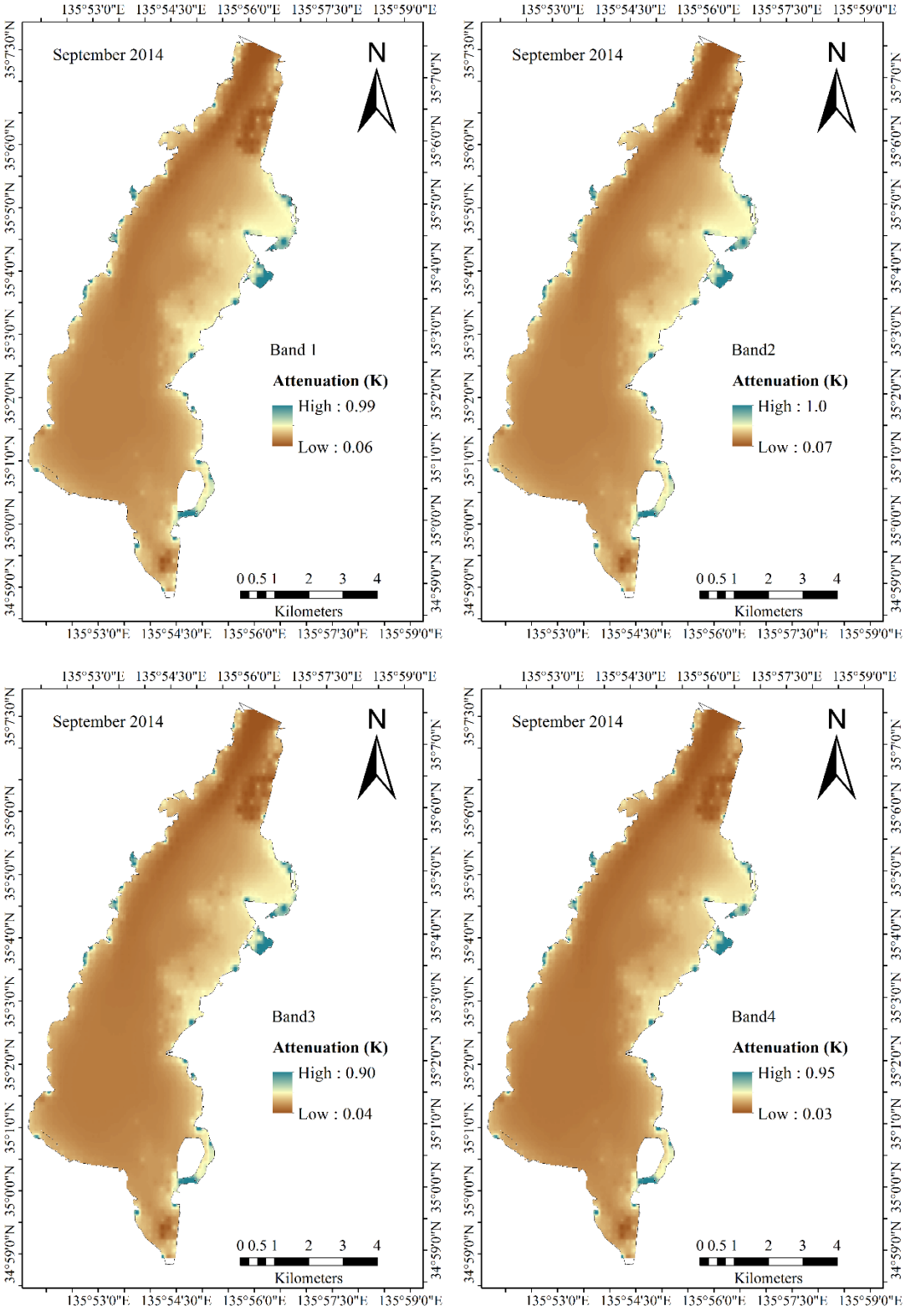

Figure 5.12. The satellite-derived diffuse attenuation coefficients for each Landsat-8 bands (band1 -4), for September 2014.

The retrieved result shows that the diffuse attenuation coefficient decreases with the increase in water depth and with increase in wavelength.

To classify the SAV species, we first selected the appropriate band in which the species can be distinguished appropriately. Thus for that, we refer to the SAV graph and chose to classify using the visible region of the spectrum, that is the green band of Landsat-8 which shows the visible variation in spectra along with NIR band. However, with band 3 (green band Landsat-8), we decided the threshold for classification based on the SAV species reflectance spectra (reintegrated to Landsat-8 bands) in Table 5.8.

The threshold for each species are: *Egeria Densa* (R > 4.5%), *Potamogeton Maackianus* (R > 3.2 %), *Hydrilla Verticillata* (R > 6.9%) and *Myriophyllum Spicatum* (R > 7.2%).

Thus the SAV species classification map was generated using the ArcMap 10.3.1, for only the SAV classified pixels of the image, is shown in Figure 5.13.

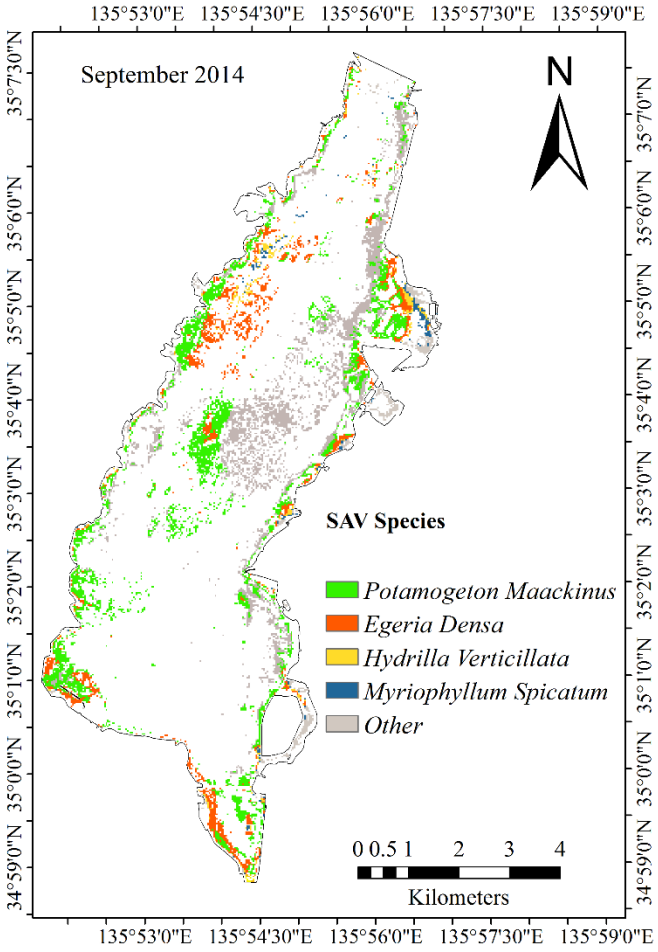

Figure 5.13. The classified SAV species map for September 2014. The dominant species classified are, *Egeria Densa*, *Potamogeton Maackianus*, *Hyrilla Verticillata* and *Myriophyllum Spicatum*.

The classified species locations match well with the observed SAV species data for September 2014, in the south basin of the Lake Biwa.

5.9 Result Discussion and Conclusion

5.9.1 Discussion

In this study an attempt to monitor the change of SAV distribution and its biomass was made using the multispectral Landsat-8 OLI image. The SAV was classified taking in to account the influence of optically active components in the eutrophic south basin of Lake Biwa (details in Chapter 4). Since the south basin of Lake Biwa is relatively shallow, therefore the influence of bottom substrate is considered while mapping the SAV. In addition, more than 90% of the basin is covered with SAV [2] thus, this further supports our assumption in this study.

The decision tree is sensitive to the changing thresholds for the images of different time. Therefore, in this study, each image was classified using the binary decision tree respective of that image, where beforehand area information was used to select the important endmembers for each image. A good classification accuracy of 84.6% was achieved when compared with the available ground truth data (2014) with an omission and commission error of 23.5% and 18.8 %, respectively. In the south basin, the SAV coverage area is >90% [6,2]. Nevertheless, due to the increased eutrophication in the basin and the deep water areas (> 6 m), only 21% (2013), 18% (2014), 30% (2015 and 40% (2016) of the basin area could be mapped for SAV using satellite image.

Healthy vegetation growth often related with the water clarity in an aquatic system [30,31]. In the south basin of Lake Biwa, the amplified SAV growth is considered as a key driving factor for improved water clarity[6,8]. In this study however, the mapped SAV coverage area does not rise as expected, with increased water clarity for the same year. For instance, water clarity obtained in 2014 is higher than 2013, 2015 and 2016, while the mapped SAV area is rather low (9.6 km^2), in the same year. It could be attributed to the fact that aquatic macrophyte reacts slowly and progressively (i.e., in years) to the changes in an aquatic system (such as nutrient conditions and turbidity), in contrast to phytoplankton and other micro-algae [1]. Principally, in lakes with increasing eutrophication, SAV communities often show a considerable delay response time [32]. However, another factor such as SAV stand height could simultaneously contribute to its low detection. In lake Biwa, SAV stand height tend to increase at the water depth of 4-6 m and decrease in relatively shallow turbid water area [8]. Therefore, if the water is relatively turbid in the shallow basin even with extensive SAV bed

of short growing species, the detection of SAV is restricted using the satellite image. Therefore, the turbid water pixels were excluded before the SAV mapping, in this study. Moreover, in the deep water if the stand height of SAV is not within the optical depth limit the detection of SAV is not possible using the satellite image [33]. Consequently, an increased SAV distribution can be seen in the following year of 2015 (15.7 km^2) and 2016 (21.0 km^2), in this study (Table 5).

The new spectral decomposition algorithm was used for SAV biomass estimation for the south basin. Each decomposition coefficients in the algorithm hold the mass information of each endmember and were used independently in the estimation model (SAV biomass model). Therefore, compared to the conventional models, this approach is less sensitive to geographical and temporal variability. If the standard reflectance spectra of the respective endmember remain consistent with similar spectral sensitivity, this model could be applied to other satellite images [16,34]. The new model is capable of estimating the SAV biomass for the whole image, thus, to avoid any confusion with other mixed pixels, we extracted the SAV biomass information only for the SAV classified pixels in the satellite image.

In 2014, SAV coverage area is comparatively lower than other years conversely, the maximum biomass density is substantially high (4.89 kg DW m^{-2}) in the same year. It could be the result of improved water clarity which allowed sufficient light penetration. Light is predominantly an important environmental factor regulating the SAV growth [17], which is directly affected by the transparency, depth of plant growth and shading from other plants. Whereas, noticeably high total SAV biomass was estimated for 2015 and 2016, following the clear water year (2014). In some instances, the eutrophication or invasive aquatic species result in excessive growth of the SAV biomass, manly in locations where previously nutrient levels were not supporting the extensive SAV growth [4,17,35].

Distinguishing aquatic vegetation from the other sources of confusion, such as deep water and turbid water is an essential step before mapping SAV in eutrophic lakes. The prior knowledge of water depth and transparency help to detect and classify aquatic vegetation from turbid water area. Nevertheless, SAV detection in inland waters is often restricted by meteorological (i.e. weather condition, cloud cover, sun, wind speed, view angle), physical (i.e. water depth, wave action) and biological (i.e. phenology of plant species) heterogeneity [36,5,37,3,38,39]. Furthermore, the apparent optical properties (i.e. surface reflectance and

diffuse attenuation) and inherent optical properties (i.e. absorption and scattering) of water largely affect the SAV detection in the water bodies [40,17,39]. Even in a pixel with 100% SAV cover, its reflectance is still dominated by absorption of water [5]. In Lake Biwa, the SAV species often grow in clusters, thus it is hard to find the pure pixel representing the single SAV specie in a medium resolution image (30 x 30 m) thus the species level classification could not be performed.

In this paper, we successfully estimated and evaluated the distribution and biomass of SAV using the Landsat-8 image. The *in-situ* measurement data (i.e. SAV Biomass and water transparency) was not available for all the years, particularly during the satellite acquisition time. Therefore, we validated the SAV classification result and developed model using the available *in-situ* field data, which coincides with the satellite acquisition time (± 3 days) they are, 2014 (52 Observation points) and 2016 (8 observation points) and applied to other years. Whereas, the water transparency result was validated using the measured data of 2013 for 95 observation points in the south basin, divided into training and validation points. The obtained result also correspond well with the research conducted by LBERI for the south basin of Lake Biwa [2,6,41]. Furthermore, the SAV species classification mainly the dominant SAV species such as *Egeri Densa*, *Potamogeton Maakicanus*, *Hydrilla Verticillata*, and *Myriophyllum Spicatum*. The classified result shows that *Potamogeton Maackianus* occupy the larger portion of the classified area in the basin, than other species. It also indicates the dominance of the specie in the south basin. The yearly changes in coverage area and biomass was analyzed. Considering the weak SAV signal in water and the time lag between the image acquisition and *in-situ* measurement, an image with high spatial, temporal and spectral resolution is recommended for detailed SAV studies in the future.

5.9.2 Conclusions

We tested the applicability of multispectral Landsat-8 satellite image to map the distribution and biomass of the Submerged Aquatic Vegetation (SAV) infested area in the eutrophic shallow basin of the Lake Biwa. The SAV in the basin was classified using the Spectral mixture Analysis (SMA), Spectral Angle Mapper (SAM) image along with the reflectance of NIR and SWIR bands in the Binary Decision Tree. A new Spectral Decomposition Algorithm was developed which involves the influence bottom albedo, to

estimate the biomass of the SAV classified pixels in the south basin. The technique was applied to images of the different year (2013-2014) for the peak growing period of the SAV, mainly in September and October, to quantify the changes in the basin.

A binary decision tree discriminated the aquatic vegetation in three categories emergent, floating and submerged vegetation with an overall accuracy of 84.6% and SAV classification accuracy of 76.5%. The SAV coverage area was estimated for four consecutive years (2013-2016). The detected SAV coverage area in the recent years, particularly in 2016 where the estimated coverage area approximately doubled (i.e. 40% of the south basin area) from 2013 (i.e. 20% of basin area). The overall trend indicates the proliferation of SAV in the basin even with decreased water clarity in recent year. However, a long-term monitoring (i.e., monthly variation in SAV) is required to understand the influence of water clarity on the SAV detection using satellite image.

The biomass of the SAV classified area was estimated using the biomass model developed from the Spectral Decomposition Algorithm for all the images. Alike the SAV coverage area, the total SAV biomass also increased in the recent year. The estimated biomass density was significantly high for 2014 with high water transparency. An upsurge in SAV biomass to 16% (2014), 55% (2015) and 34% (2016), was noted when compared to the biomass in 2013. The technique provides the biomass estimate that is consistent with the *in-situ* measurements. The satellite-derived results suggest that SAV growth significantly influenced by the water quality conditions, however, the changes may not occur immediately, can be seen in the following years. The application of the satellite-based technique to assess the extent of SAV and it biomass will be useful for the lake water managers and concerned stakeholders in monitoring and deciding the effective management activity and remediation efforts, for maintaining a healthy lake ecosystem. Furthermore, the SAV classified result shows that *Potamogeton Maackianus* occupy the larger portion of the classified area in the basin, than other species. It also indicates the dominance of the specie in the south basin.

References

1. Melzer, A. Aquatic macrophytes as tools for lake management. *Hydrobiologia* **1999**, *395/396*, 181–190.
2. HAGA, H.; Ishikawa, K. Spatial Distribution of Submerged Macrophytes in the Southern Lake Biwa basin in the summer of 2014, in comparison with those in 2002, 2007 and 2012. *Japanese Journal of Limnology (Rikusuigaku Zasshi)* **2016**, *77*, 55–64.
3. Silva, T. S. F.; Costa, M. P. F.; Melack, J. M.; Novo, E. M. L. M. Remote sensing of aquatic vegetation: Theory and applications. *Environmental Monitoring and Assessment* **2008**, *140*, 131–145.
4. Madsen, J. D. Biomass Techniques for Monitoring and Assessing Control of Aquatic Vegetation. *Lake and Reservoir Management* **1993**, *7*, 141–154.
5. Hestir, E. L.; Khanna, S.; Andrew, M. E.; Santos, M. J.; Viers, J. H.; Greenberg, J. A.; Rajapakse, S. S.; Ustin, S. L. Identification of invasive vegetation using hyperspectral remote sensing in the California Delta ecosystem. *Remote Sensing of Environment* **2008**, *112*, 4034–4047.
6. Hamabata, E.; Kobayashi, Y. Present status of submerged macrophyte growth in Lake Biwa: Recent recovery following a summer decline in the water level. *Lakes and Reservoirs: Research and Management* **2002**, *7*, 331–338.
7. Pinnel, N. A method for mapping submerged macrophytes in lakes using hyperspectral remote sensing, Technical University of Munich, 2007.
8. Haga, H.; Ohtsuka, T.; Matsuda, M.; Ashiya, M. Echosounding observations of coverage, height, PVI, and biomass of submerged macrophytes in the southern basin of Lake Biwa, Japan. *Limnology* **2007**, *8*, 95–102.
9. Brooks, C.; Grimm, A.; Shuchman, R.; Sayers, M.; Jessee, N. A satellite-based multi-temporal assessment of the extent of nuisance Cladophora and related submerged aquatic vegetation for the Laurentian Great Lakes. *Remote Sensing of Environment* **2015**, *157*, 58–71.
10. Güttler, F. N.; Niculescu, S.; Gohin, F. Turbidity retrieval and monitoring of Danube Delta waters using multi-sensor optical remote sensing data: An integrated view from the delta plain lakes to the western-northwestern Black Sea coastal zone. *Remote Sensing of Environment* **2013**, *132*, 86–101.
11. Pacheco, A.; Horta, J.; Loureiro, C.; Ferreira Retrieval of nearshore bathymetry from Landsat 8 images: A tool for coastal monitoring in shallow waters. *Remote Sensing of Environment* **2015**, *159*, 102–116.
12. Zhang, Y.; Liu, X.; Qin, B.; Shi, K.; Deng, J.; Zhou, Y. Aquatic vegetation in response to increased eutrophication and degraded light climate in Eastern Lake Taihu: Implications for lake ecological restoration. *Scientific Reports* **2016**, *6*, 23867.
13. Shuchman, R. A.; Sayers, M. J.; Brooks, C. N. Mapping and monitoring the extent of submerged aquatic vegetation in the laurentian great lakes with multi-scale satellite remote sensing. *Journal of Great Lakes Research* **2013**, *39*, 78–89.
14. Villa, P.; Mousivand, A.; Bresciani, M. Aquatic vegetation indices assessment through radiative transfer modeling and linear mixture simulation. *International Journal of Applied Earth Observation and Geoinformation* **2014**, *30*, 113–127.
15. Heege, T.; Bogner, a; Pinnel, N.; Bostater, C. R.; Santoleri, R. Mapping of submerged aquatic vegetation with a physically based process chain. *Remote Sensing of the Ocean and Sea Ice 2003* **2004**, *5233*, 43–50.
16. Oyama, Y.; Matsushita, B.; Fukushima, T.; Matsushige, K.; Imai, A. Application of spectral decomposition algorithm for mapping water quality in a turbid lake (Lake Kasumigaura, Japan) from Landsat TM data. *ISPRS Journal of Photogrammetry and Remote Sensing* **2009**, *64*, 73–85.
17. Kirk, J. T. O. *Light and photosynthesis in aquatic ecosystems*; 3rd ed.; Cambridge University Press, 2011.
18. Hale, G. M.; Querry, M. R. Optical Constants of Water in the 200-nm to 200-μm Wavelength Region. *Applied Optics* **1973**, *12*, 555.
19. Pope, R. M.; Fry, E. S. Absorption spectrum (380–700 nm) of pure water II Integrating cavity

measurements. *Applied Optics* **1997**, *36*, 8710.
20. Liu, Y. S.; Islam, M. a; Gao, J. Quantification of shallow water quality parameters by means of remote sensing . *Progress in Physical Geography* **2003**, *27*, 24–43.
21. Ackleson, S. G.; Klemas, V. Remote sensing of submerged aquatic vegetation in lower chesapeake bay: A comparison of Landsat MSS to TM imagery. *Remote Sensing of Environment* **1987**, *22*, 235–248.
22. Watanabe, F. S. Y.; Imai, N. N.; Alcântara, E. H.; Rotta, L. H. da S.; Utsumi, A. G. Signal Classification of Submerged Aquatic Vegetation Based on the Hemispherical-Conical Reflectance Factor Spectrum Shape in the Yellow and Reg Regions. *Remote Sensing* **2013**, *5*, 1856–1874.
23. Goodwin, N.; Coops, N. C.; Stone, C. Assessing plantation canopy condition from airborne imagery using spectral mixture analysis and fractional abundances. *International Journal of Applied Earth Observation and Geoinformation* **2005**, *7*, 11–28.
24. Underwood, E.; Ustin, S.; DiPietro, D. Mapping nonnative plants using hyperspectral imagery. *Remote Sensing of Environment* **2003**, *86*, 150–161.
25. Kruse, F. A.; Lefkoff, A. B.; Boardman, J. W.; Heidebrecht, K. B.; Shapiro, A. T.; Barloon, P. J.; Goetz, A. F. H. The spectral image processing system (SIPS)—interactive visualization and analysis of imaging spectrometer data. *Remote Sensing of Environment* **1993**, *44*, 145–163.
26. Oyama, Y.; Matsushita, B.; Fukushima, T.; Nagai, T.; Imai, A. A new algorithm for estimating chlorophyll-a concentration from multi-spectral satellite data in case II waters: a simulation based on a controlled laboratory experiment. *International Journal of Remote Sensing* **2007**, *28*, 1437–1453.
27. Lyzenga, D. R. Passive remote sensing techniques for mapping water depth and bottom features. *Applied Optics* **1978**, *17*, 379.
28. Lyzenga, D. R.; Malinas, N. P.; Tanis, F. J. Multispectral bathymetry using a simple physically based algorithm. *IEEE Transactions on Geoscience and Remote Sensing* **2006**, *44*, 2251–2259.
29. Gilabert, J.; Perez-Ruzafa, A.; Gutierrez, J. M. Light_Attenuation Coefficient in shallow coastal waters from airborne multispectral data.pdf. *Advances in Remote Sensing* **1995**, *4*.
30. Scheffer, M.; Jeppesen, E. Alternative stables states. In *The Structuring Role of Submerged Macrophytes in Lakes*; Erik Jeppesen, Martin Søndergaard, Morten Søndergaard, K. C., Ed.; Springer New York, 1998; pp. 397–406.
31. Takamura, N.; Kadono, Y.; Fukushima, M.; Nakagawa, M.; Kim, B. H. O. Effects of aquatic macrophytes on water quality and phytoplankton communities in shallow lakes. *Ecological Research* **2003**, *18*, 381–395.
32. Søndergaard, M.; Johansson, L. S.; Lauridsen, T. L. Submerged macrophytes as indicators of the ecological quality of lakes. **2010**, 893–908.
33. Brooks, C.; Grimm, A.; Shuchman, R.; Sayers, M.; Jessee, N. Remote Sensing of Environment A satellite-based multi-temporal assessment of the extent of nuisance Cladophora and related submerged aquatic vegetation for the Laurentian Great Lakes. *Remote Sensing of Environment* **2015**, *157*, 58–71.
34. Zhang, Y.; Ma, R.; Duan, H.; Loiselle, S.; Xu, J. A Spectral Decomposition Algorithm for Estimating Chlorophyll-a Concentrations in Lake Taihu, China. **2014**, 5090–5106.
35. Boyd, C. E.; Carolina, S. The Limnological Role of Aquatic Macrophytes and Their Relationship to Reservoir Management '. *Reserv. Fish. Limnol.* **1971**, 153–166.
36. Carpenter, S. R.; Lodge, D. M. Effects of submersed macrophytes on ecosystem processes. *Aquatic Botany* **1986**, *26*, 341–370.
37. Nelson, S. A. C.; Cheruvelil, K. S.; Soranno, P. A. Satellite remote sensing of freshwater macrophytes and the influence of water clarity. *Aquatic Botany* **2006**, *85*, 289–298.
38. Zou, W.; Yuan, L.; Zhang, L. Analyzing the spectral response of submerged aquatic vegetation in a eutrophic lake, Shanghai, China. *Ecological Engineering* **2013**, *57*, 65–71.
39. Morel, A. Optical Properties of Pure Water and Pure Sea Water 1974, 24.
40. Mobley, C. D. Radiative Transfer in the Ocean. *Encyclopedia of Ocean Sciences: Second Edition* **2008**,

619–628.
41. Ishikawa, K.; Haga, H. Ecological Regime Shift in the South Basin of Lake Biwa : Focus on Algal Blooms and Submerged Macrophyte Overgrowth. In *UNESCO International Symposium on Scientific, Technological and Policy Innovations for Improved Water Quality Monitoring in the Post-2015 SDGs Framework*; Kyoto, Japan, 2015; pp. 1–3.

Chapter 6

CONCLUSIONS AND RECOMMENDATIONS

6.1 Conclusions

In an aquatic environment, the detection of Submerged Aquatic Vegetation (SAV) using the satellite image can be influenced by several factors. For detecting the SAV particularly in the shallow eutrophic lake, it is essential to take into account all the factors influencing the SAV signal, for selecting the appropriate remote sensing method. The important factors identified in this study are; the concentration of optically active component (OAC) in the water column, SAV canopy depth, coverage area, species reflectance, water depth or SAV depth. The study shows that the absorption and scattering properties of the two dominant OAC, mainly phytoplankton (i.e., chlorophyll-a) and Non-Phytoplankton Suspended Solids (NPSS) substantially attenuates the SAV species reflectance with the increase in concentration and water depth. Whereas, colored Dissolved Organic Carbon (cDOM) has a negligible influence on the SAV spectra at low concentration (< 3mg/L), in the lakes.

In this study, the maximum canopy depth estimated for the two SAV species *Egeria Densa* and *Potamogeton Maackinus*, using the Bio-Optical model and the classified SAV image, was 1.0 m and 1.1 m, respectively. The minimum and maximum canopy depth estimated at, for *Egeria Densa* was in between 0.11 m to 1.0 m, and *Potamogeton Maackianus* was in between 0.10 m to 1.1 m, respectively. More importantly, the maximum canopy depth can be achieved in clear water condition with chlorophyll <20 μg/L and NPSS <10 mg/L. At the chlorophyll concentration >20 μg/L and NPSS >10 mg/L, the canopy depth reduced to < 0.3 m and <0.2 m. Because the input parameters used in this study are unique to Lake Biwa for SAV peak growth period, the spatial and temporal variation in the Inherent optical properties is expected, when applied to other lakes. However, with known apparent and inherent optical properties of the selected endmembers, it is possible to identify the detection depth of SAV, using the Bio-Optical model. The *in-situ* measured data of September 2016 and classified SAV image confirmed that at the maximum canopy depth (i.e., 0.40 m - 1.1 m canopy depth), the SAV could be detected using the Landsat-8 image, in the south basin of Lake Biwa. The study further suggests that the Bio-Optical model can be successfully applied to the SAV species

detailed studies in the future, for effective management efforts in the lake. In addition, the Landsat-8 image can be applied to monitor the SAV species in a shallow eutrophic lake, if the species lies with the detection depth limit (i.e., the maximum canopy depth 1.1 m). This study tried to fill the gap in depth estimation of submerged vegetation, specifically for eutrophic shallow lakes, which is limited due to the presence of OAC.

Furthermore, a new spectral decomposition algorithm was developed and applied to estimate the concentration of the dominant optically active component (i.e., mainly chlorophyll-a). The algorithm was developed based on the assumption that in a shallow eutrophic lake where > 90% of basin area (i.e., bottom surface) covered with the SAV, the bottom albedo is mainly from the SAV and is contributing significantly to the water leaving reflectance. The estimated chlorophyll using the developed algorithm (i.e., blue, green, red and NIR band of Landsat-8) was in line with the observed data ($R^2 = 0.78$) thus achieved the overall RMSE of 6.15 and 6.28 μg/L. The satellite-derived chlorophyll map shows the increased chlorophyll concentration in the 2013 and 2016, indicating the turbid water condition (> 30 μg/L), particularly towards the eastern shoreline and the outlet of the basin. The water transparency algorithm developed and applied on the Landsat-8 satellite image (2013-2016) in this study, which further supported the chlorophyll estimated result for the basin. The satellite-derived water clarity (R2 = 0.77; RMSE = 0.38 m) indicated the clear water condition in the year 2014 (i.e., maximum water transparency > 6 m). The result confirmed the reduced water clarity in 2016 and 2013, which has only 15% (8 km^2) and < 1% (1 Km^2) of the basin area with water transparency > 3.0 m than 2014 with 54% (28 km^2). Moreover, the area with low water clarity (< 1.5 m) increased in 2016 (14 km^2), when compared with the remaining years (3 km^2). The low water transparency was obtained in two particular conditions, the location with high turbidity and where the vegetation emerge out of the water surface. The estimated average water transparency for all year based on the satellite-derived data of the 52 stations in the basin are 2.2 m (October 2013), 2.9 m (September 2014), 2.6 m (September 2015) and 2.0 m (September 2016). The satellite-derived result in this study is in line with the data from Lake Biwa Environmental Research Institute (LBERI), Otsu. To develop the robust chlorophyll and water clarity estimation model it is also essential that the satellite data acquisition time coincides well with the *in-situ* measured data. On the other hand, other sources of error which can influence the model prediction using the satellite image, are the

error in atmospheric correction as well as the field data measurement error. Therefore, it is essential to carefully consider the sources of error while dealing with medium resolution satellite image. However, the developed approach successfully applied on the south basin of Lake Biwa and possibly be tested on other shallow lakes. Mainly, for the locations not easily accessible, and the location with no sufficient data available. The obtained results are informative and are used to distinguish the turbid water pixels from clear water and SAV, before mapping the SAV using satellite image

Moreover, we assessed the SAV distribution (i.e., coverage area) and its biomass for the eutrophic south basin of Lake Biwa, using the multispectral Landsat-8 OLI image. In eutrophic lake, due to the mixed pixel effect, it is crucial to isolate the SAV pixels from the turbid water pixels which often contribute to the misclassification of the SAV. In this study, the SAV was classified by applying the Spectral mixture analysis (SMA), Spectral Angle Mapper (SAM), Minimum Noise Fraction (MNF) and the binary decision tree as a classification technique, on the atmospherically corrected Landsat-8 image (2013 - 2016). A good classification accuracy of 84.6% was achieved when compared with the available ground truth data (2014) with an omission and commission error of 23.5% and 18.8 %, respectively. The study also supports the conclusion drawn in chapter 3, where with the increase in turbidity the detection of the SAV is affected. The obtained result shows that due to the increased eutrophication varying SAV canopy depth as well as water depth only 21% (2013), 18% (2014), 30% (2015 and 40% (2016) of the basin area could be mapped for SAV using Landsat-8 image. Most of the locations where SAV canopy depth > 2m were not detected using the satellite image, which further supports the fact that canopy depth is an important parameter for SAV detection and that SAV can easily be detected to the maximum canopy depth of 1 m. The detected SAV coverage area approximately doubled in 2016 (i.e., 40% of the south basin area) from 2013 (i.e., 20% of basin area). The SAV was detected at the maximum water transparency of 3.7 m. In this study, the mapped SAV coverage area does not rise as expected, with increased water clarity for the same year. However, the prolific growth noted in the following years. Thus, in this study the SAV dispersal shows a delayed response to the changing water clarity conditions in the lake.

A new spectral decomposition algorithm was developed to estimate the SAV biomass. The algorithm was successfully applied to the satellite image, with an overall RMSE of 0.13

Kg DW m^{-2}. A biomass estimation model can be applied to other images for biomass estimation using the satellite image. An upsurge in SAV biomass to 16% (2014), 55% (2015) and 34% (2016), was noted when compared to the biomass in 2013. Likewise the SAV coverage area, the total SAV biomass also increased in the recent year. The increase in estimated biomass density (4.89 kg DW m^{-2}) but a low coverage area, in the year with high water transparency (2014, water transparency > 6m) indicates that water clarity can significantly influence the biomass density, however, less significantly to SAV distribution process in a eutrophic lake. Thus we found, the increased SAV distribution in the year following the clear water year, 2015 (15.7 km^2) and 2016 (21.0 km^2). The technique provides the biomass estimate that is consistent with the in-situ measurements, in the south basin of the Lake Biwa. This study also shows that a new spectral decomposition algorithm which accounts for the bottom albedo in the shallow basin can be applied effectively for estimating the SAV biomass, using the Landsat-8 image. Furthermore, the SAV species classification performed by generating the bottom substrate map using the satellite-derived diffuse attenuation coefficient. The result indicates that the dominant species (such as *Potamogeton Maackianus*) with large biomass can be detected more extensively than more fragmented species (such as *Myriophyllum Spicatum*).

The technique provides the biomass estimate that is consistent with the *in-situ* measurements. The satellite-derived results suggest that SAV growth is significantly influenced by the water quality conditions, in the eutrophic basin. However, the changes may not occur immediately but are more visible in the following years. Long-term monitoring is essential to understand the influence of water clarity on the SAV distribution and biomass.

Landsat-8 images were successfully utilized for SAV abundance mapping in the eutrophic basin of the large lake. Furthermore, with the appropriate information of the potential optically active components (i.e., based on the water condition of the lake), their respective standard reflectance spectra and the water clarity of the lake, the developed method could be tested on other shallow lakes for SAV biomass estimation.

The developed satellite-based approach to assess the extent of SAV and its biomass will be useful for the lake water managers and concerned stakeholders in monitoring and deciding the effective management activity and remediation efforts, for maintaining a healthy lake ecosystem.

6.2 Recommendations

The time gap in the satellite acquisition and the *in-situ* measurement often result in the reduced accuracy. Thus, an adequate field data collected for the same day of the satellite overpass may provide better validation for the satellite-based models. For detailed SAV species studies, the application of medium resolution satellite images may not be very feasible with limited *in-situ* field data information. In addition, considering the several limiting factors in SAV abundance mapping, it is essential to develop the SAV classification technique to detect the deeper SAV in the lakes. In addition, it is essential to have a long-term monitoring of SAV (i.e., with monthly variation) using the satellite remote sensing is recommended to understand the influence of the water clarity on the growth and distribution of SAV in the eutrophic water body. Considering the all the limitation, an area-specific Bio-Optical model which can represent the study area should be developed, along with the radiative transfer model.